RESEARCH ON THE MORPHOLOGICAL BEHAVIOUR OF BIFURCATIONS IN RIVERS

by

P. den Dekker
J.M. van Voorthuizen

May 1994

supervisors: Prof.Dr.Ir. M. de Vries
Dr.Ir. Z.B. Wang
Dr.Ir. H.L. Fontijn
Dr. R.J. Fokkink

Preface

This report is a presentation of the research done for the completion of our MSc. thesis-work. The topic involved is the problem of bifurcations in rivers, a challenging subject which led to both a theoretical and an experimental analysis.
The experimental part of the research was realized within the framework of a linkage project between DUT (Delft University of Technology) and BUET (Bangladesh University of Engineering and Technology), a project coordinated by CICAT (Centre for International Co-operation and Appropriate Technology). In this context we spent four months in Dhaka, Bangladesh, during which time an experimental model of a bifurcated river was built.
As a result we had the unique opportunity to combine theoretical and experimental research with practical experience in a developing country. This combination is rather exceptional, as for most students going abroad the practical design and experience is the only thing accomplished.
We would like to thank a number of people, without whom this report could never have been completed. First of all Prof. de Vries, and the other members of our examination committee, Dr. Wang, Dr. Fontijn and Dr. Fokkink, who put forward the idea of going to Bangladesh for a research project, and whose advice during the course of our thesis work was essential.
We would also like to thank Cees Timmers, and the others at CICAT, for the coordination of the project and the continued interest and concern for our well-being during our stay in Dhaka.
In Bangladesh we would like to thank Mr. van Mierlo, Prof. Hannan, Dr. Kabir and all the other members of the educational staff of the Water Resources Department at BUET. Without their help the model would never have been built.
Also thanks to Mr. van der Wal, who spent some of his spare time in helping to start up the model during the absence of Mr. van Mierlo. The practical advice given was very useful.
A special thanks goes to Bob van Kappel for the hospitality given in his flat in Dhaka. The moral support given during our stay was indispensable.
And finally we would like to thank Michael van Lieshout for his critical observations in reading the report, and Jos van Kerckhoven and Ernst Rob, for the help given in making the drawings and scans presented in the report.

Peter den Dekker
Johan van Voorthuizen

Summary

Introduction

The morphological behaviour of bifurcations in rivers is a poorly understood problem with which many river engineers are confronted. Bifurcations are mostly found in deltas, but also in braided sections of a river. The course of a braided river is highly unstable and unpredictable; serious problems can therefore arise if an attempt is made to regulate the river. The stability of the islands in these braided rivers is strongly influenced by the morphological behaviour of the bifurcations. A better understanding of the processes occurring at a bifurcation would contribute to the understanding of the behaviour of the braided river system, which in turn could help in modelling the river system as a whole.

Thesis work

The research done for the thesis work is a continuation of the research done by Wang et al. (1993) for the modelling of estuaries. Wang analyzed the influence of the relations describing a bifurcation on the stability of one-dimensional network morphodynamic models.

The thesis work is an expansion of his analysis to the research on the stability of bifurcated rivers; it comprises two parts:

- a theoretical analysis in which an analytical model leads to a number of conclusions verified by numerical computations;
- the design and construction of an experimental model of a bifurcation in a river; this model can and will be used to conduct experiments which should complement the results of the theoretical analysis.

Theoretical analysis

The important problem in the modelling of bifurcations is the choice to be made for the relation describing the distribution of the sediment at the bifurcation (the *nodal-point relation*). With the help of an analytical model, the influence of the chosen relation on the stability of the one-dimensional network morphodynamic model is examined. This leads to a number of theoretical predictions, which are verified by numerical computations with the computer model WENDY. These computations agree very well with the predictions, and lead to the conclusion that the stability of the system is completely determined by the choice of the nodal-point relation. The general nodal-point relation proposed by Wang et al. (1993) is used to determine conditions of stability; these are the same as for the case of an estuary. Another conclusion drawn from the analysis is that the

morphological time scale is also completely determined by the chosen nodal-point relation. The effect of the general nodal-point relation on the morphological time scale is quantified in the report.

Experimental model

The experimental model was designed and built in Dhaka, Bangladesh within the framework of a linkage project between DUT and BUET.

The goal of the experimental part of the research is to relate the local three-dimensional configuration of a bifurcation to the relevant parameters of the different general nodal-point relations.

The experiments did not fit within the time frame of this thesis work, so none were performed. However, a detailed description of the necessary measurements is given in the report, as well as recommendations for possible experiments.

Link between theory and experiments

In order to link experimental results to theoretical results, the configuration of the experimental model was used as input for computations with WENDY. The dimensions of the model are too small for WENDY to handle, so the experimental model was scaled-*up* to a larger fictitious prototype.

The computations performed lead to a value for the morphological time-scale, which can be compared to the time scale in the experimental model. Since the value of the morphological time-scale in the numerical computation is determined by the chosen nodal-point relation, this nodal-point relation can be calibrated until the same time scale is obtained as in the experiments. In this way a link is made between theory and experiments.

Contents

Introduction

In this report, the complex problem of bifurcations in rivers is addressed. The study, performed for this Msc-thesis, is partly theoretical and partly experimental, and should be seen as a first approach of what will hopefully become a series of thesis-work research projects. This report is therefore oriented towards the potential successor, who will be able to do the experimental work recommended at the end of the report.
The report includes three parts, which each comprise several chapters. In the first part a general background is given on bifurcated rivers. This includes a description of the problem, as well as a brief review of what is known about the processes involved at a bifurcation.
The second part is a theoretical analysis of the problem. An analytical model for the morphological behaviour of the branches at a bifurcation is presented; with this model it is possible to make a number of theoretical predictions. These predictions are then verified with numerical computations, using the computer program WENDY.
In Part III the design of an experimental model of a bifurcated river is presented. Suggestions for possible experiments are made and the necessary measurements are described. The results of the experiments will hopefully relate the theoretical results presented in Part II to the physics in nature.

Part I

General background on bifurcated rivers

Chapter 1 - Description of the problem

1.1 Introduction

The morphological behaviour of bifurcations in rivers is a poorly understood problem. This is exemplified by the fact that very little literature can be found dealing with this subject. The scarcity in available literature must, however, not be seen as an indication of the unimportance of the subject, but rather as a token of the difficulty of the problem with which many river engineers are confronted.
A general description of the problem, and its relevance to the task of the engineer are given in the next section.

1.2 Description of the problem

Bifurcations can be found in different places along the stretch of a river. This is illustrated in figure 1.1 where the course of an "idealized" river is depicted.
• The braided river in the upstream end of the middle course has more than one channel, with a sequence of confluences and bifurcations forming a multitude of islands in the river. The course of a braided river is very unstable and unpredictable, leading to serious problems for an engineer trying to "tame" the river with hydraulic structures. The morphological behaviour of the islands in the braided river, and the effect of the bifurcations on the stability of the downstream branches strongly influence the stability of the braided river system as a whole. A better understanding of the morphological processes at a bifurcation would clearly contribute to the understanding of the behaviour of the islands in the braided river. This could help improve the prediction of the course of such a river, facilitating the task of the engineer trying to regulate the river.
• In the lower course (figure 1.1) the river forms a delta, which is also dominated by bifurcations. Because of the unknown behaviour of bifurcations, it has proven to be difficult to implement the layout of a delta into a one-dimensional morphodynamic model. The research on the behaviour of bifurcations in rivers is therefore relevant for the development of these models. Wang et al. (1993) analyze the influence of so-called *nodal-point relations* (see Chapter 2) on the behaviour of the one-dimensional network morphodynamic models.

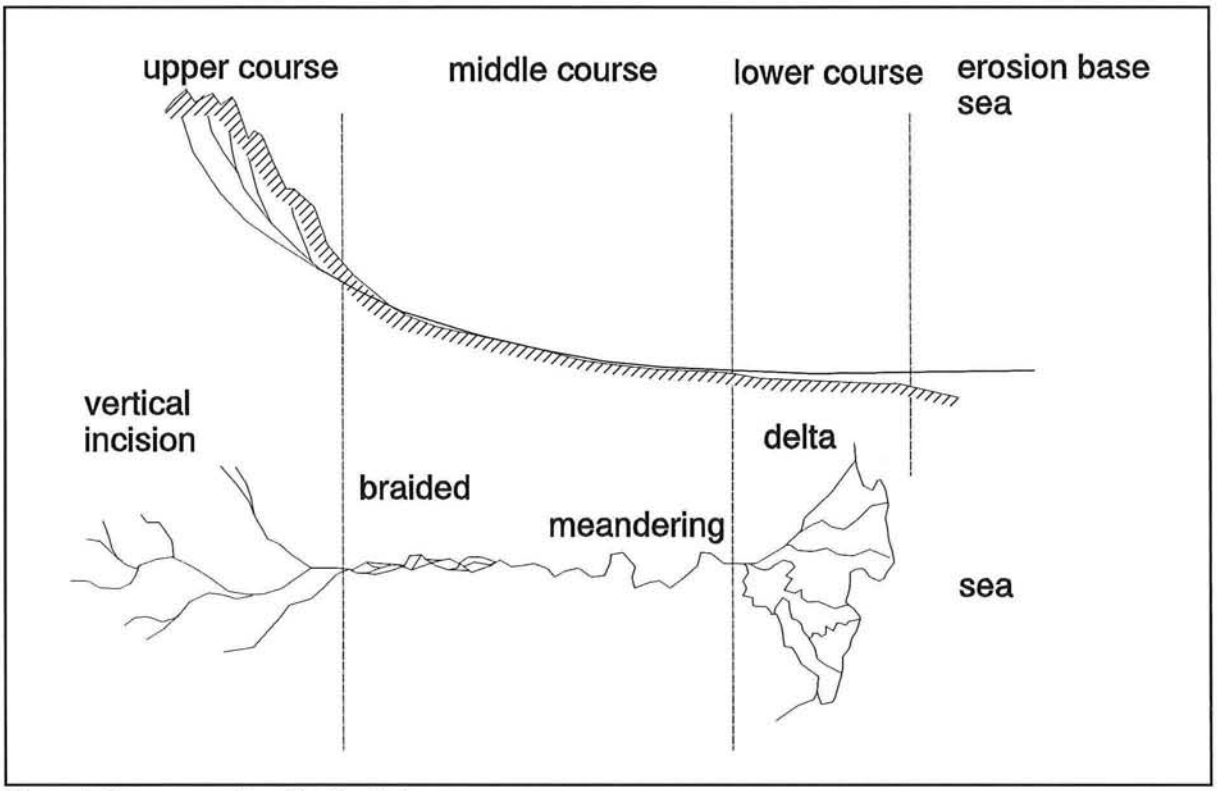

figure 1.1 - course of an idealized river

• An "artificial" bifurcation also occurs at an off-take (for example for irrigation purposes). These sometimes have a tendency to silt up if preventive measures such as dredging are not undertaken. The reason for this silting-up is not well understood, but is related to the problems of "natural" bifurcations. Boreli and Bruck (1956) attempted to analyze the conditions of stability of a river branch for the sake of off-take design; they considered a river branch a natural off-take, whose properties could be used in diversion design. Further research on bifurcations will no doubt benefit the design and construction of off-takes.

Example:

An example of a current river engineering problem involving the behaviour of a bifurcation is the construction of the bridge over the Jamuna River in Bangladesh. The main channel of this river is known to displace up to several kilometres a year, in a rather unpredictable way. Major flow guiding constructions are being built to try to stabilise the course of the river, to keep the river flowing *under* the bridge. In order to minimise costs and to align the flow guiding structures in an effective way, a prediction of the possible changes in the course of the river had to be made. This prediction was based on a probabilistic method using statistical data. A better physical understanding of the morphological behaviour of the bifurcations in the braided river could have

contributed to a more accurate prediction. Moreover, the design of the hydraulic structures could be improved as the effectiveness of the applied hydraulic structures would be better understood. The relevance of the present study is thus illustrated.

1.3 Goal of the research

After the general description of the problem given above, it is possible to define a general *goal* of the study presented in this report.

General goal: *Analyze the morphological behaviour of bifurcations in rivers, with respect to the stability of islands in rivers.*

Restrictions:
In nature situations may occur where three or more downstream branches diverge from the main channel. In this report only the case of a bifurcation with two downstream branches is considered. Moreover it is assumed that the sediment transport is related to the local flow condition by a power-law relation.

In the next chapter, a theoretical introduction of the processes describing a bifurcation is given. This brief description is a presentation of what is presently known to happen at a bifurcation, and forms the basis for the analytical model presented in Part II.

Chapter 2 - Theoretical introduction

2.1 Basic conditions

2.1.1 Introduction

When trying to analyze the stability of an island in a river, problems occur when trying to describe the processes occurring at the upstream-end of the island, at the *bifurcation* in the river. The problem arising at a bifurcation can best be displayed when comparing the basic conditions at a bifurcation with those at a confluence. The mass balances for both cases are the same, but the boundary conditions for the computations are different. Since confluences do not present any great problems during computations, they are described first.

2.1.2 Confluences

At a confluence two rivers (or river branches) meet and join into one single river.
The conditions governing the confluence are simple, as seen in the following:

* The mass balances of water and sediment have to be satisfied; these are given in the figure below, where Q_i is the discharge and S_i is the sediment transport in branch i.

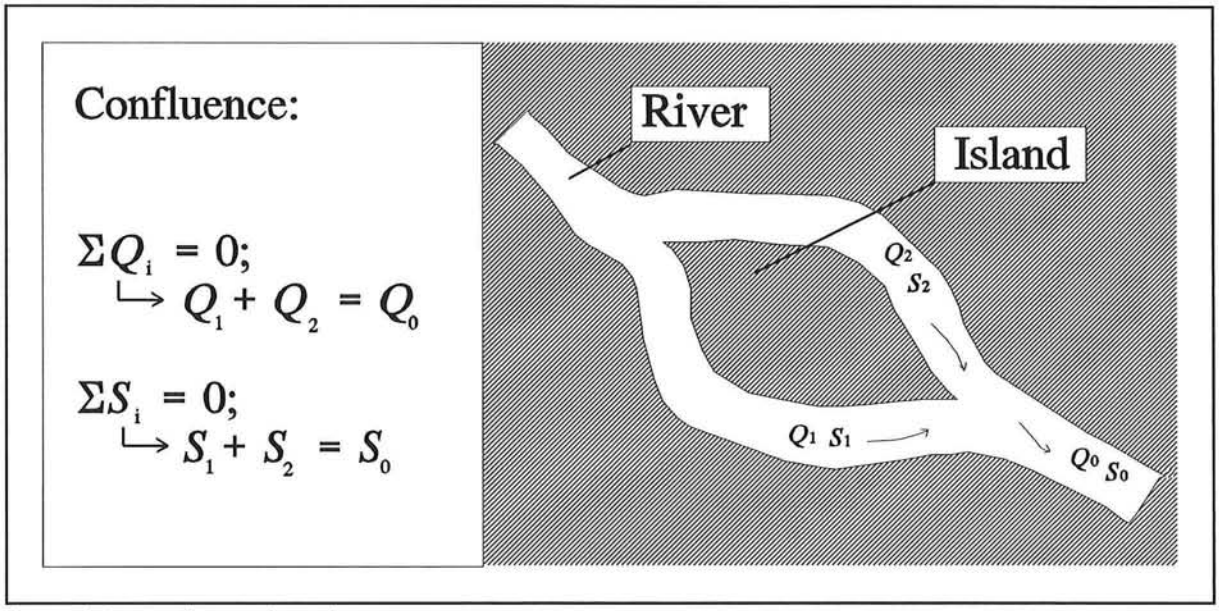

figure 2.1 - confluence in a river

* In this case Q_1, Q_2, S_1 and S_2 are known; the unknown values of Q_0 and S_0 simply follow from the two mass balance equations.

2.1.3 Bifurcations

A bifurcation occurs when a river separates into two (or more) downstream branches. The conditions governing the bifurcation are a little different from those for a confluence, as can be seen below.

* The mass balances of water and sediment are the same as for a confluence (see figure 2.2).

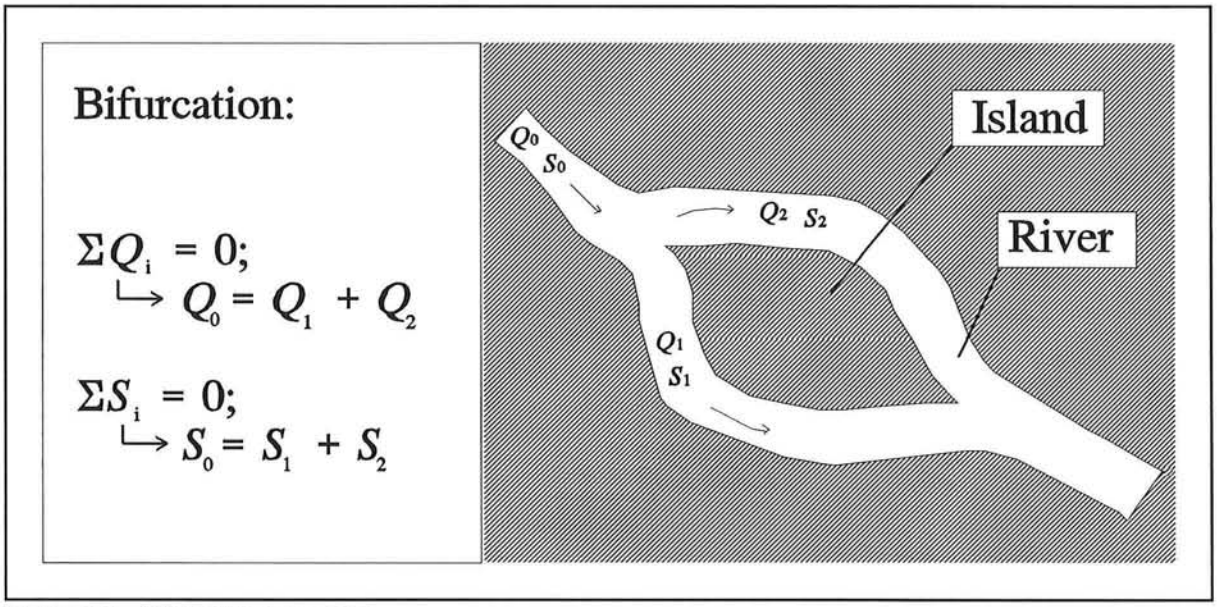

figure 2.2 - bifurcation in a river

* In this case Q_0 and S_0 are known, and Q_1, Q_2, S_1 and S_2 are unknown. As a result the two mass balance equations are not sufficient to determine the values of the unknown quantities.

With this simple description of a bifurcation, the problem arising can clearly be seen: two extra equations have to be found in order to obtain the 4 equations necessary to determine the values of the 4 unknown quantities: Q_1, Q_2, S_1 and S_2.

As shown in the sections above, the difficulty in the computations for the morphological behaviour of an island in a river largely lie in the description of the processes occurring at the upstream bifurcation. For this reason the analysis in the following mainly focuses on the bifurcation problem.

2.2 Additional equations

In order to find the values of Q_1, Q_2, S_1 and S_2, one has to know how water and sediment distribute over the downstream branches. In this way two extra equations are obtained.
Water:
The distribution of the discharge Q_0 into Q_1 and Q_2 is completely determined by the geometry and friction coefficients of the downstream branches. It is such that, given the geometry of the downstream branches, only one water level occurs at the bifurcation. This computation should not give any problems. The problem is the determination of the distribution of the sediment.
Sediment:
The distribution ratio of the sediment to the two downstream branches is determined by the local three-dimensional flow pattern (Bulle, 1926; De Vries 1992). The determination of the ratio S_1/S_2 is a difficult task; this has resulted in a multitude of proposed *nodal-point relations* (this name comes from Wang et al., 1993). A list of the different nodal-point relations is given in the next section.

2.3 Nodal-point relations

Wang et al. (1993) made an inventory of the different nodal-point relations found in literature, and analyzed the influence of these relations on the stability of one-dimensional models. The results of this inventory are presented here.

- The relation that is probably used most in operational models is the following one:

$$\frac{S_1}{S_2} = \frac{Q_1}{Q_2} \tag{2.1}$$

This relation is one of the two default options in the DELFT HYDRAULICS' one-dimensional model WENDY.

- The second default option in WENDY is the following relation:

$$\frac{S_1}{S_2} = \frac{B_1}{B_2} \tag{2.2}$$

where B_i is the width of branch i.
Wang concludes that a physically realistic stable situation is never reached with this option. Moreover, the combination of this relation with a 1D model (such as WENDY),

in which the widths of branches are constant, leads to a constant ratio S_1/S_2, which is physically unrealistic. This relation is therefore not recommended.

- Another relation involves unknown constants:

$$\frac{S_1}{S_2} = \alpha\left(\frac{Q_1}{Q_2}\right) + \beta \tag{2.3}$$

This is also an option of WENDY, in which the constants α and β have to be given by the user. This option was used in WENDY for the Beni Mazar model (Vermeer, 1990). The values of α and β were calibrated successfully on data from a run in the experimental model of the reach of the River Nile near Beni Mazar.

The analysis performed by Wang leads to the proposal of a general nodal-point relation, which is a generalisation of Eq.(2.1) and Eq.(2.2). This relation is:

$$\frac{S_1}{S_2} = \left[\frac{Q_1}{Q_2}\right]^m \left[\frac{B_1}{B_2}\right]^{1-m} \tag{2.4}$$

The influence of this relation on the stability of the 1D network morphodynamic model was analyzed and led to certain conditions of stability (see Part II of this report). This general nodal-point relation forms the basis of the analysis presented in the next chapters of the report.

2.4 Literature

Very little literature is available on the subject of bifurcations and islands in rivers. A review of the already mentioned literature is given here first.

- The analysis made by Wang et al. (1993) considers the influence of nodal-point relations on the stability of network morphodynamic models;
- Bulle (1926) states that the sediment distribution is governed by the local three-dimensional phenomena;
- Boreli and Bruk (1956) were mentioned in Chapter 1 for their analysis of the conditions of stability of a river branch for the sake of the design of off-takes;
- Vermeer (1990) was mentioned for the handling of a bifurcation in WENDY for the Beni Mazar model. Moreover, the research project of the Beni Mazar problem as a whole is worth mentioning here, since an experimental model was built which includes the local bifurcation in the River Nile (see Gasser et al., 1990).

Another study done at DELFT HYDRAULICS is that of Flokstra (1985); in this analysis the influence of a nodal-point relation is also looked at, but in this case the nodal-point relation considered is not a general nodal-point relation and moreover only a symmetrical case is analyzed.
Not yet mentioned is Klaassen et al. (1993) who approach the problem of the stability of braided rivers from a complete different angle. They are concerned with the *prediction* of changes in braided rivers from a statistical point of view, where the probability of occurrence of different potential developments play an important role. As already mentioned in Chapter 1, a better *physical understanding* of the morphological behaviour of the bifurcations in braided rivers could contribute to such a prediction. The present research is therefore relevant for the statistical models being developed.

A more general report written by De Vries (1993) gives an overview of the processes involved in braided rivers. This report is a note written for a workshop on River Engineering in Dhaka, Bangladesh, and is a good supplement to any study on the stability of islands in rivers.

Part II

Theoretical analysis

Chapter 3 - Introduction

3.1 Relevance

The previous part has made clear that relatively little is known on the subject 'bifurcations in rivers'. One-dimensional network models are hardly investigated and successful applications in numerical models are not known. From Wang et al (1993) it can be concluded that a very important place is held by the nodal-point relation which determines the distribution of the sediment transport over the downstream branches. This relation seems essential for the behaviour of a 1D-network morphodynamic model.
In this Part II it is aimed at a theoretical investigation of the general nodal-point relation as mentioned in Chapter 2

$$\left[\frac{S_1}{S_2}\right] = \left[\frac{Q_1}{Q_2}\right]^m \left[\frac{B_1}{B_2}\right]^{1-m} \tag{3.1}$$

The results hopefully lead to a better understanding of the use of this relation in morphodynamic models.

3.2 Contents of Part II

The theoretical study of the general nodal-point relation can be divided into two main aspects, viz. an analytical and a numerical aspect. First, in Chapter 4, an analytical study of a bifurcated river and the influence of the nodal-point relation is presented. The fundamental aspects are determined and hence the behaviour of a network model.
Consequently, a numerical analysis is carried out in Chapter 5 via simulations with the computer model Wendy. Several geometrical situations are computed here to compare the numerical outcome with the mathematical results from Chapter 4.
In Chapter 6 a little analytical extension is presented and linked with numerical computations.
Chapter 7 illustrates the possibility to make the experimental model parameters the input parameters for several Wendy-computations. This is possible via the application of certain scale relations.

In the last chapter of this theoretical part II, the conclusions from the analytical and numerical studies are outlined.

3.3 Description of Wendy

The mathematical computer model Wendy was developed by DELFT HYDRAULICS (DHL). The present computer model Wendy is a package consisting of five application programs:

- water flow (WAFLOW option);
- water flow with density effects (SAFLOW option);
- water flow and sediment transport (SEFLOW option);
- water flow and suspended sediment transport (SUSFLOW option);
- water flow and measured water level data (NETFIL option).

Considering the subject of this report only the SEFLOW option has been used. An important restriction of the Wendy program is that it is a one-dimensional model. Problems strongly governed by two- or three-dimensional effects are not represented well. In the context of this study on bifurcations in rivers (network models), Wendy needs therefore additional information on the sediment distribution over the downstream branches, in order to represent this three-dimensional phenomenon in a one-dimensional model. The extra information (i.e. an internal boundary condition) is given by the nodal-point relation (see Equation (3.1), (4.6)).

The momentum equation and mass balance for water and sediment are solved numerically by finite difference methods. The difference equations are expressed on a non-uniform staggered grid.

Chapter 4 - Mathematical analysis

4.1 Schematisation

In this chapter, the set-up of a simple mathematical model is outlined in order to describe the influence of the nodal-point relation on the morphological changes around a bifurcation in a river. The bifurcation is part of a network system as schematised in the figure below.

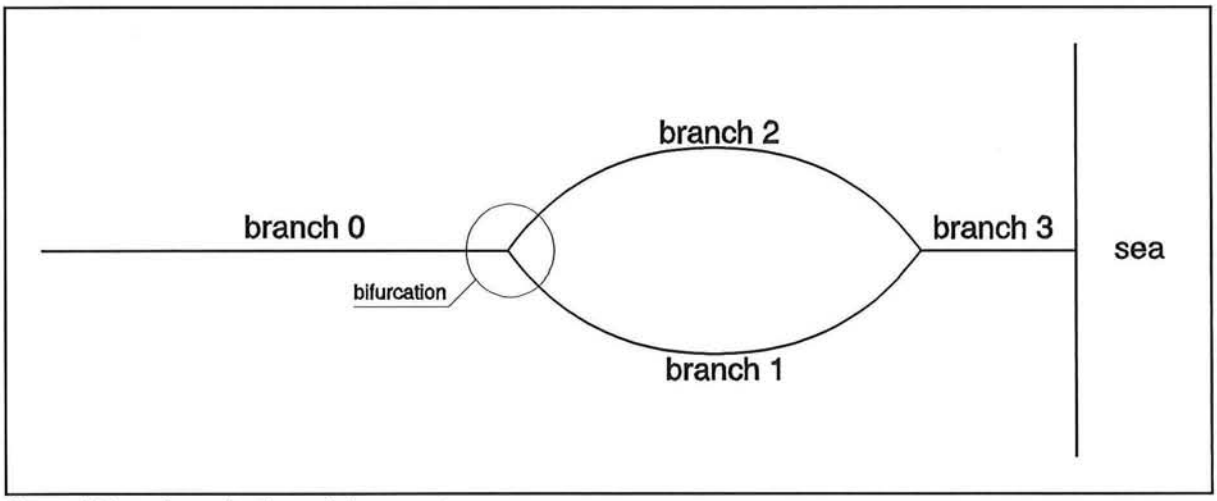

figure 4.1 - schematisation of river system

The figure represents in fact an island in a river. This schematisation is applied for the numerical computations in the following chapters as well. The mathematical analysis also holds for half an island (see Chapter 7).

4.2 Mathematical model

The main part of the mathematical analysis in this section was derived from Wang, Fokkink and Karssen (Wang et al, 1993). The basis of the analysis is formed by the following four equations:

- the momentum equation for the water movement

$$\frac{\partial u}{\partial t} + u\frac{\partial u}{\partial x} + g\frac{\partial a}{\partial x} + g\frac{\partial z_b}{\partial x} = -g\frac{u|u|}{C^2 a} \tag{4.1}$$

- the mass balance for the water movement

$$\frac{\partial a}{\partial t} + u\frac{\partial a}{\partial x} + a\frac{\partial u}{\partial x} = 0 \tag{4.2}$$

- the momentum equation for the sediment movement

$$s = f(u, \text{ parameters}) \tag{4.3}$$

which can be substituted by the power law $s = f(u) = m'u^n$ in case the transport formula is approximated (m' is a transport coefficient).

- the mass balance for the sediment movement

$$\frac{\partial z}{\partial t} + \frac{\partial s}{\partial x} = 0 \tag{4.4}$$

Considering the problem of the sediment distribution at a bifurcation a few assumptions can be made.

- the time needed for a wave caused by disturbances at the bed to travel through a downstream branch is much smaller than the morphological time scale of the system;
- the height of the bedforms is much smaller than the water depth;
- the two assumptions mentioned above implies that each of the branches can be represented by a single water depth if the processes on the morphological time scale are considered;
- the water level at the downstream boundary does not change;
- the morphological changes in the upstream river due to disturbances in the downstream branches can be neglected.

Furthermore assuming steady uniform flow and applying the simple wave model, the changes of the water depth in the branches follow now from the mass balance of sediment

$$B_i L_i \frac{\partial a_i}{\partial t} = -(S_i - S_{ie}) \tag{4.5}$$

with: B_i = width of the branch;
L_i = length of the branch;
S_i = sediment transport inflow into the branch according to the nodal-point relation;

S_{ie} = sediment transport outflow from the branch according to the transport capacity of the branch, determined by the transport formula of Engelund-Hansen (n=5).

The sediment inflow S_1 and S_2 in the respective downstream branches is determined by the nodal-point relation

$$\frac{S_1}{S_2} = \left[\frac{Q_1}{Q_2}\right]^m \left[\frac{B_1}{B_2}\right]^{1-m} \tag{4.6}$$

Combining Equation (4.5) and (4.6), the next system of differential equations expressed in a_1 and a_2 is obtained

$$\frac{\partial a_1}{\partial t} = -\frac{m' Q_0^5}{B_0^5 L_1}\left[\left(\frac{B_0}{B_1}\right)^m \frac{1}{a_0^5}\left(\frac{\beta_1 a_1^{3/2}}{\beta_1 a_1^{3/2}+\beta_2 a_2^{3/2}}\right)^m - \left(\frac{B_0}{B_1}\right)^5 \frac{1}{a_1^5}\left(\frac{\beta_1 a_1^{3/2}}{\beta_1 a_1^{3/2}+\beta_2 a_2^{3/2}}\right)^5\right] \tag{4.7}$$

$$\frac{\partial a_2}{\partial t} = -\frac{m' Q_0^5}{B_0^5 L_2}\left[\left(\frac{B_0}{B_2}\right)^m \frac{1}{a_0^5}\left(\frac{\beta_1 a_2^{3/2}}{\beta_1 a_1^{3/2}+\beta_2 a_2^{3/2}}\right)^m - \left(\frac{B_0}{B_2}\right)^5 \frac{1}{a_2^5}\left(\frac{\beta_1 a_2^{3/2}}{\beta_1 a_1^{3/2}+\beta_2 a_2^{3/2}}\right)^5\right] \tag{4.8}$$

in which: m' = transport coefficient;
m = power in the nodal-point relation;
β_j = $B_j/L_j^{1/2}$.

This system of differential equations describes the morphological behaviour of a river at a bifurcation. Although the system is too complicated to solve analytically, it is possible to gain qualitative insight in the behaviour of these equations by means of studying the nature of the *singular points*. A point (a_1, a_2) is called a singular point if both derivatives vanish. This means physically that the singular points (a_1,a_2) represent the equilibriums of the river system. They are the solutions of the equations:

$$-\frac{m'Q_0^5}{B_0^5 L_1}\left[\left(\frac{B_0}{B_1}\right)^m \frac{1}{a_0^5}\left(\frac{\beta_1 a_1^{3/2}}{\beta_1 a_1^{3/2}+\beta_2 a_2^{3/2}}\right)^m - \left(\frac{B_0}{B_1}\right)^5 \frac{1}{a_1^5}\left(\frac{\beta_1 a_1^{3/2}}{\beta_1 a_1^{3/2}+\beta_2 a_2^{3/2}}\right)^5\right] = 0 \tag{4.9}$$

$$-\frac{m'Q_0^5}{B_0^5 L_2}\left[\left(\frac{B_0}{B_2}\right)^m \frac{1}{a_0^5}\left(\frac{\beta_1 a_2^{3/2}}{\beta_1 a_1^{3/2}+\beta_2 a_2^{3/2}}\right)^m - \left(\frac{B_0}{B_2}\right)^5 \frac{1}{a_2^5}\left(\frac{\beta_1 a_2^{3/2}}{\beta_1 a_1^{3/2}+\beta_2 a_2^{3/2}}\right)^5\right] = 0 \tag{4.10}$$

Three singular points can be derived from the system of differential equations. One singular point represents an equilibrium in which both branches downstream of the bifurcation in the river are open; the other two represent the equilibrium in which one of the branches is closed. The stability of the three singular points depends on the value of m. This is shown by the following analysis of the singular points.
A system of differential equations of the form

$$\begin{bmatrix}\frac{dx}{dt}\\ \frac{dy}{dt}\end{bmatrix} = \begin{bmatrix}f(x,y)\\ g(x,y)\end{bmatrix} \tag{4.11}$$

with singular point (x_0,y_0) can be linearized locally by taking the Jacobian.

$$\begin{bmatrix}\frac{\partial x}{\partial t}\\ \frac{\partial y}{\partial t}\end{bmatrix} = \begin{bmatrix}\frac{\partial f}{\partial x}(x_0,y_0) & \frac{\partial f}{\partial y}(x_0,y_0)\\ \frac{\partial g}{\partial x}(x_0,y_0) & \frac{\partial g}{\partial y}(x_0,y_0)\end{bmatrix}\begin{bmatrix}x-x_0\\ y-y_0\end{bmatrix} = J(x_0,y_0)\begin{bmatrix}x-x_0\\ y-y_0\end{bmatrix} \tag{4.12}$$

A singular point is stable if both eigenvalues of the Jacobian matrix $J(x_0,y_0)$ have a negative real part.
First the equilibrium state with both branches open is looked at. This equilibrium is represented by the singular point (a_1,a_2) in the general case. For the simple case that $B_1 = B_2 = B_0/2$ and $L_1 = L_2$ the singular point is determined at (a_0,a_0). The Jacobian at this point (a_0,a_0) is equal to

$$\frac{m'Q^5}{32a_0^6 B_1^5 L_1}\begin{bmatrix}-\frac{3m+5}{4} & -\frac{15-3m}{4}\\ -\frac{15-3m}{4} & -\frac{3m+5}{4}\end{bmatrix} \tag{4.13}$$

The matrix in Equation (4.13) has the following eigenvalues

$$-5 \ , \ -\frac{3m-5}{2}.$$

The second eigenvalue is dependent on the value of the power m. In the case $m<5/3$, one eigenvalue is positive. The singular point at (a_0,a_0) is then a *saddle* point resulting in an unstable equilibrium (see figure 4.2). In the case $m>5/3$, both eigenvalues are negative. The singular point at (a_0,a_0) is now a *sink* representing a stable equilibrium with both branches open (see figure 4.3).

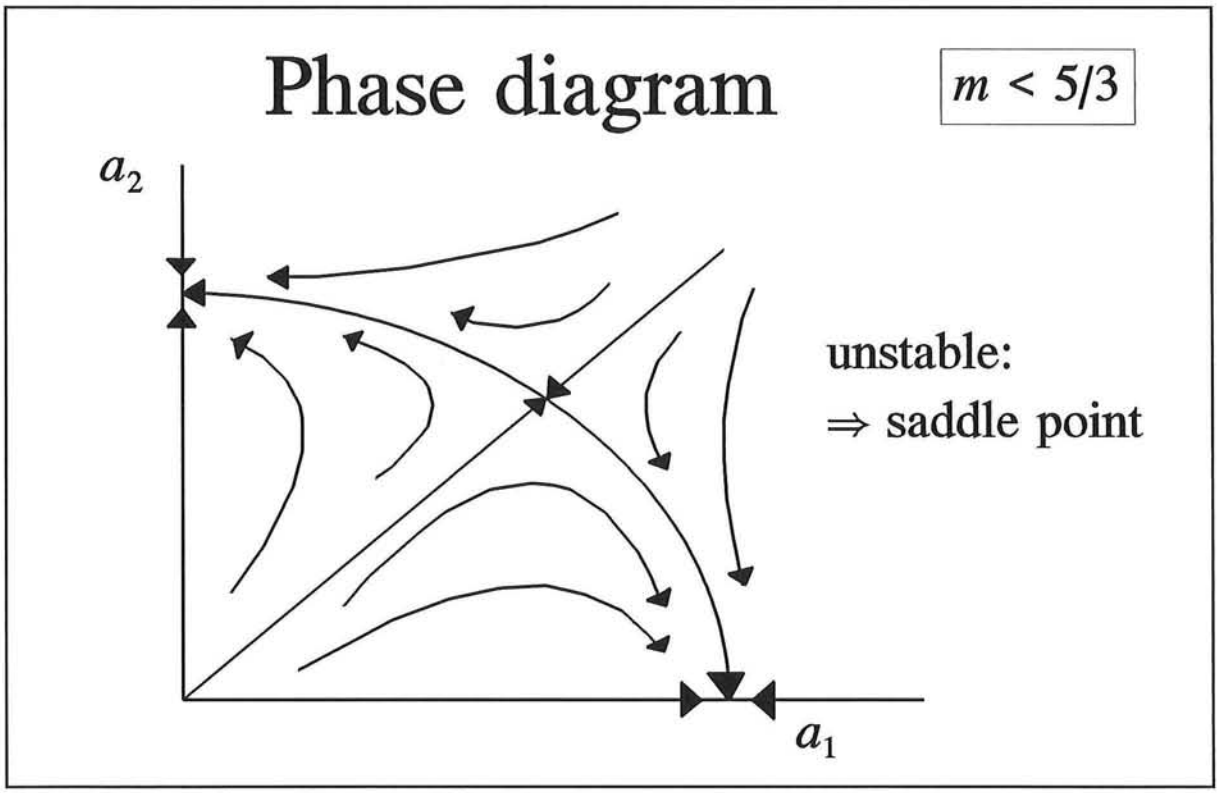

figure 4.2 - phase diagram in case $m<5/3$

The two equilibriums in which one of the branches closes and all the water and sediment goes through the remaining channel are represented by the respective singular points $(a_1,0)$ and $(0,a_2)$. The water depths can be derived from equilibrium considerations. For the simple case that $B_1 = B_2 = B_0/2$ and $L_1 = L_2$ the respective singular points are $(2^{4/5}a_0,0)$ and $(0,2^{4/5}a_0)$. Linearising these points again by taking the Jacobian, it can be shown that both equilibria are stable in case $m<5/3$ and unstable when $m>5/3$, as illustrated in figure 4.2 and figure 4.3.

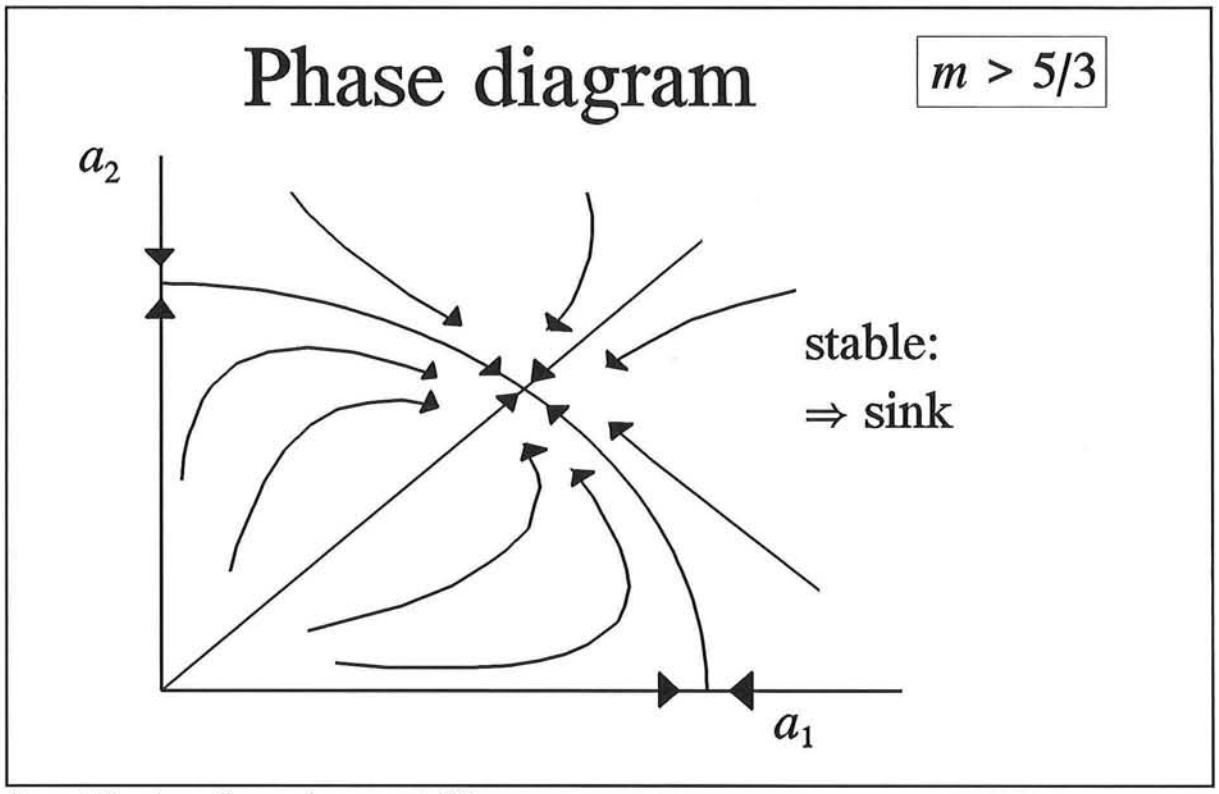

figure 4.3 - phase diagram in case $m>5/3$

Both figures are set up under the special assumption $B_1 = B_2 = B_0/2$ and $L_1 = L_2$ leading to the fact that the line $a_1 = a_2$ represents a line of saddle points and sinks, respectively. For general values of B_1, B_2, L_1 and L_2 the analysis and figures are more complicated, but they do not change qualitatively.

4.3 Conclusion

Describing a bifurcation in a river system with a mathematical model leads to three possible equilibriums: two situations in which one of the downstream branches is closed, and one equilibrium state with both branches open. The value of the power in the general nodal-point relation of Equation (3.1), (4.6) determines the stability of these equilibriums. In case $m<5/3$ the situation with two branches open is unstable; only a small disturbance is enough to close one of the branches, a stable situation. When $m>5/3$ the system always stabilises with two branches open, even when a very large disturbance is present (for example when one branch is almost closed).

Chapter 5 - Numerical computations

5.1 Introduction

As mentioned in Chapter 3, numerical computations are carried out with the computer program WENDY to verify the outcome of the theoretical analysis presented in Chapter 4. The computations complement those made by Wang et al. (1993), who considered bifurcations and simple network models under tidal flow conditions.
In this report the behaviour of an island in a *non-tidal* river is analyzed. The results of three series of simulations for three different configurations are presented in this chapter. The first set of simulations includes an island surrounded by branches with an equal width; this is referred to with the term *symmetrical case*. The second set of simulations is that of an *asymmetrical case*, where the island is surrounded by branches with different widths. The third set of simulations involves the disturbance of the system by the placement of a groyne in one of the branches.

5.2 The symmetrical case

5.2.1 Configuration

The first set of simulations involves the simple case of an island surrounded by two branches with equal width. The schematisation of the island is given in figure 5.1.
The channels are rectangular and of constant width.

Geometrical and hydraulic parameters:

L_0	=	100 km	B_0	=	100 m	i	=	0.00004
L_1	=	10 km	B_1	=	50 m	C	=	45 $m^{1/2}/s$
L_2	=	10 km	B_2	=	50 m	D_{50}	=	0.0002 m
L_3	=	10 km	B_3	=	100 m			

where L_j is the length of branch j;
B_j is the width of branch j;
i is the slope of the bed;
C is the Chézy value;
D_{50} is the grain diameter.

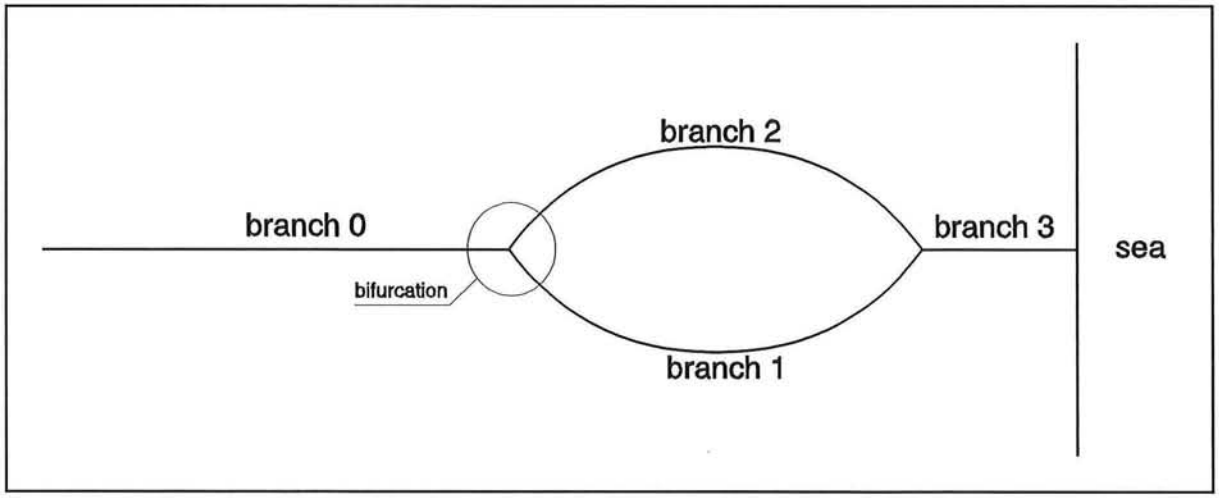

figure 5.1 - schematisation of an island in a river

The Engelund-Hansen transport formula is used, with:

- relative density $\Delta = 1.65$
- porosity $p = 0.4$

Boundary conditions:

* water	→ Q	=	500 m^3/s	(upstream)
	H	=	0 m	(downstream)
* morphology	→ S	=	0.01 m^3/s	(upstream)
	S	=	S-equilibrium	(downstream)

One internal boundary condition is needed: the general nodal-point relation (Eq. (2.4)). The theoretical analysis presented in Chapter 4, predicts that this relation leads to a stable network with open channels if m is larger than 5/3. For smaller values the theory predicts that one of the branches closes.

Disturbance of the system:

Several runs are performed for this configuration to check whether the behaviour of the model for different values of m agrees with the theory. Two values of m are tested: $m=1$ and $m=3$. For each run a disturbance in the bed level is applied, which causes overloading and/or underloading of the branches, resulting in the equilibrium situations mentioned above.

5.2.2 Simulations 1 & 2

Two simulations were done for $m=1$.

• In the first simulation no disturbance is applied to the branches of the network. The initial depths of branches 1 and 2 are the equilibrium depths. According to the theoretical analysis this results in an unstable equilibrium in which both branches remain open (see the phase diagram for $m<5/3$ in Chapter 4).

The results of the simulation are shown in figure 5.2 and figure 5.3.

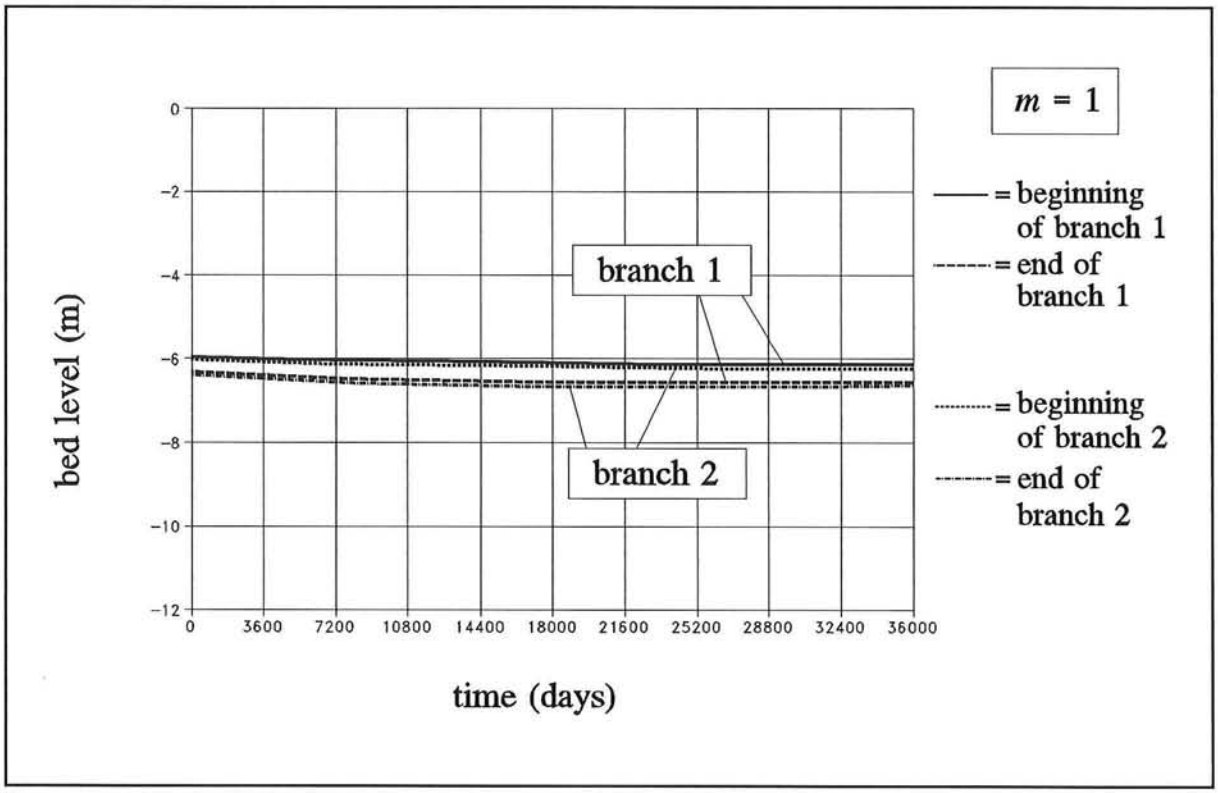

figure 5.2 - bed levels for the symmetrical case, $m=1$ and no disturbance.

In figure 5.2 the bed level in both branches stays the same so that both branches remain open. Each branch receives half of the sediment transport from the upstream branch, as shown in figure 5.3.

Thus the results match with the theoretical prediction that for $m=1$ an unstable equilibrium with both branches open is possible; it is obtained if no disturbance is applied.

• In the second simulation the same configuration is used, but here a small disturbance is applied: branch 1 is made 1 cm deeper, and branch 2 made 1 cm shallower. The theory predicts that this small disturbance is enough to result in the closure of one of the two branches, because it is a disturbance of an *unstable* equilibrium.

The results of the simulation are shown in figure 5.4 and figure 5.5.

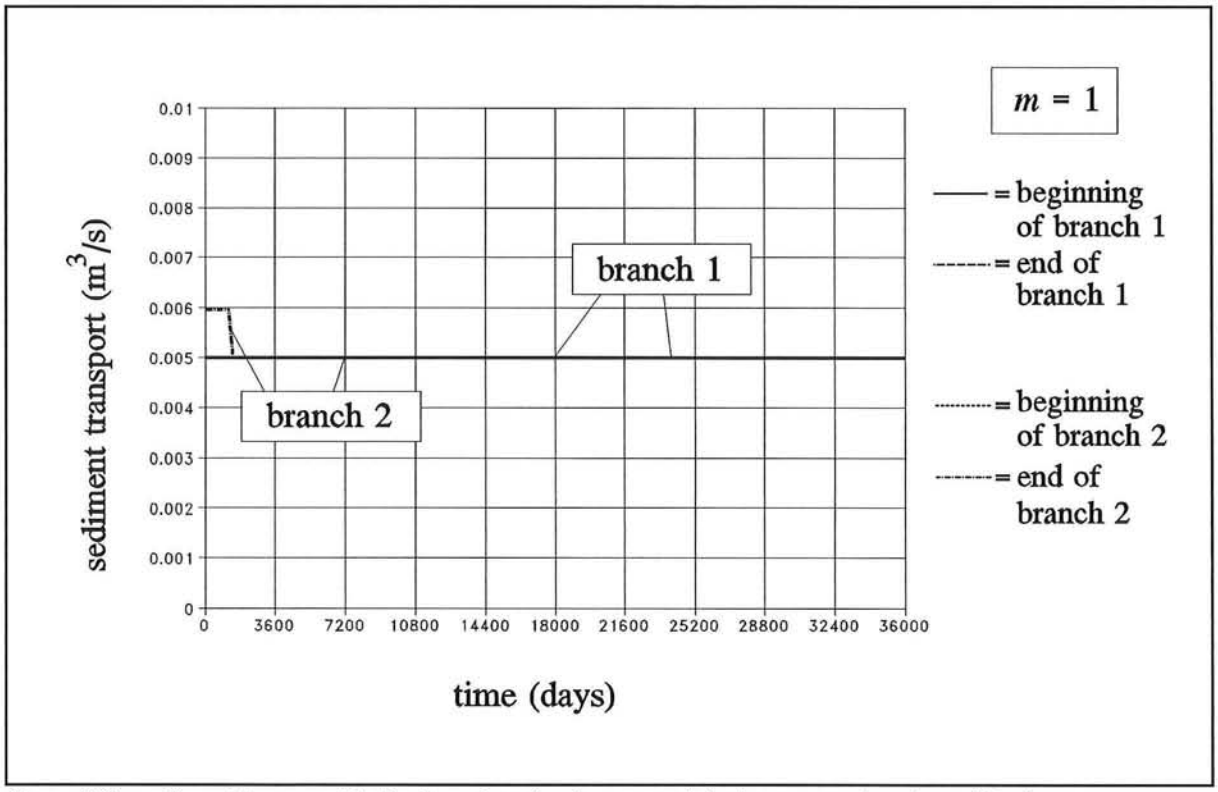

figure 5.3 - sediment transport in the branches for the symmetrical case, $m=1$ and no disturbance.

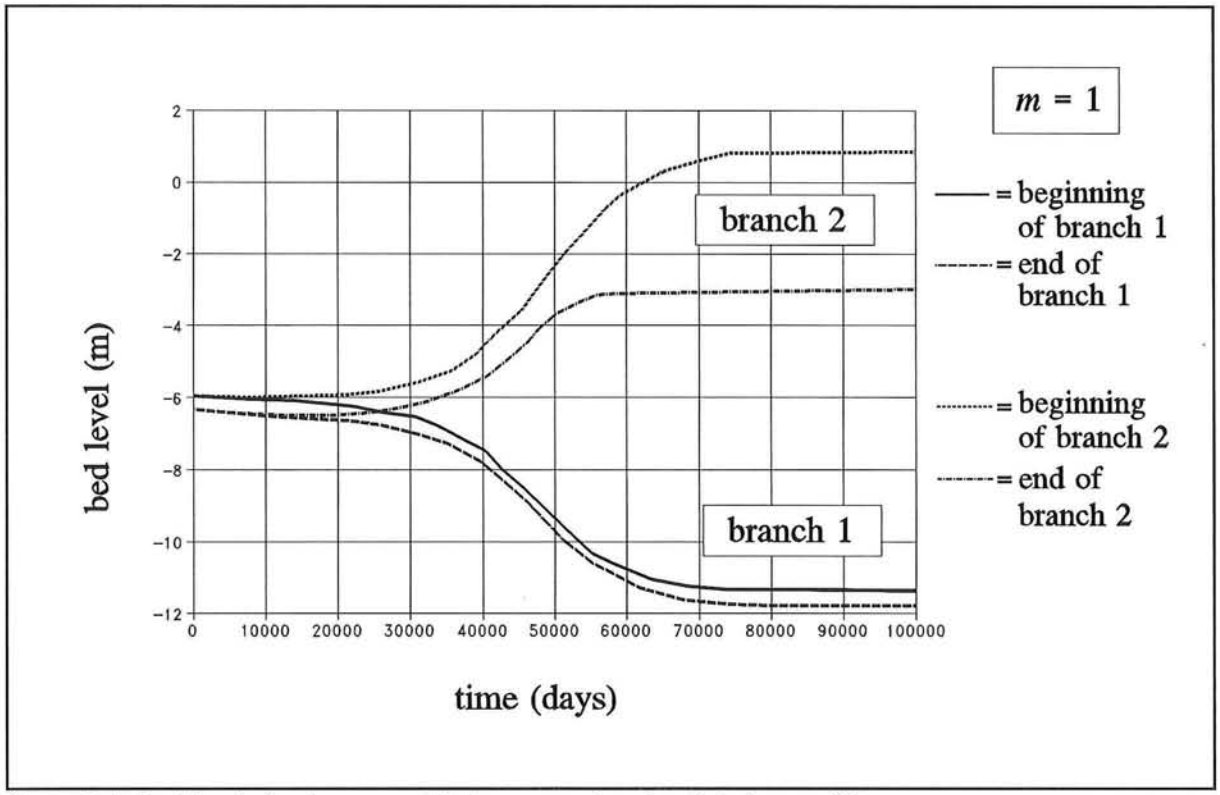

figure 5.4 - bed levels for the symmetrical case, $m=1$ and a disturbance of 2 cm.

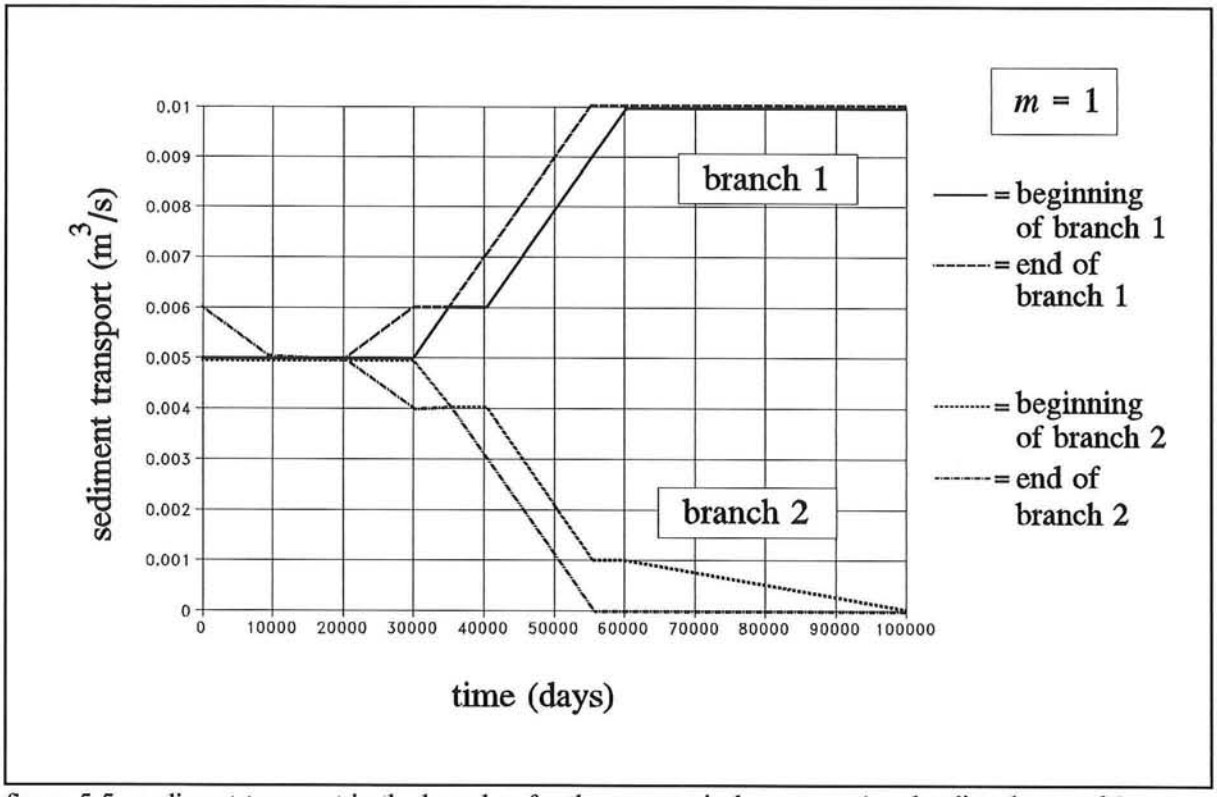

figure 5.5 - sediment transport in the branches for the symmetrical case, $m=1$ and a disturbance of 2 cm.

Both figures clearly show that the numerical results agree with the theoretical predictions. As seen in figure 5.4, the difference between the bed levels in branch 1 and 2 grows until branch 2 finally closes. At that point branch 2 no longer transports any sediment, as shown in figure 5.5; all of the sediment coming from upstream is transported through branch 1.

5.2.3 Simulation 3

The nodal-point relation is also tested for $m=3$. According to the theory this leads to a morphologically stable network with open channels, no matter what disturbance is applied. A rather large disturbance is therefore applied to the same configuration given in figure 5.1. Branch 1 is made 1 m deeper, and branch 2 made 1 m shallower.
The result shown in figure 5.6 is clearly in accordance with the predictions, because the network stabilises with both branches open. These branches are of exactly the same slope and depth.

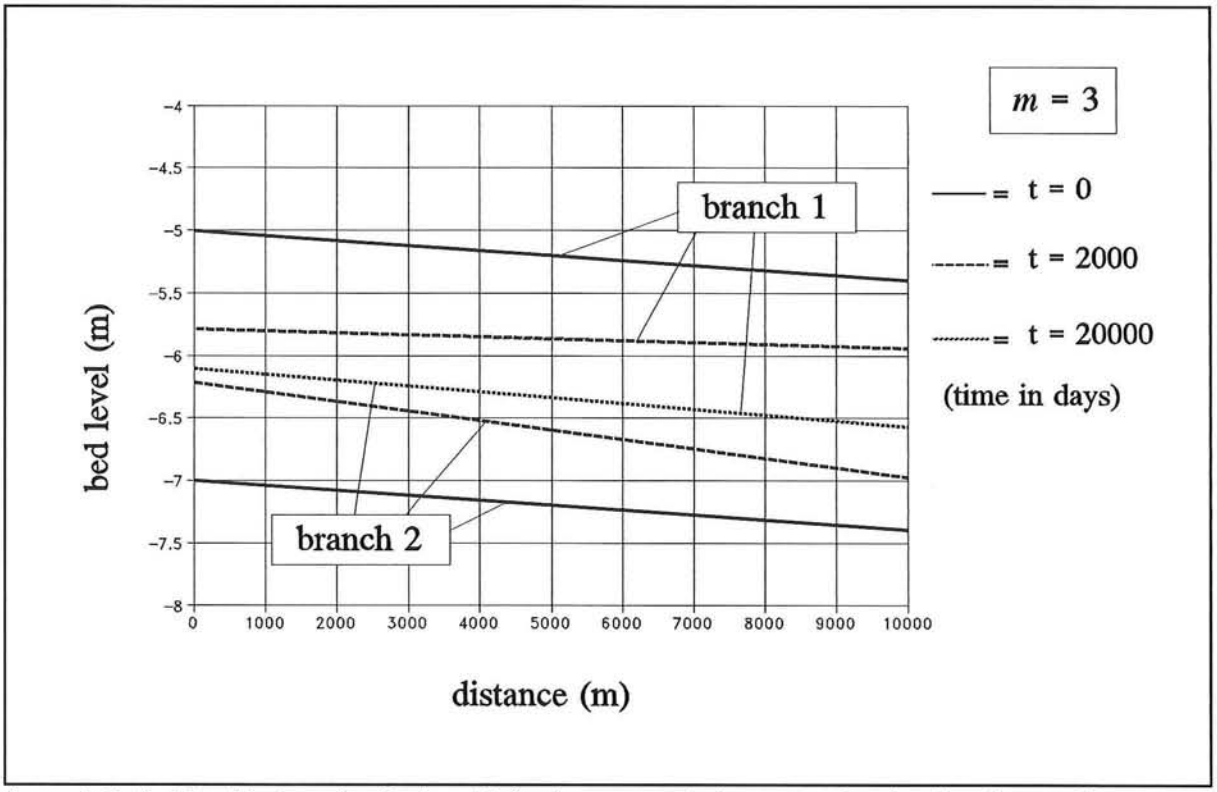

figure 5.6 - bed level in branches 0, 1 and 3 for the symmetrical case, m=3 and a disturbance of 2 m.

5.3 The asymmetrical case

5.3.1 Configuration

Just as for the symmetrical case, a set of simulations is carried out for the case of an island surrounded by two branches with different widths. The schematisation of the problem is the same as for the symmetrical case (see figure 5.1), but now the values of the widths of the branches are different.

Geometrical and hydraulic parameters:

L_0 = 100 km	B_0 = 100 m	i	= 4.10^{-5}
L_1 = 10 km	B_1 = 75 m	C	= 45 $m^{1/2}/s$
L_2 = 10 km	B_2 = 25 m	D_{50}	= 0.0002 m
L_3 = 10 km	B_3 = 100 m		

Boundary conditions:

* water	→ Q = 500 m^3/s		(upstream)
	H = 0 m		(downstream)
* morphology	→ S = 0.01 m^3/s		(upstream)
	S = S-equilibrium		(downstream)

The general nodal-point relation (Eq.(2.4)) is used as an internal boundary condition. Once again the theory predicts that one of the branches closes for $m=1$ and that for $m=3$ both branches remain open.
In this case, however, the difference in width for branch 1 and 2 results in a difference in the hydraulic radius, so that the conveyance of the two branches is not the same. The consequence is that the equilibrium depths of the branches is not the same.
Two simulations are performed for this asymmetrical configuration: for $m=1$ and $m=3$.

5.3.2 Simulation 4

This is the simulation for $m=1$. The initial depths for branches 1 and 2 are the same, just as in Simulation 1. But whereas for Simulation 1 this meant a simulation with *no* disturbance, the equal depths in this case *do* represent a "disturbance" of the system. This is because the initial values for the depths are not located in the *saddle point* of the phase diagram (see Section 4.2). As a result the theoretical analysis predicts that one of the two branches closes.
The results of the simulation are given in figure 5.7 and figure 5.8.

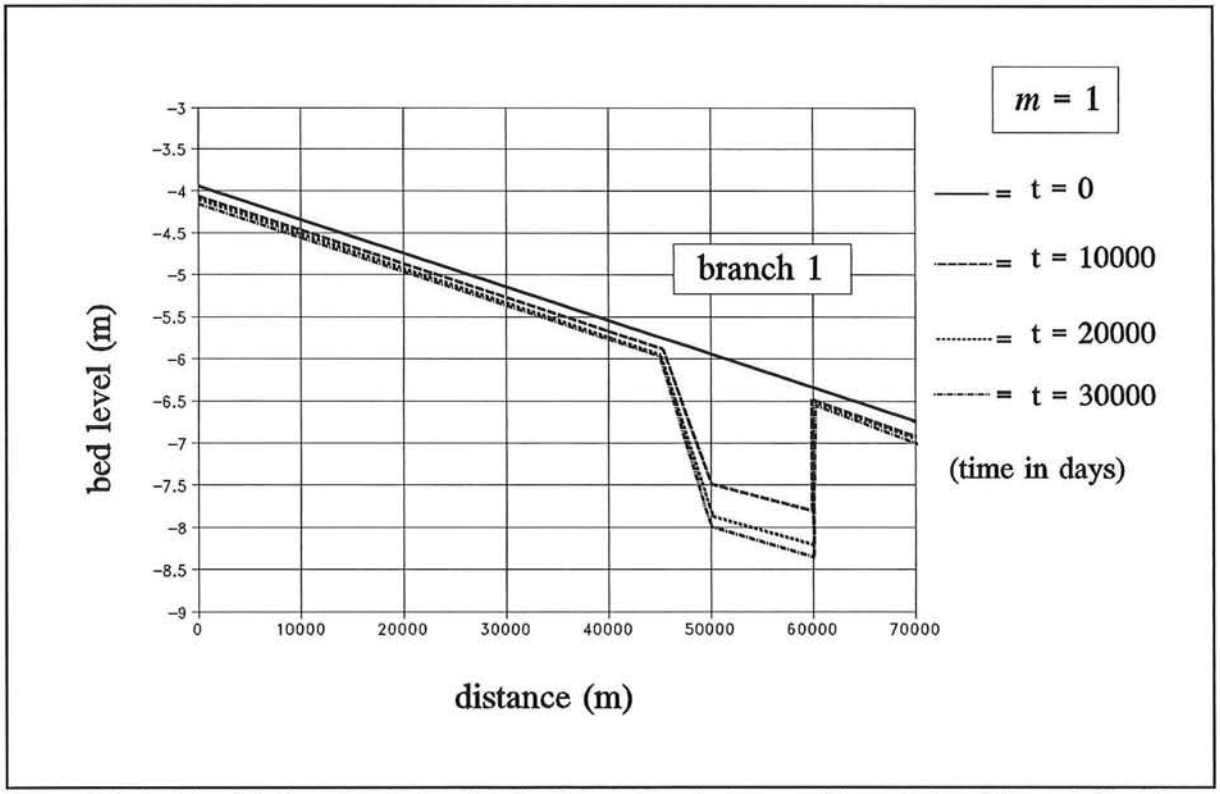

figure 5.7 - bed level in branches 0, 1 and 3 for the asymmetrical case with $m=1$, $B_1=75$ m and $B_2=25$ m.

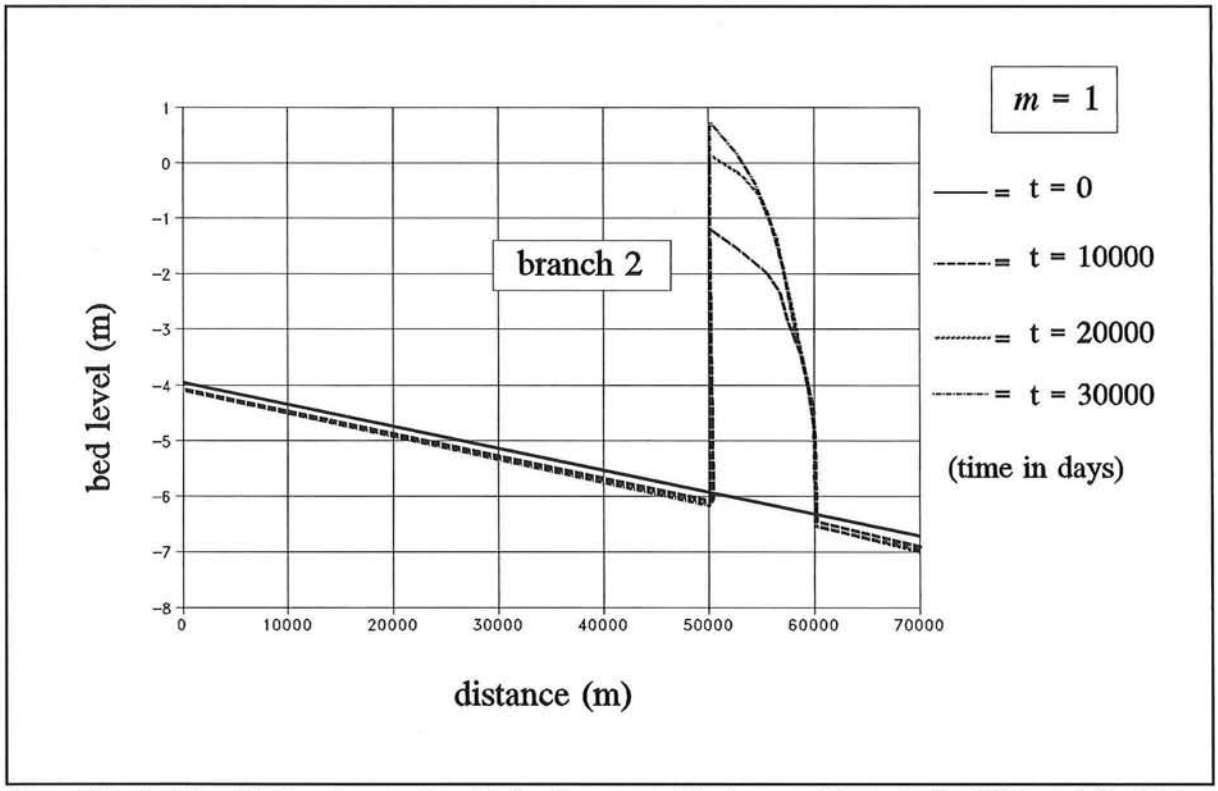

figure 5.8 - bed level in branches 0, 2 and 3 for the asymmetrical case with $m=1$, $B_1=75$ m and $B_2=25$ m.

The results shown in these figures confirm the theoretical predictions: for $m=1$ the nodal-point relation leads to the closure of one of the two branches. Moreover, because of this instability, it is clearly shown that the initial *equal* waterdepths are not located in the saddle point of the phase diagram: if so, both branches would have remained open.

5.3.3 Simulation 5

The nodal-point relation is also tested with $m=3$ for this asymmetrical case. The theory predicts that it leads to a stable network, with both branches open. The equilibrium depths are different for each branch as the widths are not equal (see also Section 5.3.1).

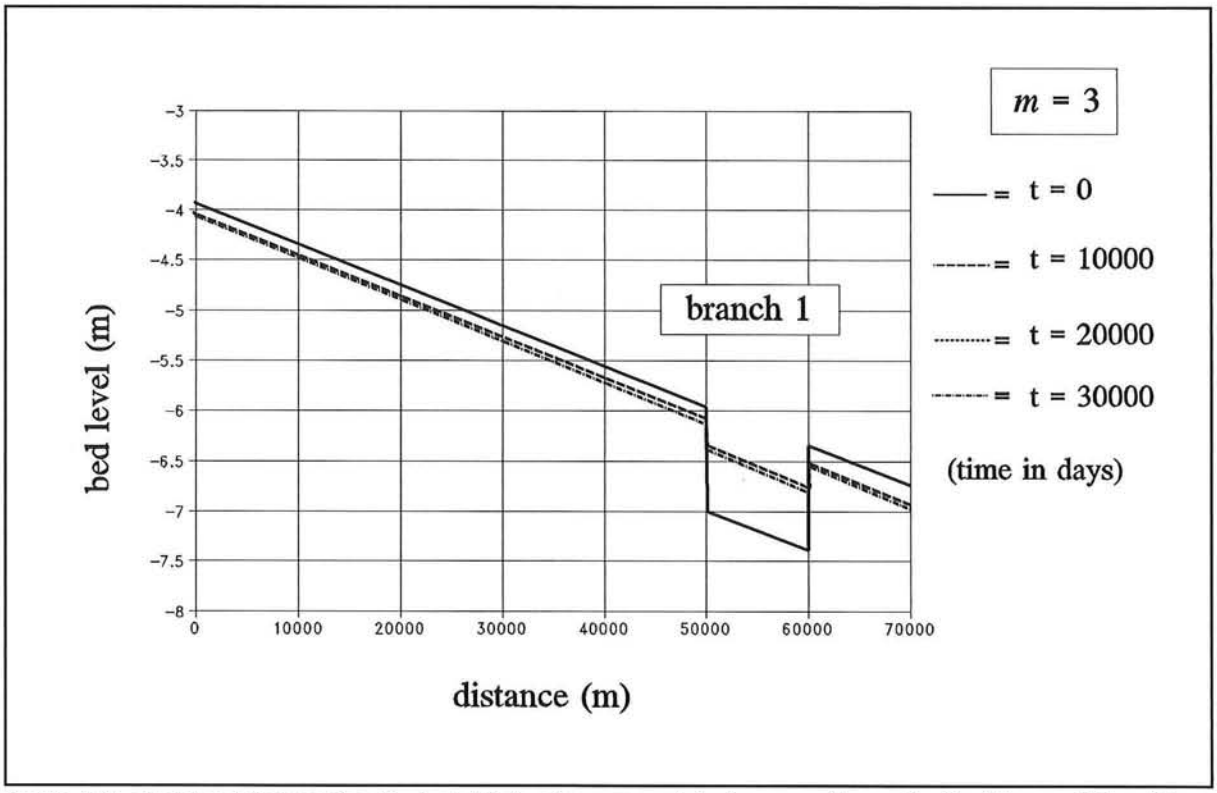

figure 5.9 - bed level in branches 0, 1 and 3 for the asymmetrical case, with m=3, B_1=75 m and B_2=25 m.

The results shown in figure 5.9 and figure 5.10 confirm these predictions: both branches stay open and the bed level in branch 1 is lower than in branch 2.

5.4 Groynes

5.4.1 Introduction

In the third set of simulations the system is disturbed by a groyne in one of the branches. This groyne is placed at different places of the branch, for both m=1 and m=3, leading to the four simulations presented below. These computations are performed to stress the fact that the stability of the nodal-point relation in a 1D-network model of an island is solely determined by the value of m. Once the value of m is fixed, the configuration of the downstream branches no longer influences the stability of the system.

5.4.2 Configuration

The configuration for these simulations is the same as for Simulation 1 (see figure 5.1). The values of the parameters are presented here once again:

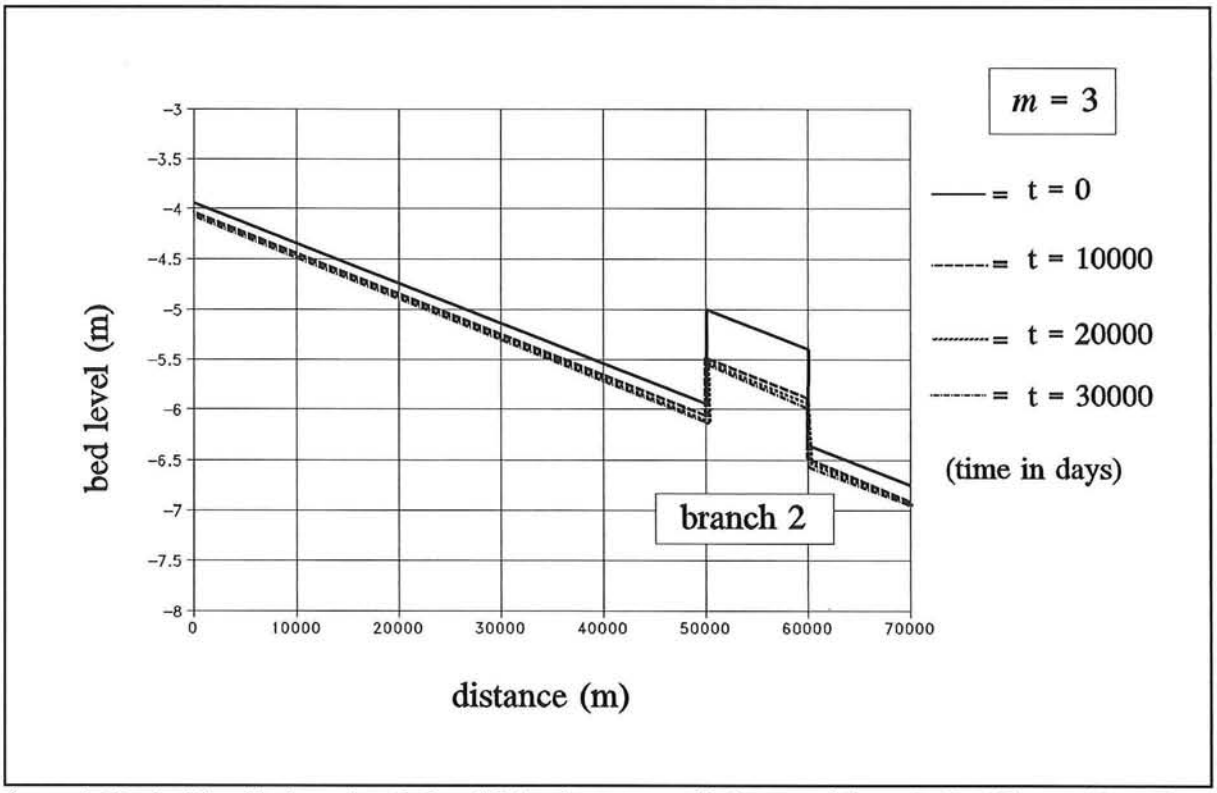

figure 5.10 - bed level in branches 0, 2 and 3 for the asymmetrical case, with m=3, B_1=75 m and B_2=25 m.

Geometrical and hydraulic parameters:

L_0	=	100 km	B_0	=	100 m	i	= 0.00004
L_1	=	10 km	B_1	=	50 m	C	= 45 m$^{1/2}$/s
L_2	=	10 km	B_2	=	50 m	D_{50}	= 0.0002 m
L_3	=	10 km	B_3	=	100 m		

Boundary conditions:

* water	→ Q =	500 m^3/s	(upstream)
	H =	0 m	(downstream)
* morphology	→ S =	0.01 m^3/s	(upstream)
	S =	S-equilibrium	(downstream)

One internal boundary condition is needed: the general nodal-point relation (Eq. (2.4)). Two sets of simulations are performed: one set with the groyne placed half-way the length of branch 1, and the other set with the groyne placed at the upstream end of the branch.

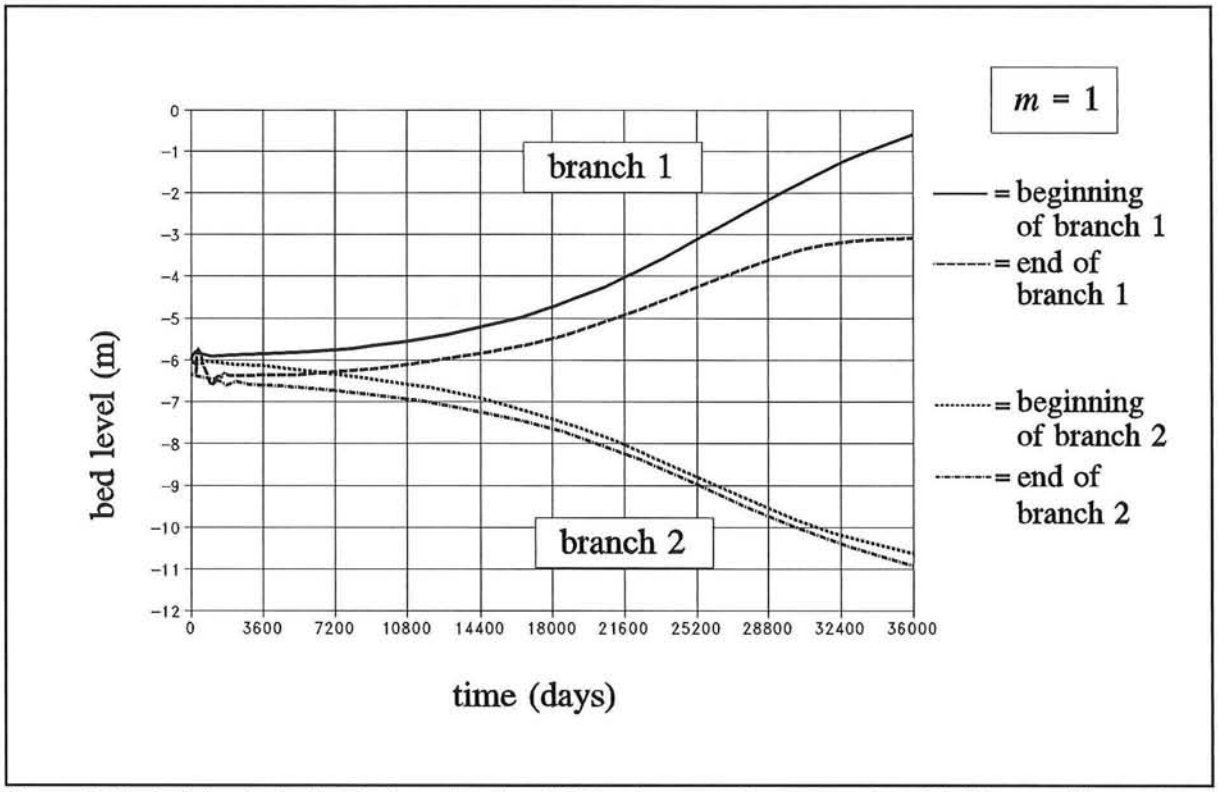

figure 5.11 - bed levels in time in branches 1 and 2 for the case of a groyne placed half-way, with m=1.

5.4.3 Simulations 6 and 7

The first two simulations with groynes have the groyne placed half-way between the beginning and end of branch 1. The groyne has a length of 25 m, so that the width of branch 1 is reduced by 50%. This "disturbance" is applied both for m=1 and m=3.

Simulation 6:

Simulation 6 is the simulation with m=1. The results presented in figure 5.11 and figure 5.12 show that the theoretical prediction of an unstable nodal-point relation resulting in the closure of one of the two branches is correct.

In figure 5.11 the bed level in branch 1 gradually rises until the branch is completely closed. This is also clearly illustrated in figure 5.12, where it can be seen that the local depression in the bed level near the groyne also gradually disappears as the bed level rises.

Simulation 7:

Simulation 7 is the simulation with m=3. Once again the results of the simulation are in complete accordance with the theoretical prediction. This is shown in figure 5.13, where it is seen that both branches remain open. The equilibrium depth for branch 1 is not exactly the same as for branch 2: the presence of the groyne reduces the conveyance of branch 1, so that its sediment transport and equilibrium depth are slightly smaller.

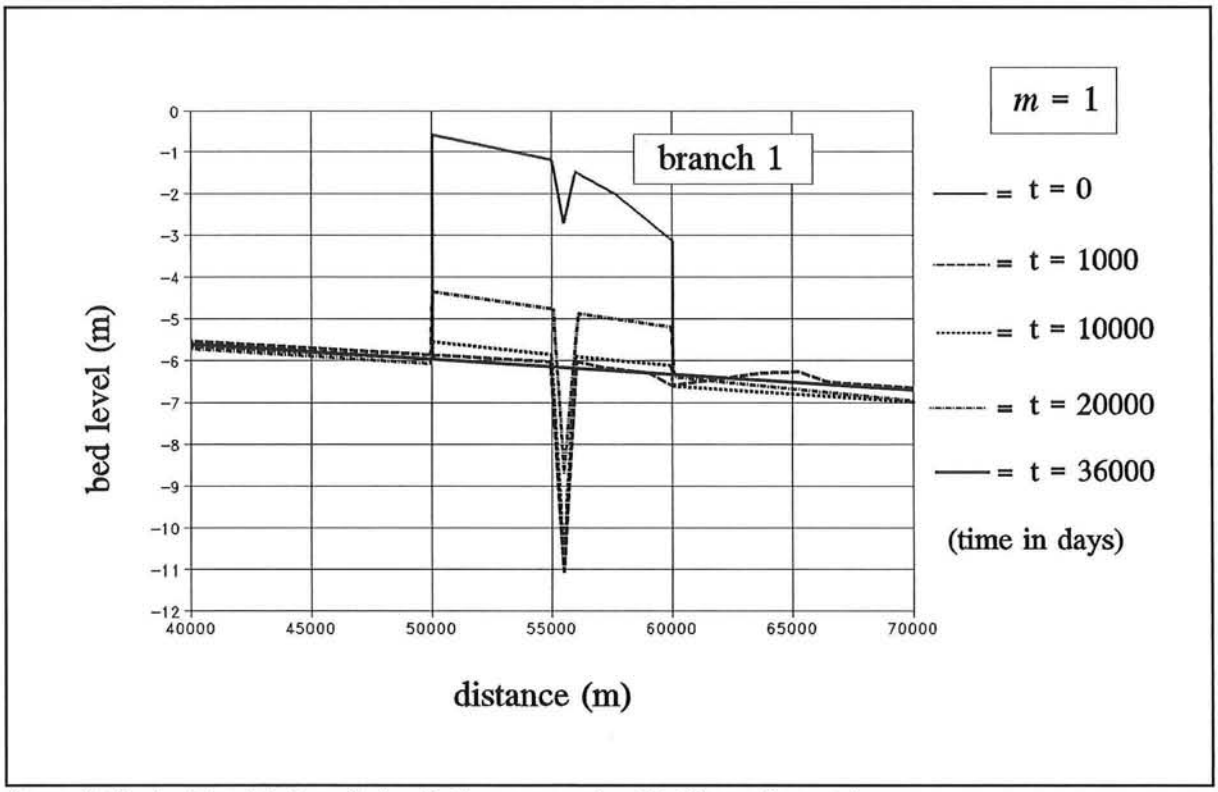

figure 5.12 - bed level in branch 1 with the groyne placed half-way for $m=1$.

From the results of Simulations 6 and 7 it can be concluded that a groyne half-way in one of the branches does not influence the behaviour of the network. It is simply another disturbance of the system, the stability of which is determined by the value of m.

5.4.4 Simulations 8 and 9

In practice the value of m will depend on the 3D geometry at and around the bifurcation. It might therefore be tempting to think that the placement of a groyne near the bifurcation at the entrance of a branch will influence the stability of the network in the 1D model. However, the flaw in the train of thought is that the value of m is an *input parameter* for a simulation, and will stay *constant* during a run. So a groyne at the entrance of one of the branches has no effect on the stability of the network, just the groynes half-way (see previous section).

This is demonstrated in Simulations 8 and 9, with a groyne at the entrance of branch 1. The groyne has a length of 25 m, reducing the entrance of the branch by 50%. The result of Simulation 8, in which $m=1$, is found in figure 5.14. Simulation 9 was done for $m=3$, and its result is found in figure 5.15.

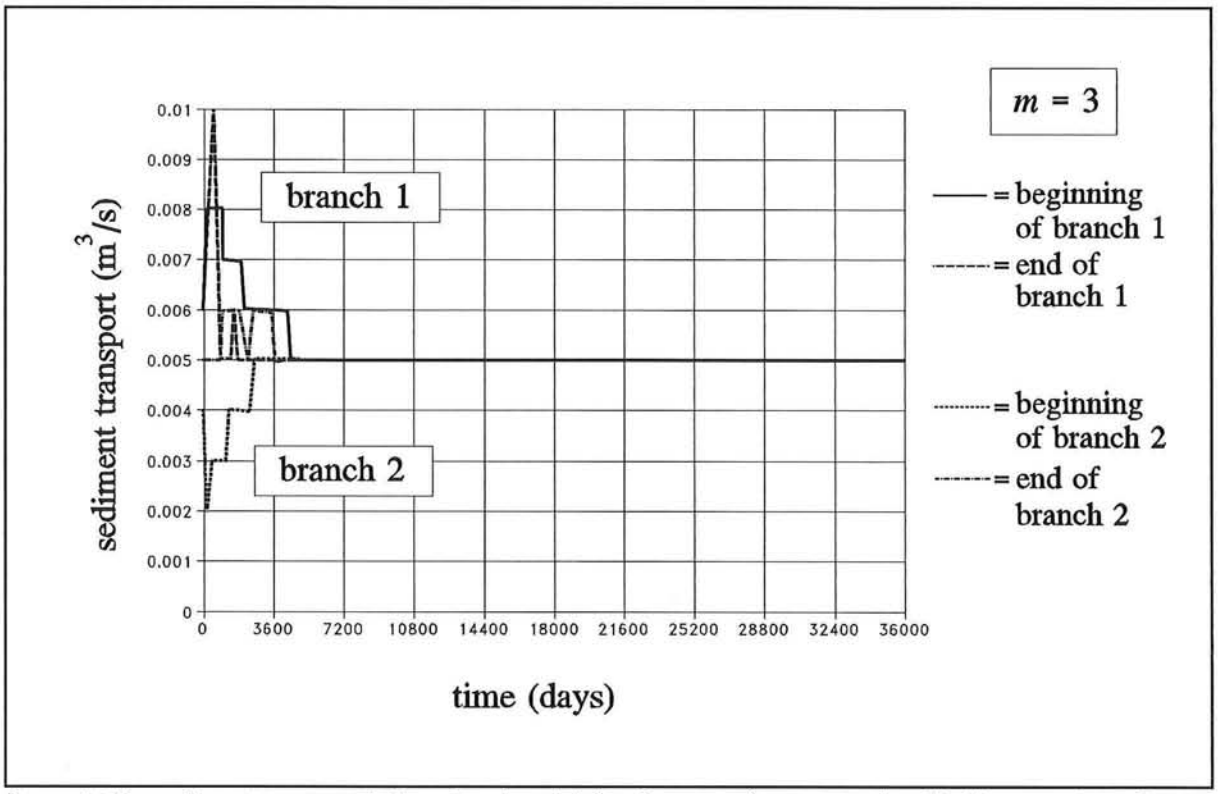

figure 5.13 - sediment transport in branches 1 and 2 for the case of a groyne placed half-way and $m=3$.

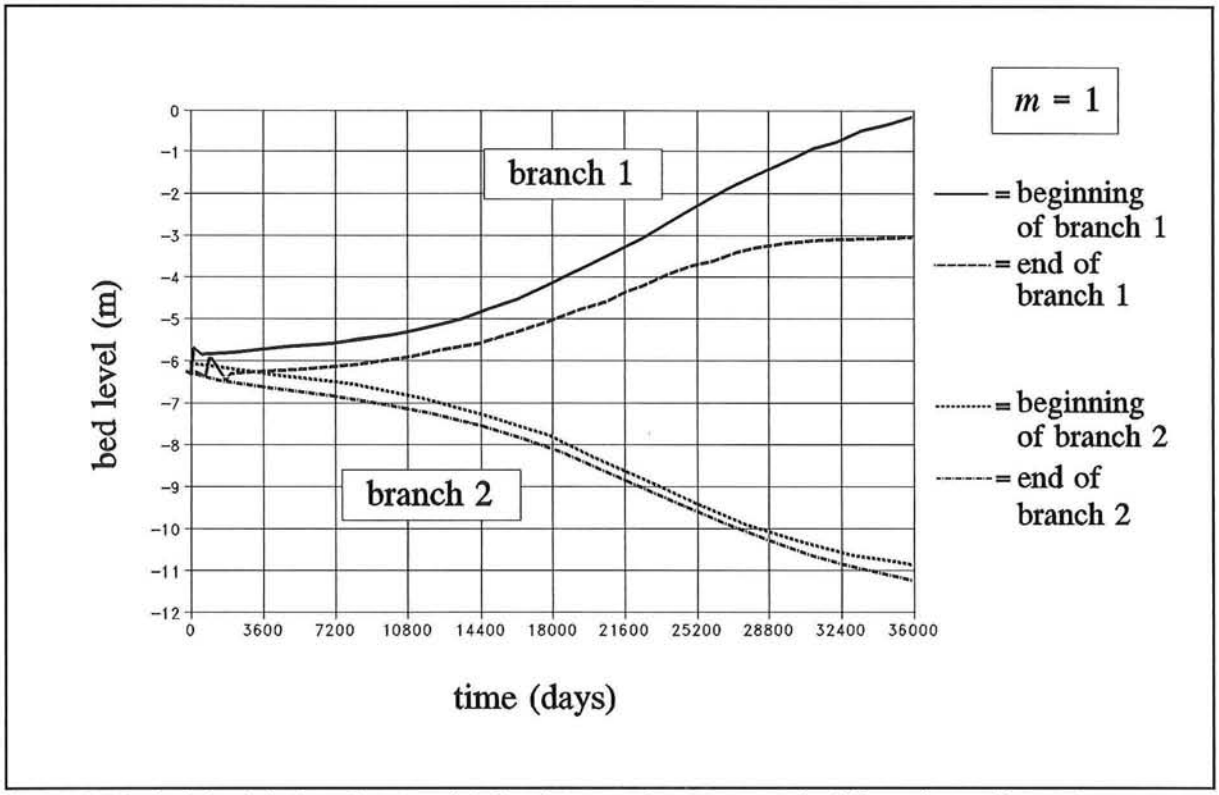

figure 5.14 - bed level in branches 1 and 2 for the case of a groyne at the bifurcation, with $m=1$.

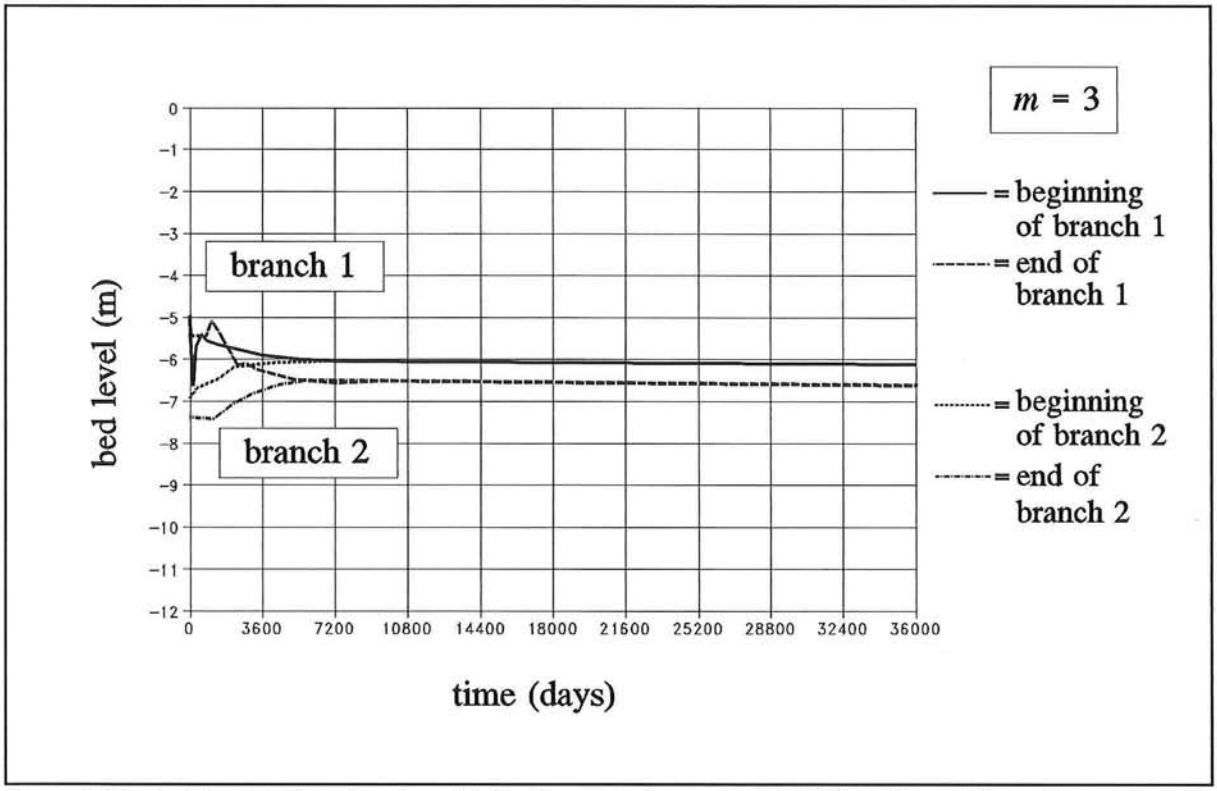

figure 5.15 - bed level in branches 1 and 2 for the case of groyne at the bifurcation, with m=3.

The figures clearly show that a groyne at the bifurcation by no means influences the stability of the branches. The groyne only acts as a disturbance of the system, so that branch 1 closes for the case of m=1 (see figure 5.14). Both branches remain open for m=3, as can be seen in figure 5.15.

The results of the simulations strongly confirm the outcome of the theoretical analysis: the stability of the nodal-point relation in the 1D-network morphodynamic model is completely determined by the value of m. A groyne, or any other type of disturbance in one of the branches, will not affect this stability. The configuration of the branches *will*, however, affect the ultimate equilibrium depths of the branches.

Chapter 6 - Influence of the power *m*

6.1 Influence on the morphological time-scale

The mathematical model, as presented in Chapter 4, has shown that the nodal-point relation plays an important role in the stability of the branches in a bifurcated river. In fact, the value of the power m in the nodal-point relation determines the behaviour of the possible equilibria of the branches downstream of a bifurcation. In other words, if $m<5/3$ the equilibrium state with both branches open is an unstable situation and the two equilibria with one channel remaining open are both stable. In case $m>5/3$ the stability of the equilibria is the opposite (see both phase diagrams in Chapter 4).
From the mathematical model additional information can be derived concerning the behaviour of the equilibrium states. Linearization of the singular points results into two eigenvalues. These eigenvalues belong to two eigenvectors. This is shown in figure 6.1 for the case with both branches open.

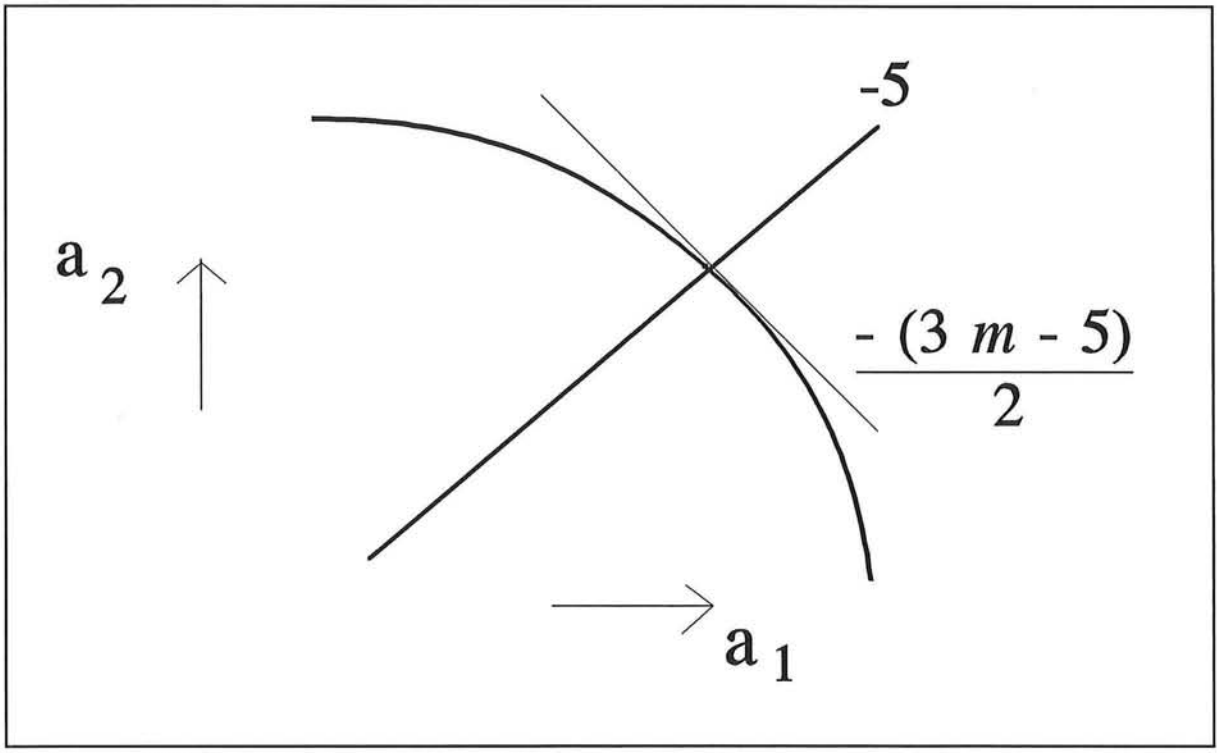

figure 6.1 - visualisation of the eigenvalues and eigenvectors

At first the figure illustrates that a deviation from the equilibrium situation either stabilises to this equilibrium or moves away from this state, dependent on the value of m. Moreover the value of m determines the time necessary to reach the final equilibrium. As m influences directly one eigenvalue, m determines the rate between attraction and repulsion. In other words, the morphological time-scale depends on the power m. The process develops faster when a larger value of m is used. For example, the final equilibrium is obtained much earlier if $m=3$ is applied instead of $m=2$.
An important aspect as well is the initial disturbance in the bed level. The influence of m increases when the deviation from the equilibrium is chosen more in the direction of the eigenvector which depends on the value of m.

This result of the mathematical model is verified by numerical computations. Various simulations are carried out and they confirm the mathematical analysis, as illustrated in the following figure where the influence of a different value of m on the morphological time-scale is visualised. For the stable case of the equilibrium with both branches open, two different values of m are applied. The difference in the bed level of the downstream branches is chosen in the direction of the eigenvector which is dependent on m.

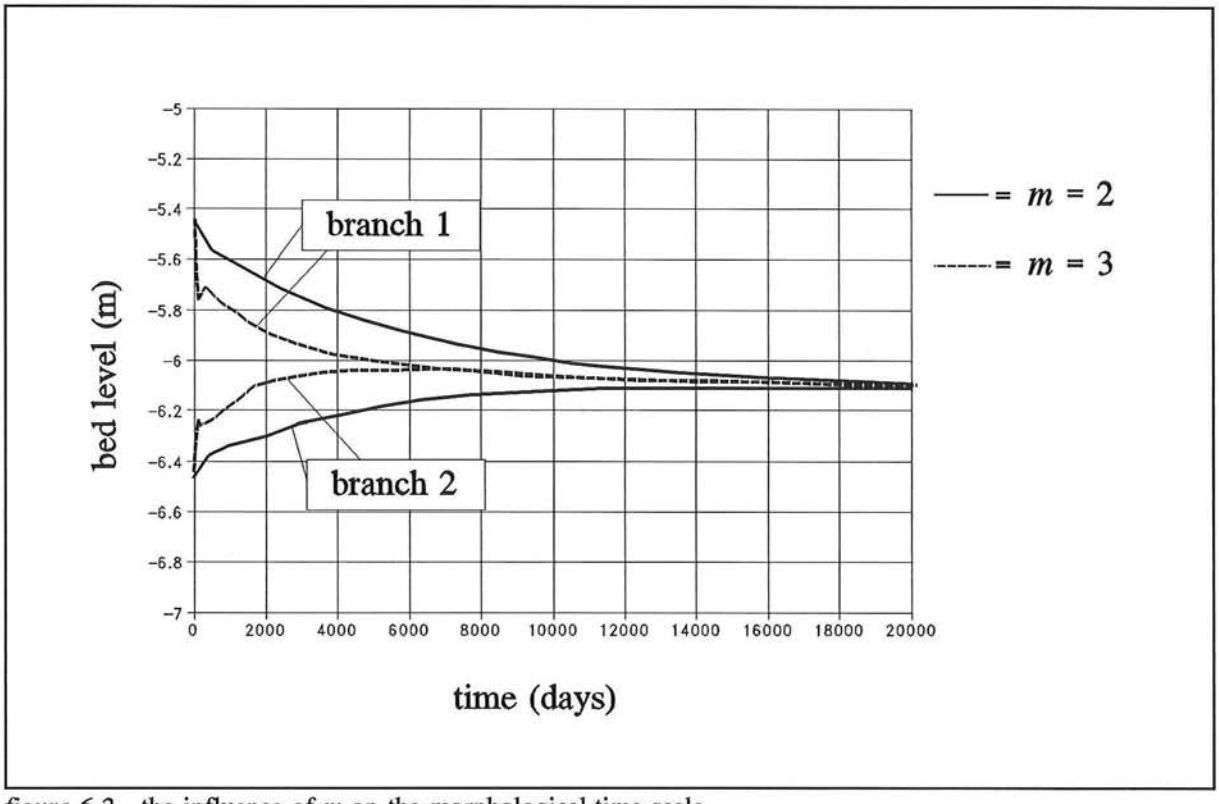

figure 6.2 - the influence of m on the morphological time-scale

From figure 6.2 it is seen that in case $m=3$, the equilibrium is reached much earlier compared to the simulation in which $m=2$ is used, just as expected from the mathematical results.

6.2 The critical value of *m*

The analytical study has shown that the transition point for either stable or unstable behaviour of the network is determined by a value of the power in the nodal-point relation of $m=5/3$. From Wang et al (1993) it can be learned that an analytical improvement is possible concerning this critical value of m.
In the mathematical model the hydraulic radius R has been approximated by the water depth a. This approximation is only valid if B is much larger than a and if the channel has smooth side walls. In fact the hydraulic radius is determined by

$$R = \frac{a}{1+2\frac{a}{B}} \tag{6.1}$$

Taking the hydraulic radius into account, steady flow is now given by

$$Q = CBa\sqrt{Ri} \tag{6.2}$$

Carrying out the analysis as in Chapter 4, the conclusion can be drawn that the critical value of m changes due to the influence of R. The network is stable if m is larger than 5. If m is in between 5/3 and 5, it can be stable or unstable. An unstable situation is reached when m is smaller than 5/3.
This result can be verified via several numerical computations. The following two figures illustrate that the critical value of m lies within 1.4 and 1.5. A small initial disturbance results in an unstable network in case of $m=1.4$ (see figure 6.3). When $m=1.5$, the network stabilises with two branches open (see figure 6.4).
The results of the mathematical model and the numerical computations are not in agreement with each other. A solution for this discrepancy is not yet found.

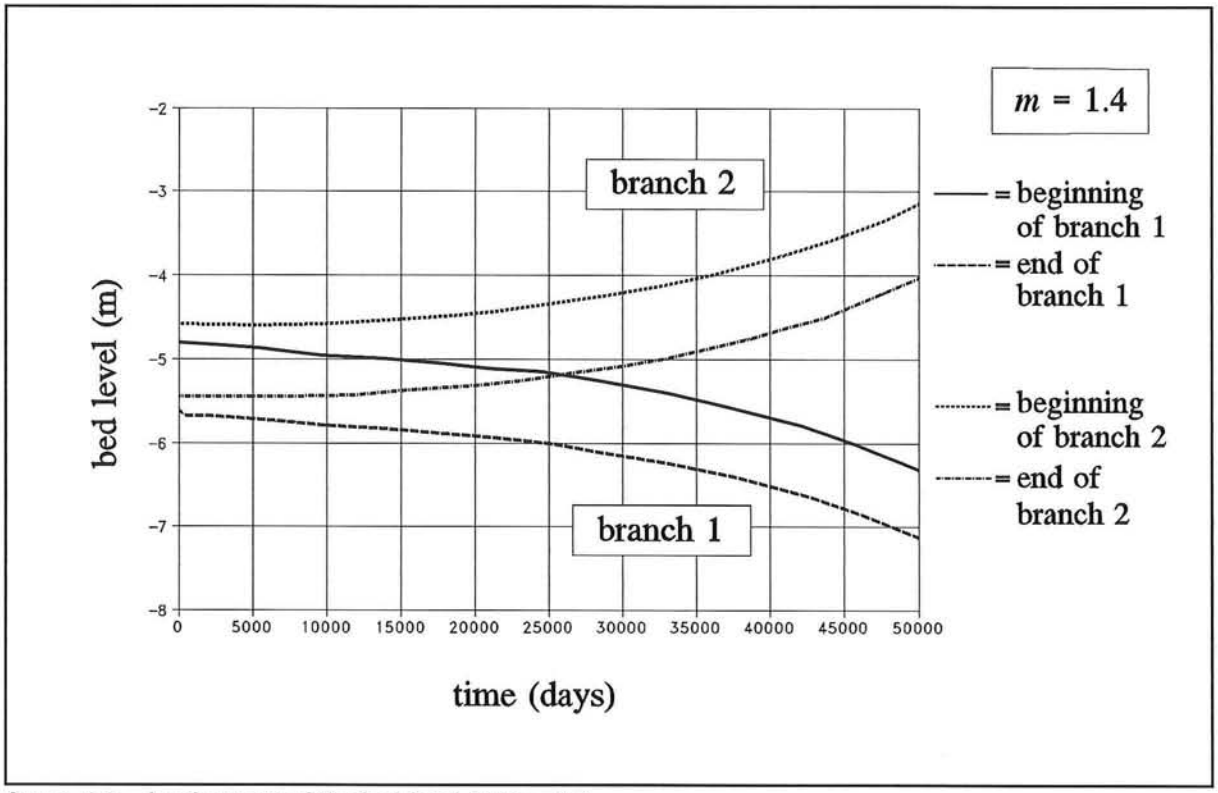

figure 6.3 - development of the bed level for $m=1.4$

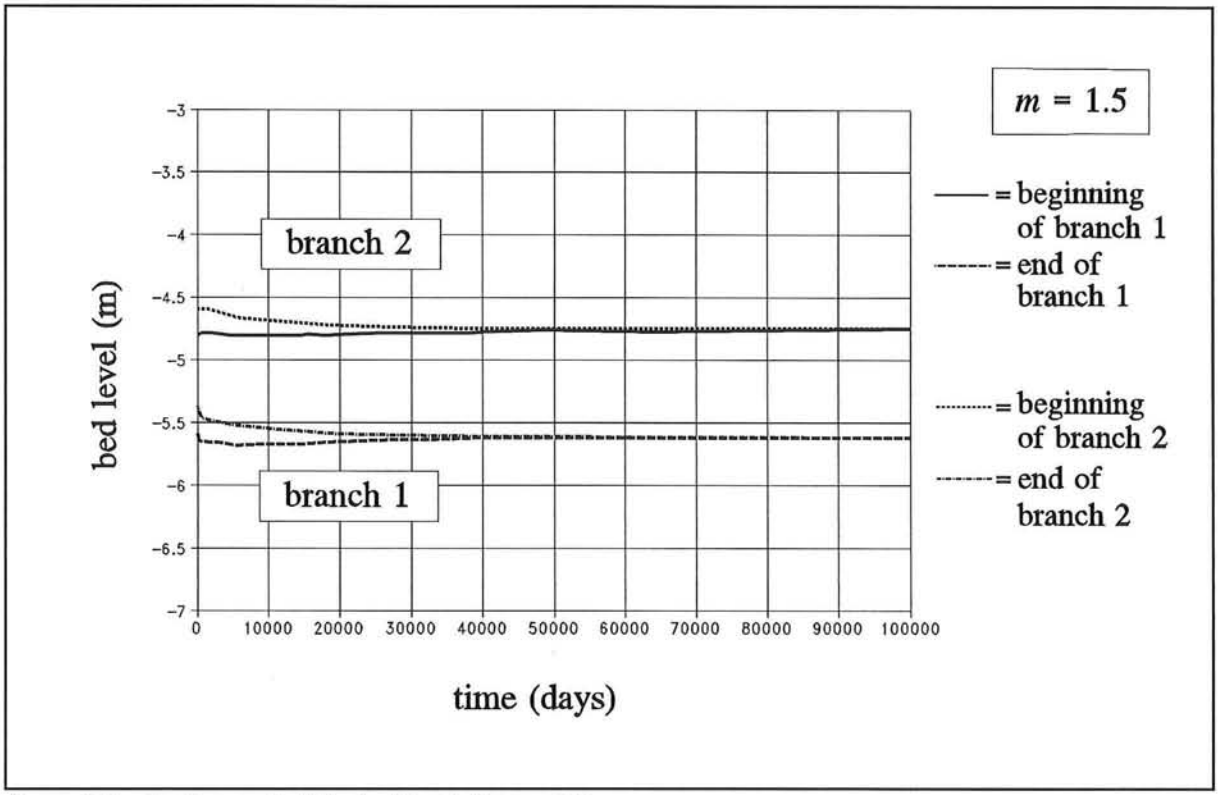

figure 6.4 - development of the bed level for $m=1.5$

Chapter 7 - Scaling, from model to prototype

7.1 Relevance

The previous chapters show that countless variations can be made concerning a river bifurcation problem. Taking the experimental model of Part III into account, a few more calculations are relevant to carry out. An interesting problem is to make the parameters of the experimental model the input for a Wendy calculation. Moreover, in the future it may be essential to compare data from experiments with numerical computations.
A problem, however, is that the experimental parameters are too small to implement in Wendy. Therefore it is necessary to enlarge the experimental model by means of scaling. Hence a *fictitious prototype* is determined from a physical model, an inverse and unconventional way. In this chapter the following terminology is followed: the experimental model is considered to be the *model* and after applying the scale relations, the writers use the term *fictitious prototype* as the parameters represent in fact not a real prototype, but only the input for a numerical computation.

7.2 Derivation of the important scale relations

By reproducing the physical processes concerning water and sediment movement, *scale relations* form the basis. Two types can be deduced:

- *scale laws* are scale relations that *must* be fulfilled as they come from equations that imply a definition, like $L = u.t$ or the Chézy-law;
- *scale conditions* are scale relations that have to be fulfilled in order to avoid scale effects.

The scale of a parameter (x) is defined by

$$n_x = \frac{x_{prototype}}{x_{model}} = \frac{x_p}{x_m} \tag{7.1}$$

There exist different scaling methods (De Vries, 1993) from which the Delft method is applied. This method is outlined below.
Analyzing the momentum equation for the water movement results in two scale conditions

$$\frac{\partial u}{\partial t} + u\frac{\partial u}{\partial x} + g\frac{\partial a}{\partial x} + g\frac{\partial z_b}{\partial x} = -g\frac{u|u|}{C^2 a} \tag{7.2}$$

Combining the second and the third term the *Froude condition* is derived

$$n_u^2 = n_a \tag{7.3}$$

From the second and the fifth term the *roughness condition* is obtained

$$n_C^2 = \frac{n_L}{n_a} = \text{distortion} = r \tag{7.4}$$

To reproduce a correct sediment movement as well, additional scale relations are present. Using the Engelund-Hansen transport formula leads to the following *transport condition*

$$n_u^5 = n_\Delta^2 n_D n_C^3 n_s \tag{7.5}$$

Desiring an equal criterium for which only bed load occurs in the model as well as in the prototype, the *bed load condition* gives the following relation

$$\left(\frac{u_*}{W}\right)_m = \left(\frac{u_*}{W}\right)_p \tag{7.6}$$

These are the scale relations that have to be fulfilled in order to avoid scale effects.

7.3 Determination of the scales

While determining the scales of all parameters a few facts have to be considered. From Wendy experiences it is learned that the length of a river schematisation should not be to small. This restricts the choice of the length scale (n_L). In case the depth scale (n_a) is chosen equal to the length scale an *undistorted* fictitious prototype is applied. Otherwise the result is a *distorted* fictitious prototype. The rate of distortion is indicated by the distortion factor r. The scale of the roughness (n_C) is now also determined by Equation (7.4)
Further on preference is given to fulfilling Equation (7.5). The scale of Δ (n_Δ) and D (n_D) can be selected freely, within a certain range. The bed load condition results in a velocity scale (n_u). Hereby the Van Rijn formula for the fall velocity is used

$$W = 10\frac{\nu}{D}\left[\left(1+\frac{0.01\Delta g D^3}{\nu^2}\right)^{0.5}-1\right] \quad , 100\ \mu m \leq D_{50} \leq 1000\ \mu m \tag{7.7}$$

as well as the following relation between the flow velocity and the shear velocity

$$u = u_* \frac{C}{\sqrt{g}} \tag{7.8}$$

Now the scale of the sediment transport (n_s) is determined via the transport condition. The derived velocity scale is called the *ideal velocity scale*. It means a deviation from the Froude condition, leading to errors in the reproduction of the water levels. These errors are usually corrected by *tilting* the scaled model according to a *sloping reference level* i_t.

$$i_t = i_p - \frac{1}{r} i_m \tag{7.9}$$

resulting in the next relation

$$i_t = \left(\frac{n_u^2}{n_C^2 n_a} - \frac{1}{r}\right) i_m \tag{7.10}$$

The sign of i_t depends on the relation n_u^2/n_a as can be seen from figure 7.1.

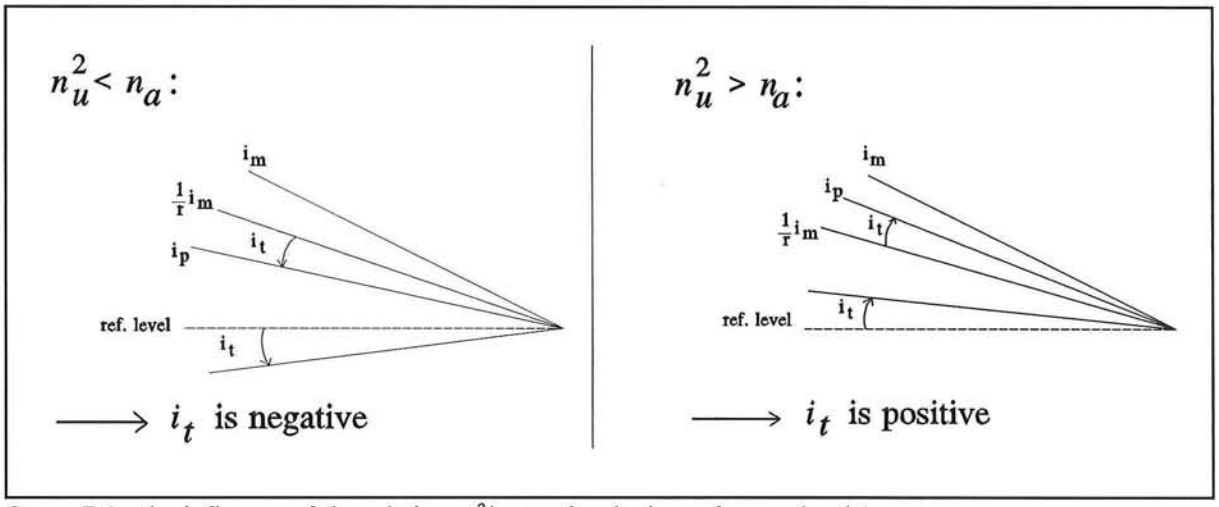

figure 7.1 - the influence of the relation n_u^2/n_a on the sloping reference level i_t

In this case of a fictitious numerical prototype, the definition of the reference level in Wendy, however, makes it impossible to implement the fictitious prototype according to the desired sloping reference level i_t. This means that afterwards the results of the computations have to be translated according to i_t.

Hereby the important scale relations are outlined. To summarize this section, the determination process of all scale parameters is given in figure 7.2.

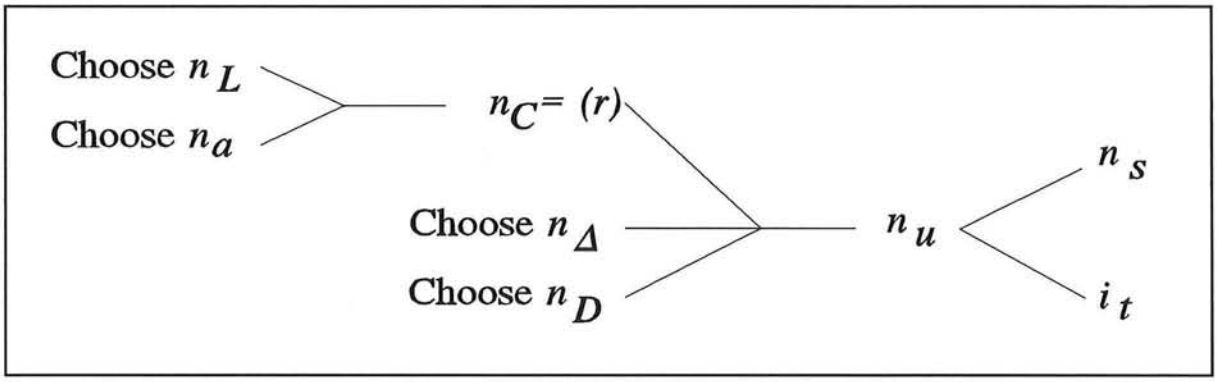

figure 7.2 - determination process of the scale parameters

7.4 Two fictitious prototype variations

7.4.1 General remarks

In this section two different fictitious prototypes are worked out. The first one is an application without distortion. The second variation shows a distorted fictitious prototype. Moreover, both examples present the two possibilities of a positive or a negative i_t.
In order to give a total view on this scaling problem, both variations have been calculated with two different values of the power m in the nodal-point relation. As in the two previous chapters, values of $m=1$ and $m=3$ are used. According to the theoretical analysis and the numerical results, these values of m lead to respectively an unstable network and a stable network.
The geometry of the experimental model is visualised by figure 7.3. Also the most important physical parameters are given (the subscript m stands for model).

The experimental parameters are:

$S_{0,m}$	$= 3.14.10^{-6}$ m^3/s	$B_{0,m}$	$= 1.00$ m
$Q_{0,m}$	$= 0.03$ m^3/s	$B_{1,m}$	$= 0.40$ m
$D_{50,m}$	$= 270$ μm	$B_{2,m}$	$= 0.60$ m
C_m	$= 30$ m^{½}/s	$L_{0,m}$	$= 4.55$ m
Δ_m	$= 1.65$	$L_{1,m}$	$= 8.60$ m
a_m	$= 0.10$ m	$L_{2,m}$	$= 8.40$ m
i_m	$= 1.10^{-4}$		

In Section 7.5 the calculations are verified and compared with each other via certain scale relations and equilibrium considerations.

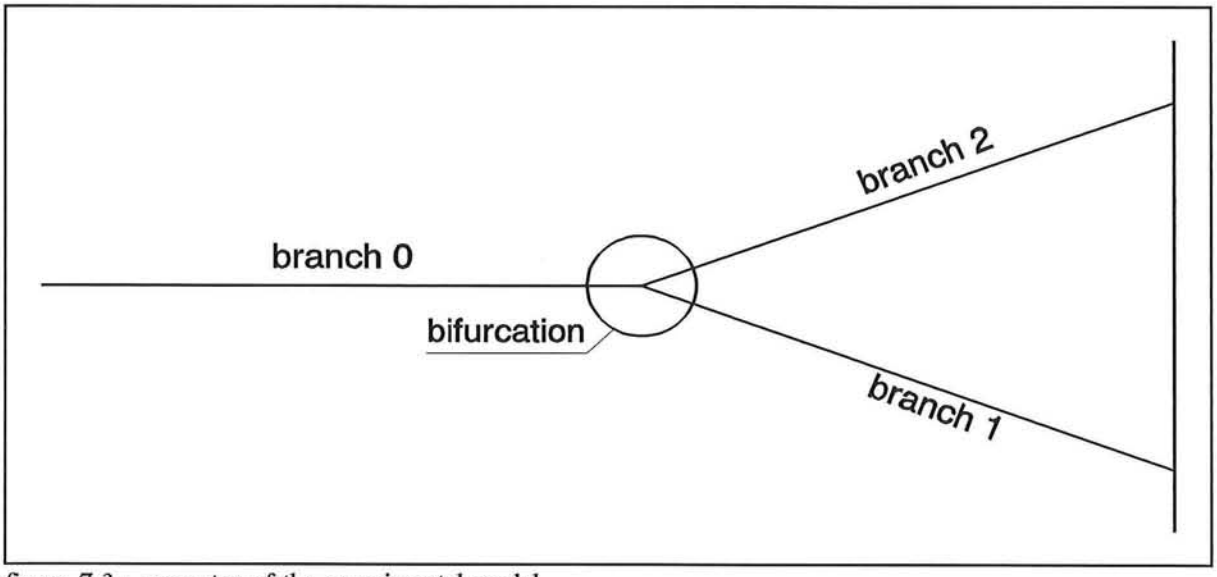

figure 7.3 - geometry of the experimental model

7.4.2 The undistorted fictitious prototype

No distortion means an identical scale of length and water depth. The scale parameters which are chosen or calculated (see figure 7.2), are:

- n_L = 1000
- n_a = 1000
- n_C = 1
- n_Δ = 2
- n_D = 3
- n_u = 3.86
- n_s = 71.4

and

- i_t = -1.10^{-3} (to be used after a computation for translating the different levels)

From these values and the experimental model parameters, the input parameters of the fictitious prototype for a Wendy calculation are derived (the subscript p stands for prototype):

- S_p = 0.23 m^3/s
- Q_p = 115800 m^3/s
- D_p = 810 μm
- C_p = 30 $m^{1/2}/s$
- Δ_p = 3.3
- a_p = 100 m
- i_p = $0.01.10^{-3}$

$B_{0,p}$ = 1000 m
$B_{1,p}$ = 400 m
$B_{2,p}$ = 600 m
$L_{0,p}$ = 4550 m
$L_{1,p}$ = 8600 m
$L_{2,p}$ = 8400 m

These input parameters are implemented in a Wendy-simulation. Three boundary conditions for the water flow are required, viz. one at the beginning of branch 0 and one at the respective end of branch 1 and branch 2. This is represented by a constant upstream discharge (Q_p) and a constant downstream water level in the sea (H = 0.00 m). The boundary condition for the sediment transport is a constant upstream supply (S_p).

First, the undistorted fictitious prototype is calculated with m=1 in the nodal-point relation. At the bifurcation, a relatively small difference in the initial bed levels of the three branches is introduced. The bed level in branch 1 is raised with 5.00 m compared to the original bed level, whereas the bed level in branch 2 is lowered with 5.00 m. The results of the calculation can be seen in figure 7.4 concerning the bed level and in figure 7.5 for the sediment transport.

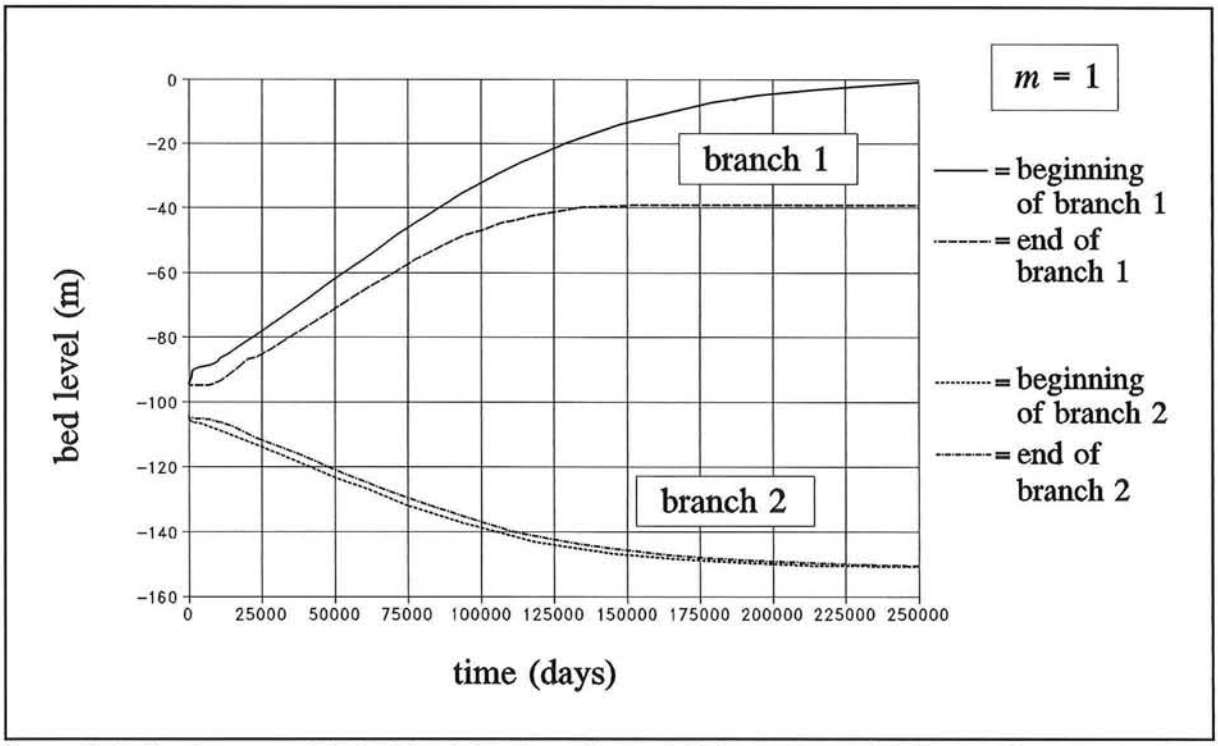

figure 7.4 - development of the bed level for the undistorted fictive prototype in the unstable case

The network of the undistorted fictitious prototype is also calculated for m=3. In this case the difference in the initial bed levels at the bifurcation is different. The bed level in branch 1 is now raised with 20.00 m and the bed level in branch 2 is lowered with 20.00 m. The outcome of the calculation is presented in figure 7.6 for the bed level and in figure 7.7 for the sediment transport.

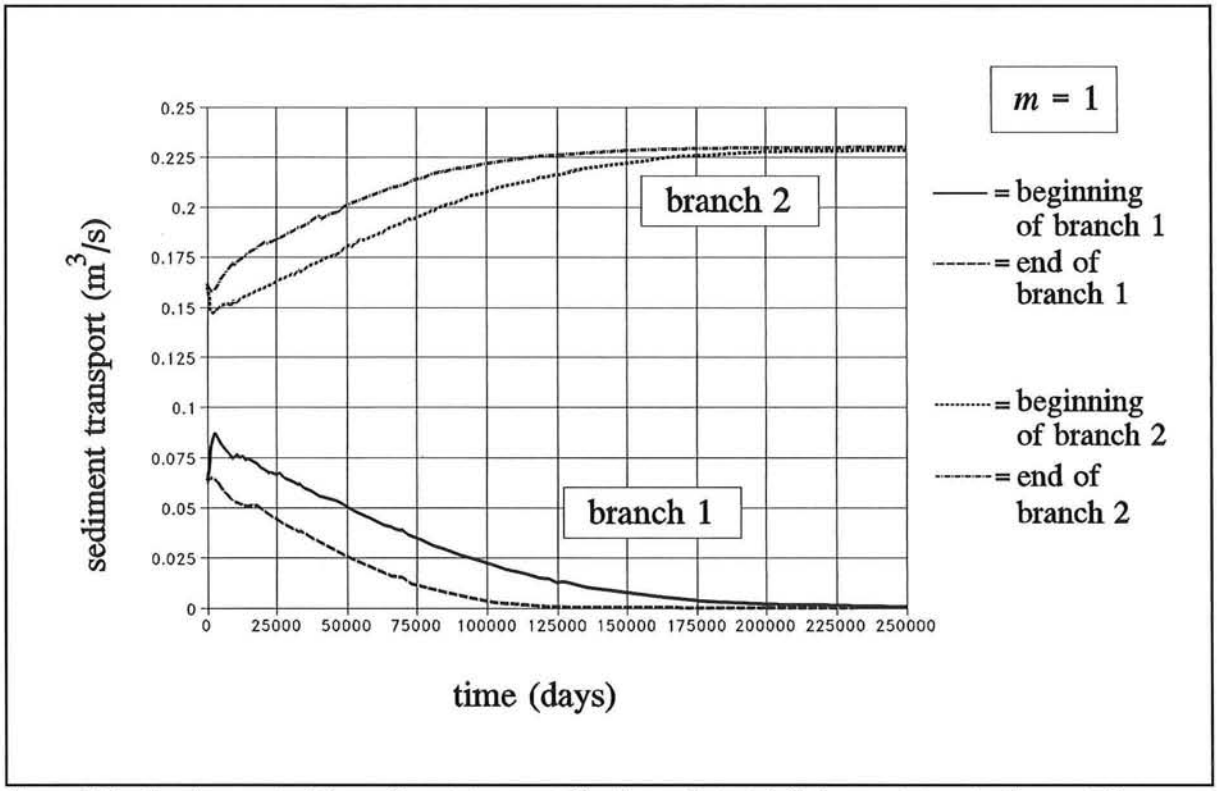

figure 7.5 - development of the sediment transport for the undistorted fictive prototype in the unstable case

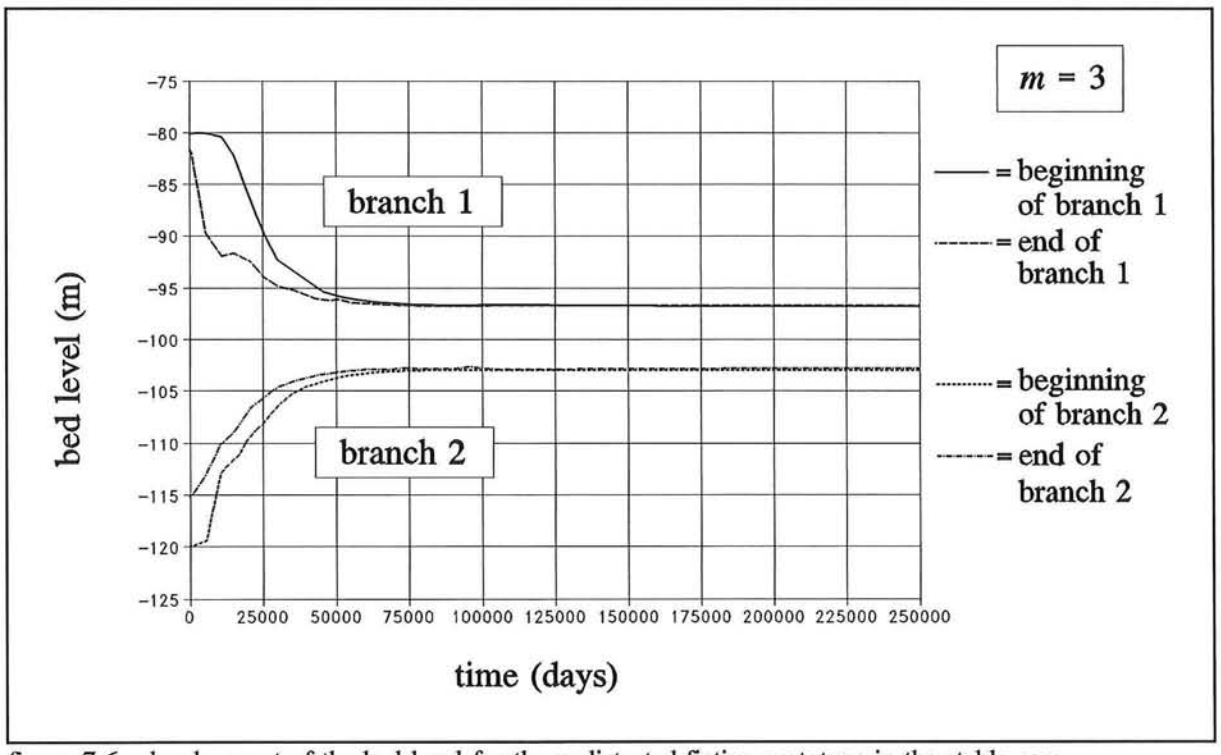

figure 7.6 - development of the bed level for the undistorted fictive prototype in the stable case

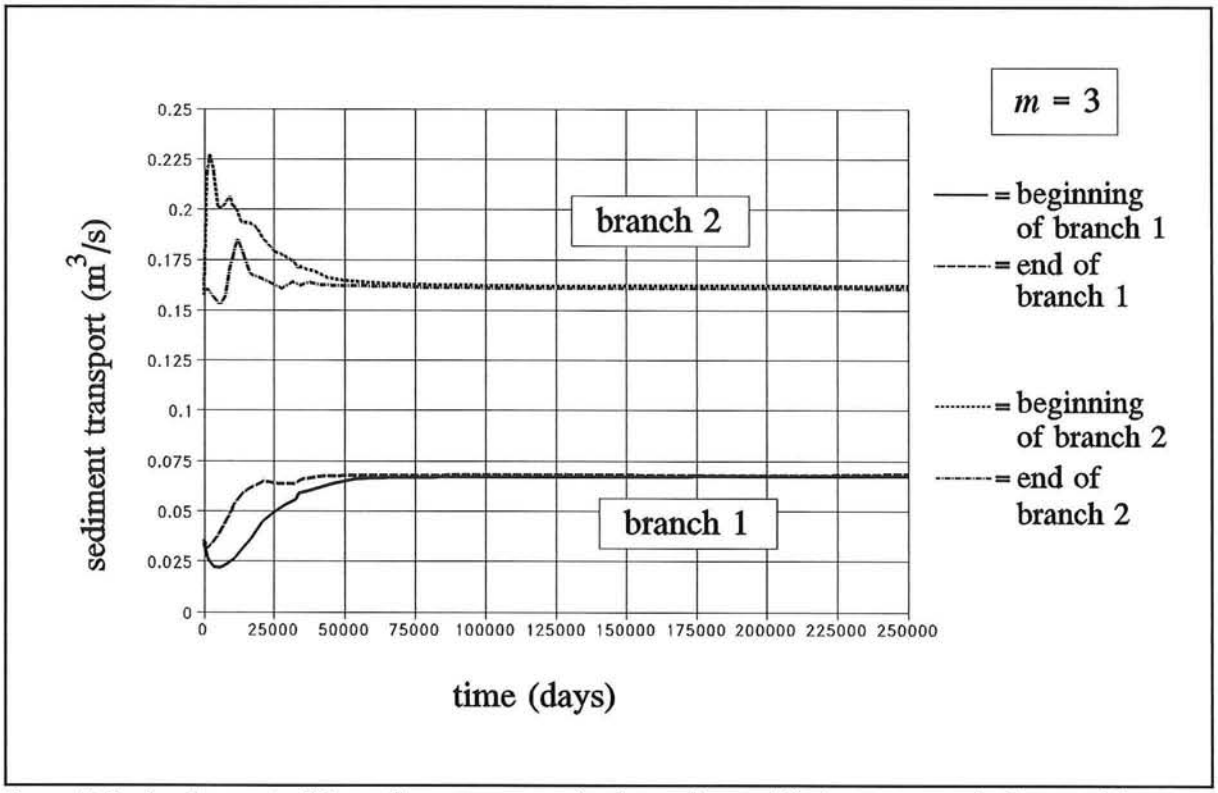

figure 7.7 - development of the sediment transport for the undistorted fictive prototype in the unstable case

Just as in Chapter 5, the results of both cases of the undistorted fictitious prototype agree with the predictions of the theoretical analysis. For $m=1$ the difference between the downstream branches grows until finally branch 1 closes and all water and sediment flows through branch 2, as clearly indicated by figure 7.4 and figure 7.5. Also the calculations for $m=3$ show expected results. The network stabilizes, both branches stay open, as demonstrated by figure 7.6 and figure 7.7.

7.4.3 The distorted fictitious prototype

In this case no identical scale for the length and water depth is chosen. The rate of distortion which is applied, is $r=10$. The scale parameters which are chosen or calculated (see figure 7.2), are:

- n_L = 1000
- n_a = 100
- n_C = 3.16
- n_Δ = 2
- n_D = 3
- n_u = 12.2
- n_s = 713.8

and

- i_t = $0.05.10^{-3}$ (to be used after a computation for translating the different levels)

The input parameters of the fictitious prototype for a Wendy calculation are now (the subscript p stands for prototype):

- S_p = 2.24 m^3/s
- Q_p = 36600 m^3/s
- D_p = 810 μm
- C_p = 94.8 $m^{1/2}/s$
- Δ_p = 3.3
- a_p = 10 m
- i_p = $0.15.10^{-3}$

$B_{0,p}$ = 1000 m
$B_{1,p}$ = 400 m
$B_{2,p}$ = 600 m
$L_{0,p}$ = 4550 m
$L_{1,p}$ = 8600 m
$L_{2,p}$ = 8400 m

Again these parameters are used as input values in a Wendy-simulation. For the four necessary boundary conditions, the same parameters are used as in case of the undistorted fictitious prototype.

First, the distorted fictitious prototype is calculated with $m=1$ in the nodal-point relation. At the bifurcation, a relatively small difference in the initial bed levels of the three branches is introduced. The bed level in branch 1 is raised with 0.50 m compared to the original bed level, whereas the bed level in branch 2 is lowered with 0.50 m. The results of the calculation can be seen in figure 7.8 concerning the bed level and in figure 7.9 for the sediment transport.

In the nodal-point relation, $m=3$ is also used. In this case the difference in the initial bed levels at the bifurcation is different from the previous calculation. The bed level in branch 1 is now raised with 2.00 m and the bed level in branch 2 is lowered with 2.00 m. The outcome of the calculation is presented in figure 7.10 for the bed level and in figure 7.11 for the sediment transport.

Again, the theoretical analysis is confirmed by the results of both calculations of the distorted fictitious prototype. For $m=1$ the difference between the downstream branches grows until finally branch 1 closes and all water and sediment flows through branch 2, as shown in figure 7.8 and figure 7.9. The calculations for $m=3$ show that the network stabilizes as expected, both branches stay open, as demonstrated by figure 7.10 and figure 7.11.

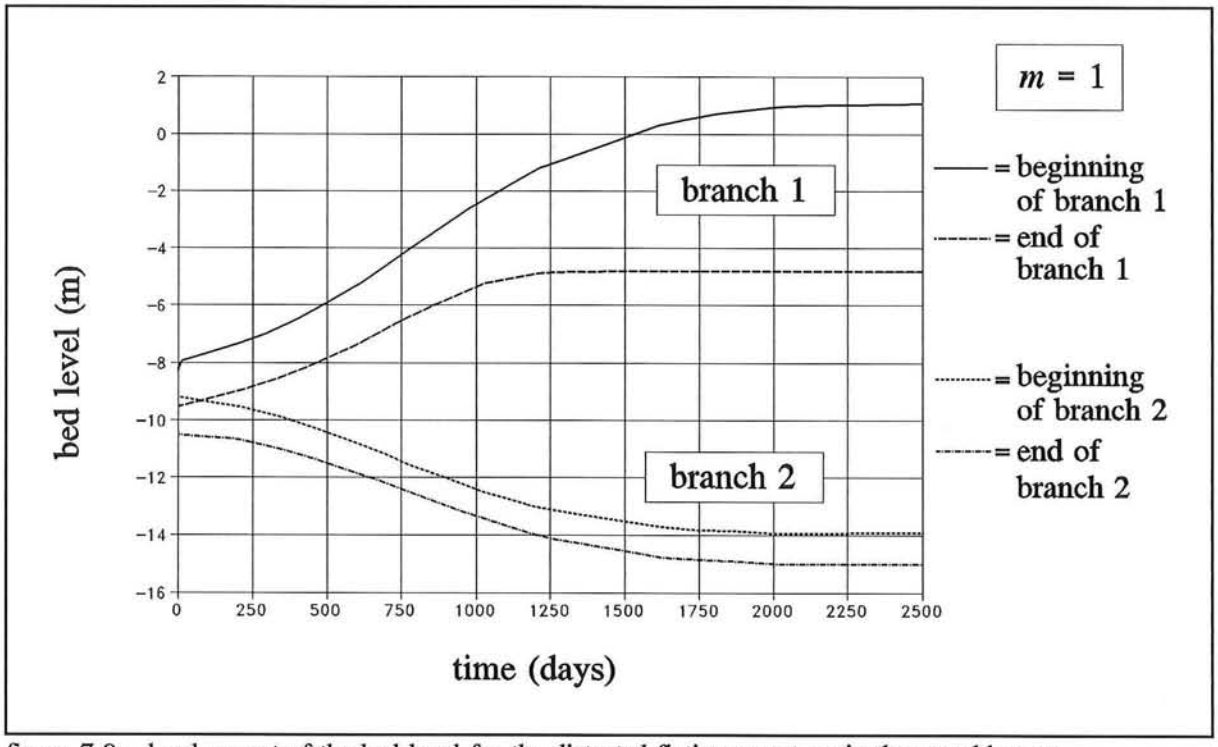

figure 7.8 - development of the bed level for the distorted fictive prototype in the unstable case

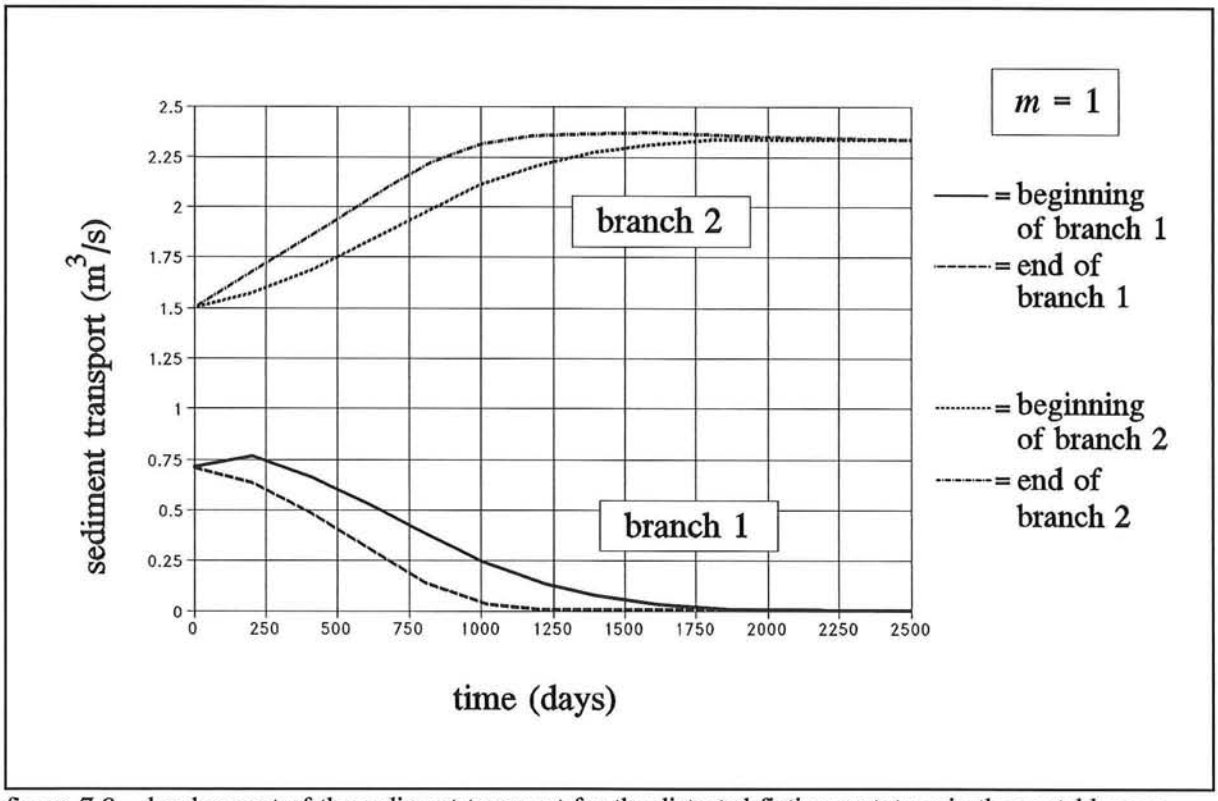

figure 7.9 - development of the sediment transport for the distorted fictive prototype in the unstable case

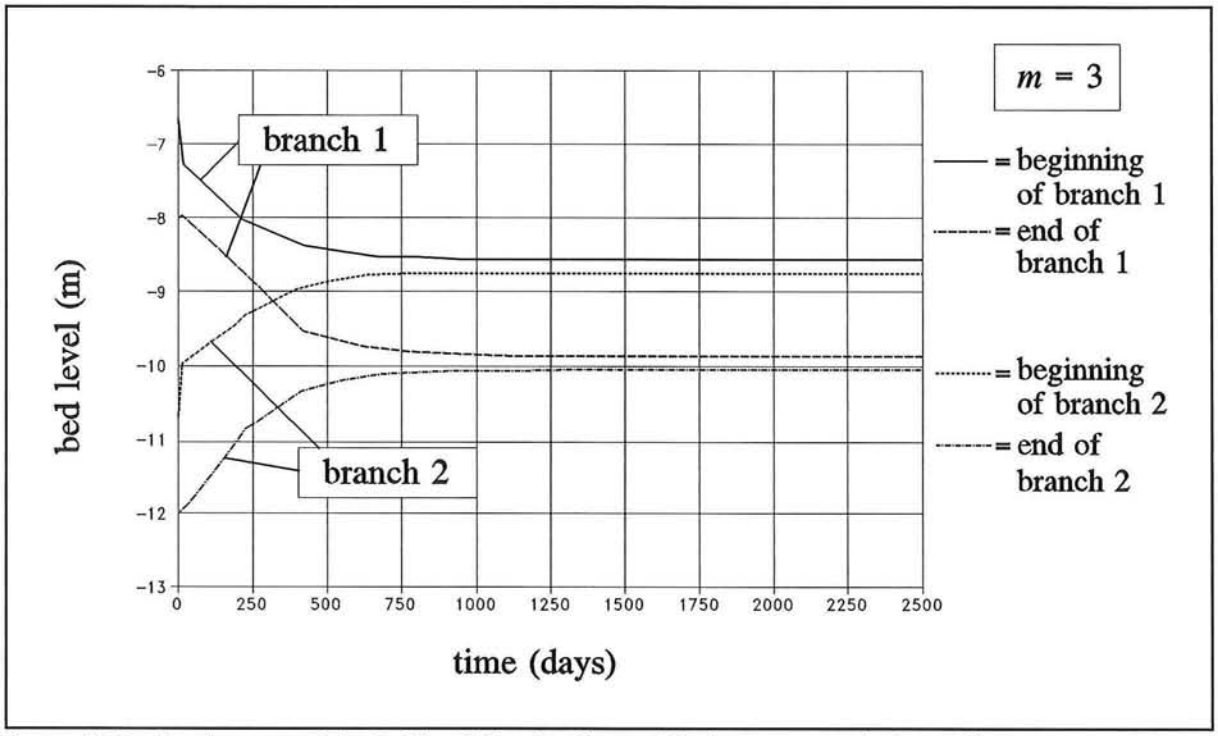

figure 7.10 - development of the bed level for the distorted fictive prototype in the stable case

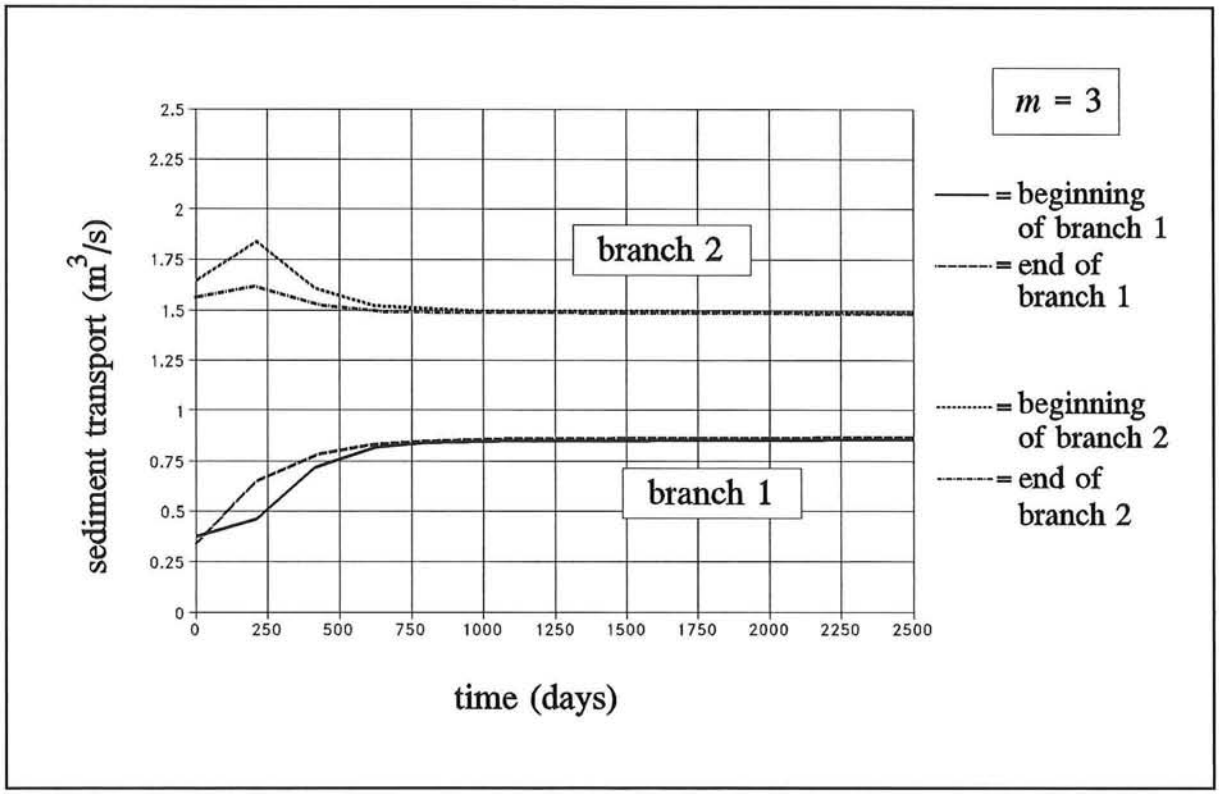

figure 7.11 - development of the sediment transport for the distorted fictive prototype in the stable case

7.5 Verification of the results

7.5.1 General

The results of the computations of both fictitious prototypes for different values of m demonstrate a good qualitative resemblance to the outcome of the theoretical analysis. In order to verify whether the scaling method and the scale relations are applied in a right way, a few specific, quantitative results have to be looked at. The check of the calculations can be divided in three elements:

- a comparison of the morphological time-scale (n_{tm}) for the two computed fictitious prototypes;
- a verification of the equilibrium depths.

These elements are described in the following sections.

7.5.2 Comparison of the morphological time-scales

The undistorted and distorted fictitious prototype can be compared with each other via the requirement for the morphological time-scale. From the continuity equation for the sediment

$$\frac{\partial a}{\partial t} + \frac{\partial s}{\partial x} = 0 \tag{7.11}$$

the morphological time-scale is deduced

$$n_{tm} = \frac{n_a n_L}{n_s} \tag{7.12}$$

Relating the morphological time-scale of both fictitious prototypes and substituting in the scales of the different parameters, the following expression is found

$$\frac{n_{tm,distorted}}{n_{tm,undistorted}} = \frac{1}{100} = 0.01 \tag{7.13}$$

The figures in the previous section show indeed a difference of a factor 100 when the time to reach an equilibrium state is considered for the undistorted and distorted fictitious prototype.

7.5.3 Verification of the equilibrium depth

Applying the value of $m=1$ in the power of the nodal-point relation leads to an unstable network. One of the downstream branches closes and the other receives all the water and sediment. The equilibrium depth of the remaining downstream branch is calculated with the formula for a long river-constriction

$$\frac{a_2}{a_0} = \left[\frac{B_0}{B_2}\right]^{\frac{n-1}{n}} \tag{7.14}$$

with $n=5$, when the Engelund-Hansen transport formula is used. The subscripts 0 and 2 are referring to the upstream branch and the open downstream branch. The equilibrium depths in case of the experimental model, the undistorted fictitious prototype and the distorted fictitious prototype are now computed. Comparing these values, the scales of the water depths for both fictitious prototypes have to be the result. This is confirmed by figure 7.4 and figure 7.8. The final equilibrium depths in the fictitious prototypes are indeed a factor 1000 and a factor 100 greater, respectively, than the values of the experimental model.

Chapter 8 - Conclusions

Since many different computations are made in this part of the report, the major results of the theoretical analysis are summarised here. This gives a clear overview of the conclusions of the theoretical study.

Stability of the network:
In continuation of the analysis made by Wang, the influence of the general nodal-point relation (Eq. (2.4)) on the stability of a 1D-network morphodynamic model is tested for the schematisation of an island in a river. Just as Wang found for the case of an estuary, the results of the computations agree very well with the predictions of the theoretical model.
The computations confirming these predictions are computations for a symmetrical case, an asymmetrical case, and a case with a groyne placed in one of the branches. The conclusion is that the stability of the network is determined by the value of m in the nodal-point relation, and not by the configuration of the downstream branches. For large values of m the bifurcation is stable (with both branches open), and for small values of m it is unstable (with one of the branches closing).
The configuration of the downstream branches (i.e. the respective widths of the branches, or the presence of a groyne etc.) does influence the equilibrium depths attained in each branch; this is due to a difference in conveyance of the respective branches.

Critical value of m:
A certain critical value for m can be assumed to exist, under or above which the system is either stable or unstable. If the hydraulic radius of a branch is taken to be equal to its depth, then the theoretical analysis leads to a critical value of $m=5/3$. If, however, the influence of the walls of the branches is large enough, then the hydraulic radius must be adjusted accordingly; the theory then leads to a critical value which is *larger* then 5/3. The computations performed with WENDY to check this prediction lead, however, to a critical value of m which is slightly *smaller* then 5/3. No direct conclusion can therefore be drawn; the problem remains unexplained, and it is thus recommended to look into this problem again.

Morphological time-scale:
The influence of the value of m on the morphological time-scale is also analyzed in the theoretical model, and the resulting predictions are once again confirmed by the numerical computations. It can therefore be concluded that, although the value of m does not influence the value of the equilibrium depths in the respective branches, it does determine the resulting morphological time-scale. The larger the m, the *faster* equilibrium is reached.

Scaling of the experimental model:
The configuration of the experimental model described in Part III of this report is used as an input for numerical computations with WENDY. This is done in order to compare data generated by the experiments with the computations made in WENDY, so that a link can be made between the analytical model and the experiments.
For the input of the configuration of the model the dimensions are scaled according to scale laws, resulting in two options (a distorted and an undistorted option) which, when put into WENDY, both agree with the theoretical predictions mentioned above.
To verify whether the scaling is done correctly, the results are checked: the morphological time-scales from the computations should be compared with the morphological time-scale observed during experimentation, and the same is done for the attained equilibrium depths. This forms the necessary link between the configurations of different experiments and the value of m (of the nodal-point relation) in the theory.

Part III

Experimental modelling

Chapter 9 - Introduction

9.1 Background

This part of the report encompasses a detailed description of the experimental test rig built in the hydraulics laboratory of the Water Resources Engineering department of the Bangladesh University of Engineering and Technology in Dhaka, Bangladesh. This test rig was built in the period of July through October 1993 within the framework of the BUET-DUT linkage project. The construction was based on a design made in the Netherlands (Den Dekker and Van Voorthuizen, 1993), which was adapted according to the local requirements with the assistance of the resident-engineer M.C.L.M. van Mierlo. A detailed drawing of the test rig is given in figure 9.1.

9.2 The experimental research

An experimental model of a bifurcated river is built in the test rig; this is described in the following section. This model will be used to conduct experiments on bifurcations.
Goal of the experiments:
Within the framework of the research project as a whole (as described in the general goal in Part I) the experiments aim to analyze the stability of the different branches at a bifurcation. Specifically the experiments will aim to relate the local three-dimensional configuration of the bifurcation to the relevant parameters of the different general nodal-point relation(s) presented in Part I.

Relevance of the experiments:
In the analytical and numerical studies (as mentioned in Part II) *one-dimensional* morphodynamic models are considered. Physically the distribution of the sediment transport rates to the different branches is determined by the local *three-dimensional* phenomena. Because of their three-dimensional nature, the experiments may present a valuable complement to the existing analytical studies.

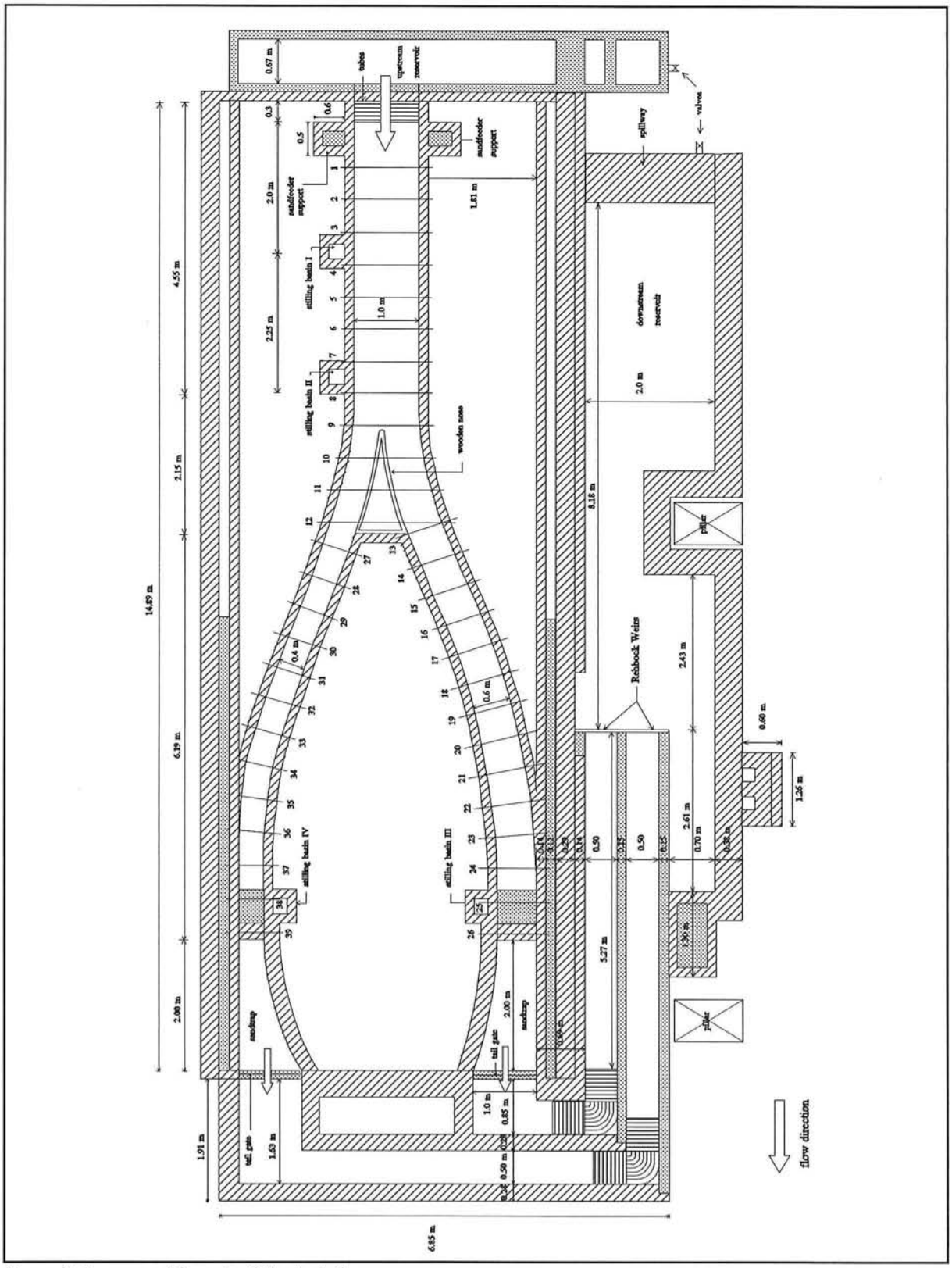

figure 9.1 - general layout of the test rig

9.3 General description of the test rig

The test rig consists of two separate parts: a *temporary* part and a *permanent* part. The permanent part is the *experimental facility* necessary for the storage and regulation of the water circulating throug the test rig, and the guidance of this water to and from the temporary part.
The temporary part contains the actual *experimental mobile-bed model* of a bifurcation in a river. It is possible to change the configuration of this part for other research projects in the future, using the permanent part of the test rig without any drastic constructive changes. The layout of the two parts is shown in figure 9.2.

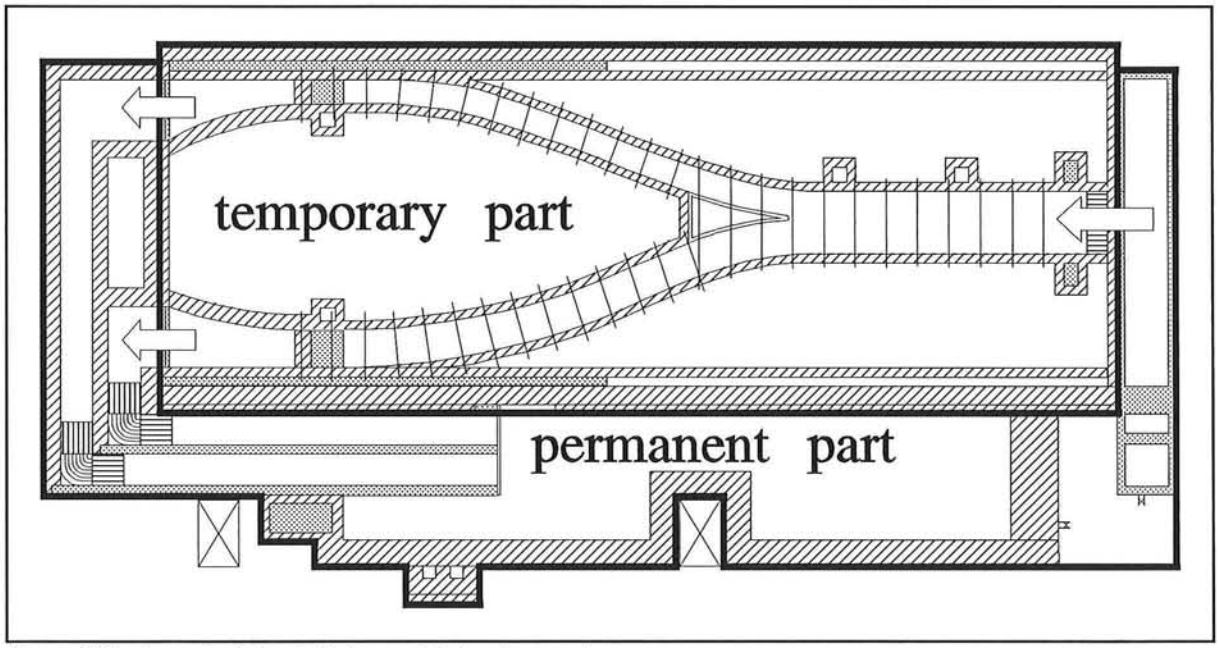

figure 9.2 - layout of the test rig containing two parts

The configuration of the temporary part, containing the experimental model, is described in detail in Chapter 10. The permanent part of the model is described in Chapter 11. The measurements necessary for the experiments on bifurcations are discussed in Chapter 12. Furthermore, practical suggestions for operating the model are given in Chapter 13, and recommendations for possible experiments are discussed in Chapter 14. Before detailing the layout of the model, a review of the main assumptions made during the design phase is given in the next section, as well as a list of the most important equations governing the design.

9.4 General considerations

9.4.1 Introduction

During the design of the model, a number of assumptions and restrictions were made. Considering the complexity and scope of the problem, a *steady flow* is taken into account. Only *bed-material transport* is considered, since this is the transport that is involved in the morphological changes.
The basic equations governing the model are given in the following sections.

9.4.2 Flow velocity

The maximum flow velocity in the model is determined by the criterium for which only bed-load transport occurs:

$$\frac{u_*}{W} \leq 1 \tag{9.1}$$

with

$$u = u_* \frac{C}{\sqrt{g}} \tag{9.2}$$

in which u : flow velocity;
u_* : shear velocity;
C : Chézy-coefficient;
W : fall velocity.

This results in an expression for the maximum flow velocity:

$$u_{max} = W \frac{C}{\sqrt{g}} \tag{9.3}$$

The fall velocity is determined using the expression found by Van Rijn (1993), which is valid for $100\ \mu m < D < 1000\ \mu m$:

$$W = \frac{10\nu}{D} \left[\sqrt{1 + \frac{0.01 \Delta g D^3}{\nu^2}} - 1 \right] \tag{9.4}$$

in which D : grain diameter;
Δ : relative density = $(\rho_s-\rho)/\rho$;
ν : kinematic viscosity.

9.4.3 Sediment transport

Sediment with a grain size D_{50}= 270 μm is used in the model, as can be seen in Section 10.8. The Engelund & Hansen (1967) sediment transport formula can be used if D_{50}>190 μm, so it is applied here:

$$S = B\frac{0.084}{D_{50}\sqrt{g}\Delta^2 C^3}u^5 \tag{9.5}$$

In the model the time-dependent process of erosion and sedimentation is governed by the celerity c of a small disturbance of the bed (De Vries, 1959). The adaptation time T for a disturbance in the model can easily be determined:

$$\frac{c}{u} = \frac{ds/du}{a}\frac{1}{1-Fr^2} \tag{9.6}$$

in which s is the sediment transport per unit width;
$Fr=u/\sqrt{ga}$ is the Froude number.

It takes a time $T=3L/c$ before an equilibrium is reached (De Vries, 1993).
With $s=mu^n$ and thus $ds/du=mnu^{n-1}=ns/u$, the adaptation time becomes:

$$T = \frac{3}{n}\frac{L}{u}\frac{1-Fr^2}{s/q} = \frac{3}{5}\frac{La}{s}(1-Fr^2) \tag{9.7}$$

in which T is the adaptation time;
L is the length of the branches;
q is the discharge per unit width.

9.4.4 Maximum bed level fluctuations

The maximum bed level fluctuations must be determined in order to estimate the necessary depth of the mobile sand bed. Furthermore it is used to compute the storage capacity of the sand traps.
The maximum decrease in the bed level occurs when one of the two branches closes due to sedimentation. The new equilibrium depth in the remaining open branch can be calculated with the formula of a long river constriction:

$$\frac{a_1}{a_0} = \left[\frac{B_0}{B_1}\right]^{\frac{n-1}{n}} \tag{9.8}$$

Chapter 10 - The experimental model

10.1 Introduction

The model of the bifurcated river is built in the temporary part of the test rig. It is a mobile-bed model with fixed banks. The layout of the river comprises three branches: a main branch, branch 0, which bifurcates into two separate branches, branches 1 and 2 (see figure 10.1). To avoid accidental equilibriums during experimentation, branches 1 and 2 have different widths. A sand trap is situated at the end of each of these two branches, followed by a tail gate for the control of the water levels. In the following sections all elements of the model are described in detail.

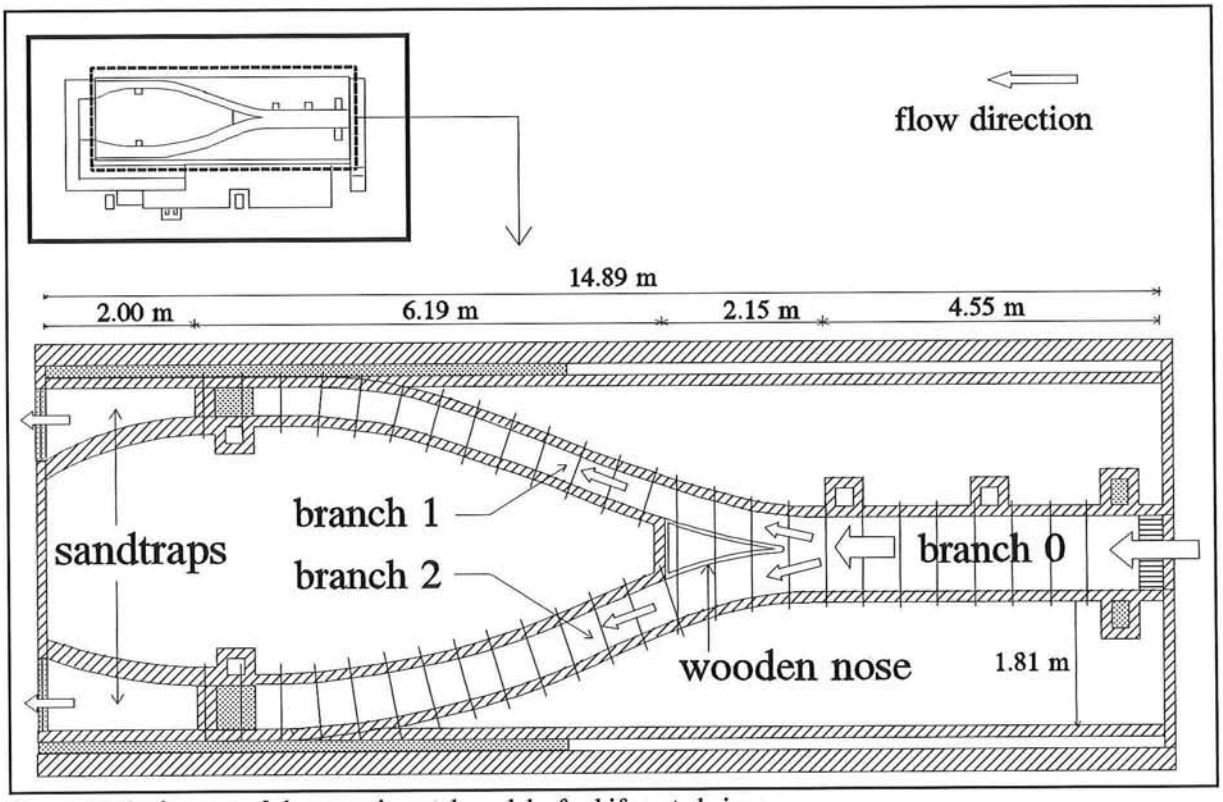

figure 10.1 - lay-out of the experimental model of a bifurcated river

Definition: The level of the laboratory floor will be used as a reference datum for measurements given in the following chapters. This level will be referred to with the abbreviation L.B.F. (LaBoratory Floor).

10.2 Inflow section and branch 0

The experiments are mainly focused on the bed level fluctuations around the bifurcation and in branches 1 and 2. An inflow section and inflow branch of considerable length are needed to insure an equal distribution of sediment transport, and stable flow conditions before the water reaches the bifurcation.

Inflow of water:
Water flows from the upstream reservoir to branch 0 via the inflow section. PVC tubes ($\varnothing$=2.7 cm; L=30 cm) placed over the width of the entrance get rid of the larger eddies present in the upstream reservoir and thus stabilise the flow (see figure 10.2 and figure 11.7).

Sandfeeder:
Directly behind the tubes a sandfeeder distributes sand over the width of the channel into the flow (see figure 11.7). For specifications of the sandfeeder capacity, see Section 11.3.

Branch 0:
This is the main branch of the river which splits up at the bifurcation. The characteristics of this branch, are given in the following (see also figure 10.2).

- Length L_0: Before the water reaches the bifurcation, the sediment from the sandfeeders should be well-distributed over the width of the branch in stable flowing conditions. For this, experimental experience learns that a minimum adaptation length $L_0 \geq 40*a$ (a is the water depth) is needed. Practical limitations result in a minimum average water depth in which it is possible to make measurements: a_0= 10 cm; therefore $L_0 \geq 4.0$ m. To make room for the tubes and the supports of the sandfeeder the branch is made a little longer: L_0= 4.55 m.
- Width B_0: To disregard the influence of the walls, experimental experience learns that $B \geq 5*a$ is required. Since branch 0 bifurcates into two *smaller* branches, this criterium governs the widths of branches 1 and 2; so branch 0 is a little wider: B_0= $10*a$ = 1.0 m.

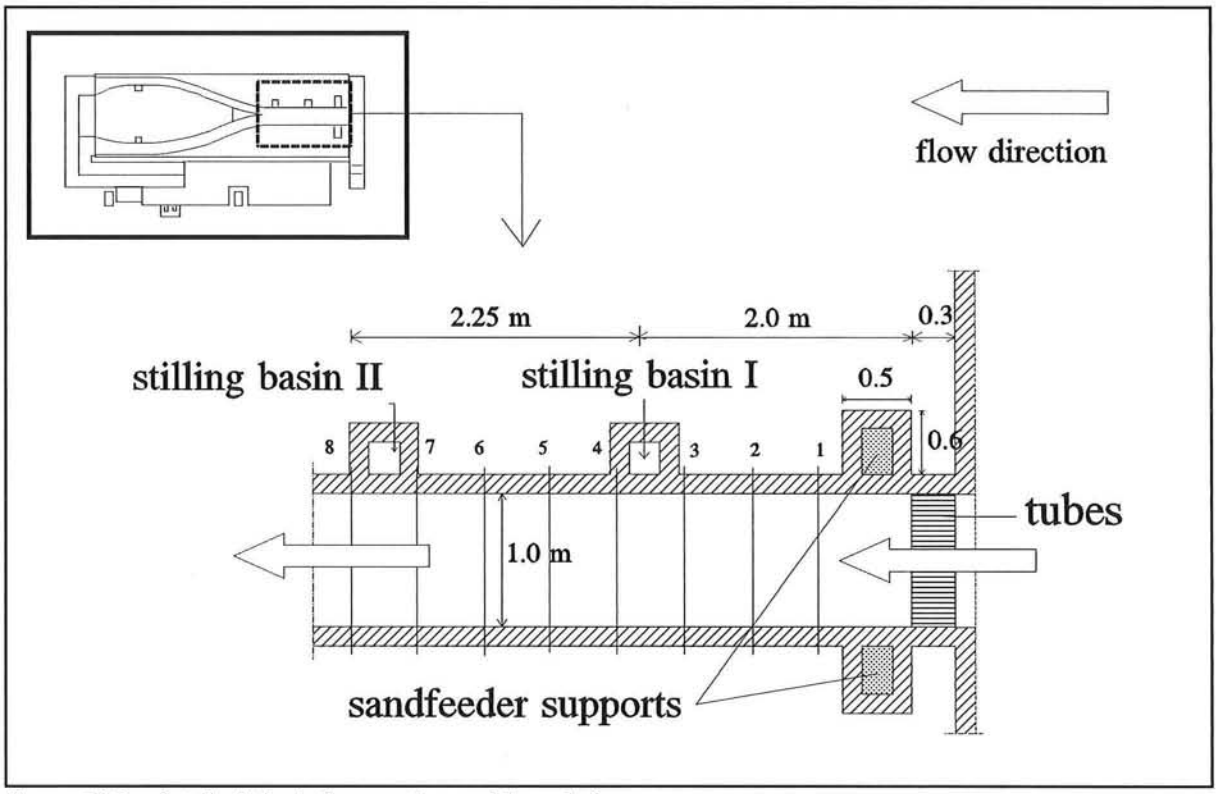

figure 10.2 - detail of the inflow section and branch 0

10.3 Dimensions of branches 1 and 2

At the bifurcation, the flow is split into branches 1 and 2. The radius, length and width of these curved branches are given in the following (see also figure 10.3).

Width B: The sum of the widths of branches 1 and 2 is equal to the width of branch 0. Thus $B_1+B_2=B_0=1.0$ m. As mentioned in Section 10.1, the branches have different widths to avoid accidental equilibriums. So $B_1=0.4$ m and $B_2=0.6$ m.

Radius R: To minimise secondary flow in the bends of these branches, the radius R of the branches must not be too small: $R \geq 5*B$. With the available space in the laboratory this is not a problem if $R_1=23.5$ m and $R_2=25.5$ m.

Length L: The resulting lengths of the two branches are: $L_1=8.6$ m and $L_2=8.4$ m.

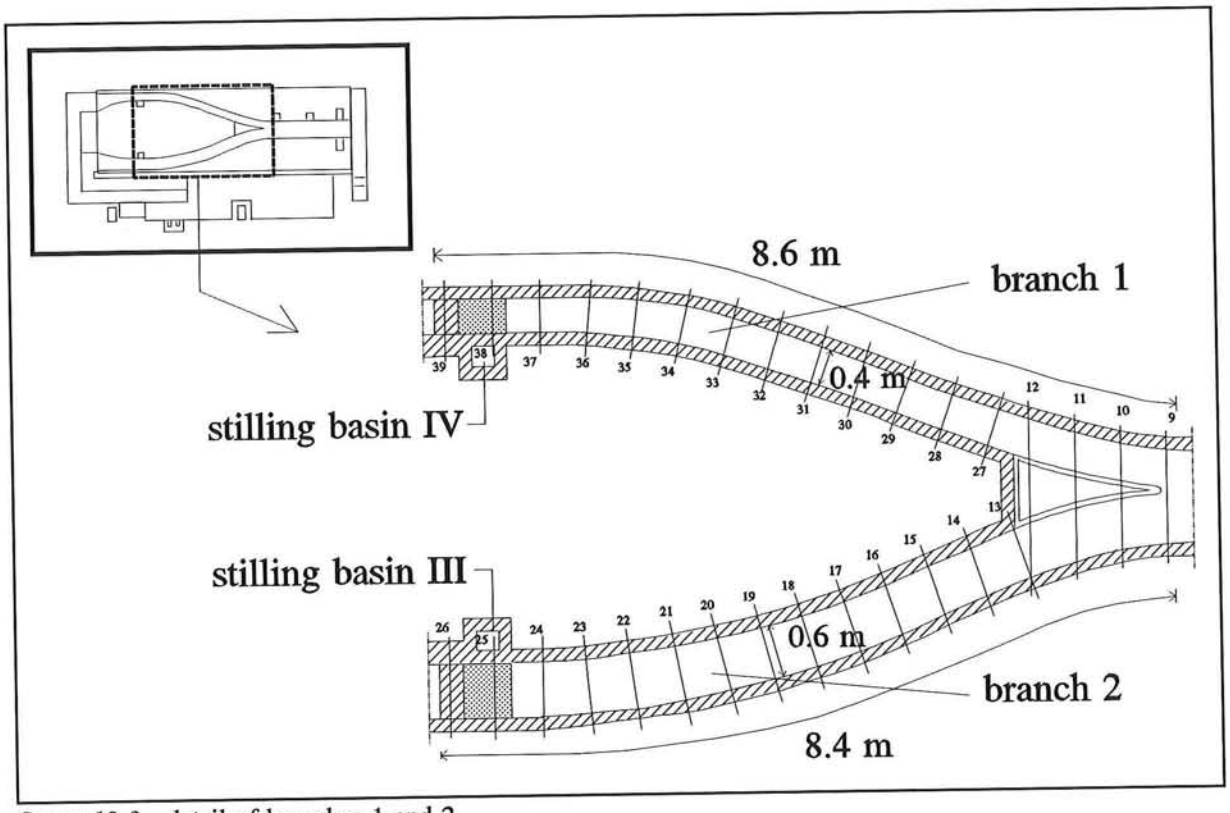

figure 10.3 - detail of branches 1 and 2

10.4 Configuration of the bifurcation

As seen in Part I of this report, the distribution of the sediment transport rates to the downstream branches is governed by the local flow pattern at the bifurcation. Consequently, the shape of the bifurcation plays an important role in this distribution. Therefore the "tip" or "nose" of the bifurcation is implemented as a flexible component of the model: whereas the entire model is made of brickwork, the nose is made of wood, so that different shapes can be applied for different experiments as proposed in Chapter 14.

10.5 Sand traps

10.5.1 Introduction

The sand traps located at the end of branches 1 and 2 have a double function:

1) they intercept the sediment transported through the branches, so that the average sediment transport rate can be determined for each branch, as detailed in Section 12.3;

2) by intercepting all the sediment, the sand traps prevent the sand from coming into the permanent part of the model, which includes the reservoir and pump system.

10.5.2 Length of the sand traps

The length L_s of the sand traps is governed by the following equation:

$$\frac{L_s}{a} = \frac{u}{W} \tag{10.1}$$

Combining Eq. (10.1) with Eq. (9.3) yields:

$$L_s = \frac{C\, a_{max}}{\sqrt{g}} \tag{10.2}$$

The maximum water depth occurs in the case that branch 2 is closed due to siltation. In that case branch 1 conveys all the water, and from Eq. (9.8) it follows that:

$$a_{max} = \left[\frac{B_0}{B_1}\right]^{\frac{4}{5}} a_0 = 0.21 \text{ m} \tag{10.3}$$

The resulting length of the sand traps is (with C= 30 m^{½}/s): L_s = 2.0 m.

10.5.3 Width of the sand traps

The sand traps do not have a constant width. The widths of the sand traps increase gradually (to avoid the formation of eddies): at the *upstream end* they have the width of the corresponding branch (0.4 or 0.6 m); at the *downstream end* they have the width of the tail gate, B_s= 1.0 m (see Section 10.6). This results in the shapes as seen in figure 10.4.

10.5.4 Capacity of the sand traps

The storage capacity of the sand traps is determined by their length, width and depth. The available depth for storage in the sand trap depends on the bed level immediately upstream of the sand trap. The *minimum* available depth occurs when the bed level is at its lowest: as can be seen in Section 10.7 the lowest possible bed level is located at +0.80 m above the laboratory floor (L.B.F). The floor of the sand trap is located at L.B.F. +0.35 m, so the resulting minimum depth of the sand trap is d_s=0.80-0.35=0.45 m (see figure 10.5).

The minimum storage capacities of the sand traps are therefore:

- Sand trap 1 (belonging to branch 1): V_{s1} = 0.63 m^3;
- Sand trap 2 (belonging to branch 2): V_{s2} = 0.72 m^3.

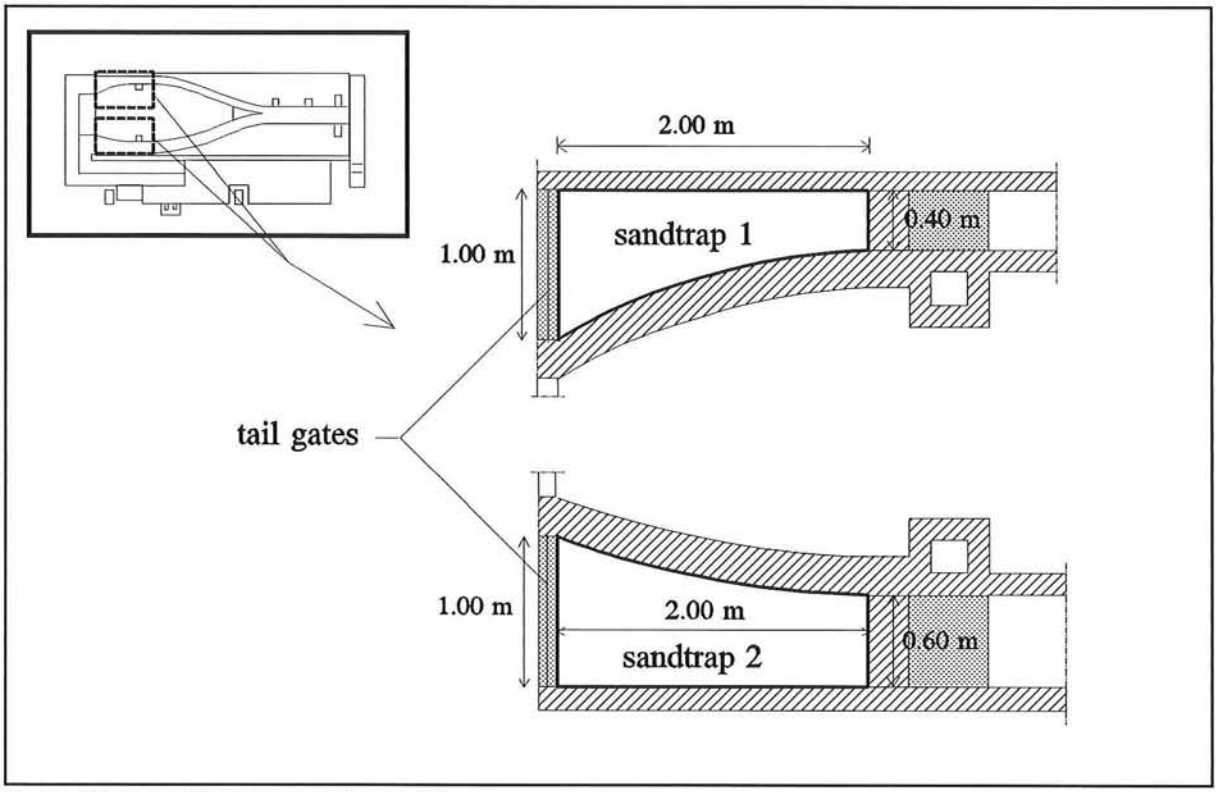

figure 10.4 - configuration of the sand traps

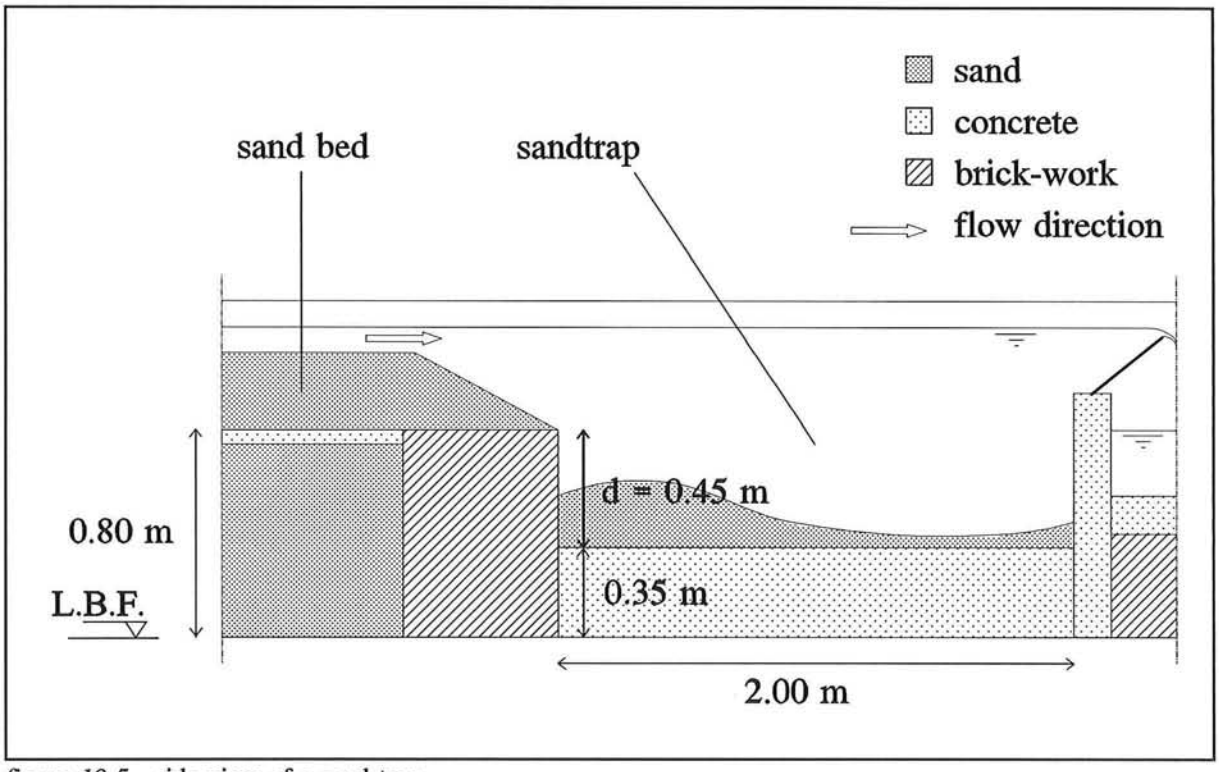

figure 10.5 - side view of a sand-trap

10.6 Outflow section

At the downstream end of the model, the water in each branch flows over a tail gate into the permanent part of the model (see figure 9.2), where the discharge is measured before spilling into the downstream reservoir. The tail gates have two functions:
a) they regulate the water level in each branch;
b) they prevent the sand bed from running dry.

ad.a) During experimentation, several types of tests can be imagined (see Chapter 14), which each dictate an own set of downstream water levels. The dimensions of the tail gates are such that they can be adjusted to induce a large range of downstream boundary conditions (see also Section 11.4).

ad.b) The adaptation time for the experiments will be about 25 hours (see Section 10.8). One experiment will therefore be divided over several days, the model being put to a standstill at the end of each day. When stopping the model it is imperative that the river bed does not come dry, because this would lead to unacceptable disturbances of the bathymetry. Water must therefore be stored in the river branches when the model is idle, resulting in the requirement for a watertight construction of the tail gates (see figure 10.6).

For a visual impression of a tail gate see also figure 11.9.

Width of the tail gates:
If a power failure occurs during experimentation, the water level in the branches will drop quickly. Thanks to the watertight construction shown in figure 10.6 the water level will stop dropping when it reaches the crest level of the tail gate. To avoid disturbances of the bed this crest level must be situated far above the bed level. For this reason the tail gates have a *larger* width than the branches: this decreases the head over the tail gate, thus *increases* the crest level of the tail gate. Since the widths of the branches are 0.4 m and 0.6 m, the tail gates have a width of 1.0 m. For further details of the tail gates see Section 11.4.

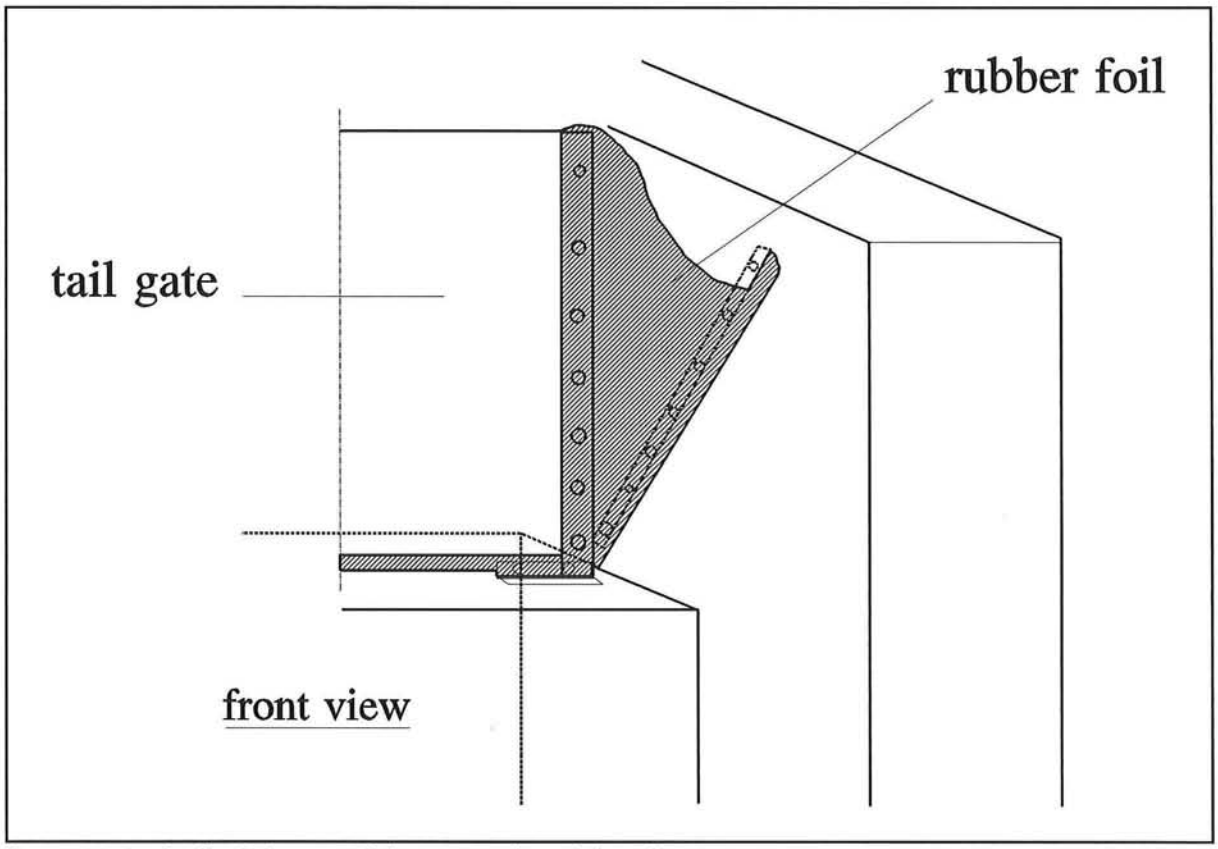

figure 10.6 - detail of the watertight construction of the tail gate

10.7 Height of the model

10.7.1 Introduction

The simulated river flows at approximately L.B.F. +1.20 m, and the brickwork is laid up to a height of L.B.F. +1.30 m. The reason for this rather large elevation is the fact that the downstream reservoir is built on the laboratory floor: this forms the base to which all depths and head-losses must be added. The factors determining the height of the model are summed up in the following sections.

10.7.2 Water levels in the test rig

The downstream reservoir contains the gross of the water present in the test rig. The pump which circulates the water through the model taps its water from this reservoir. A minimum suction head of 0.50 m is needed in the reservoir.

The permanent part of the test rig is designed to cope with a maximum discharge of 60 l/s. The corresponding water depths in the approach channels of the Rehbock weirs,

the consequent head-losses in these channels and the necessary nappes behind the Rehbock weirs and tail gates result in a minimum tail gate crest elevation of L.B.F. +1.06 m (see figure 10.7).

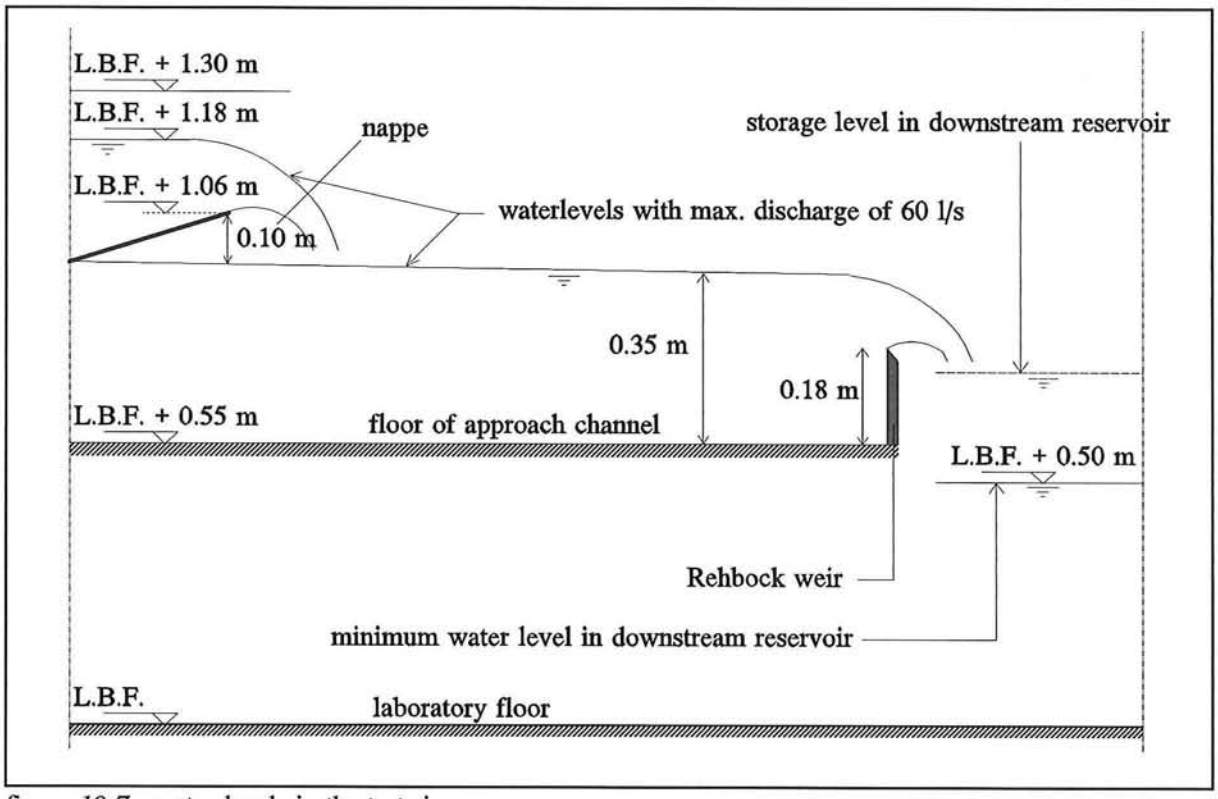

figure 10.7 - water levels in the test rig

This is the lowest position of the tail gate and it is applied when the maximum discharge of 60 l/s runs through the connecting branch. The head over the tail gate with this discharge is approximately 0.12 m. The resulting water level H_s in the sand trap is therefore: H_s=1.06+0.12= L.B.F. +1.18 m.
The water level at the inflow section is a little higher due to head-loss: taking into account a slope $i=10^{-3}$ (see Section 10.8) the head-loss over the length of the model is ΔH=0.02 m, so the resulting water level at the inflow section is H_i=1.18+0.02= L.B.F. +1.20 m. An extra freeboard of 0.10 m is taken into account, so the brick walls have an elevation of L.B.F. +1.30 m.

10.7.3 Bed levels in the model

Since the model has a mobile bed there is no fixed bed level to be given. However, an indication of the initial bed levels and extreme bed level variations give sufficient insight into the possible bed level fluctuations. This is impo*83%(for determining the thickness of the sand bed applied in the model.

As seen in Section 10.2 the average water depth is a=0.10 m. The initial bed level at the outflow section is therefore located at $z_b = H_s - a$ = L.B.F. +1.08 m.
As for the extreme case: according to Eq. (10.3) the maximum water depth is a_{max}=0.21 m. Bed forms will develop in the branches; according to Van Rijn (1993) the maximum bed-form is given by:

$$\frac{\delta}{a} = 2\left[\frac{D_{50}}{a}\right]^{0.3} \tag{10.4}$$

in which δ is the height of the bed form (difference between highest and lowest point). With a=0.21 m and D_{50}=270 μm (see Section 10.8) this results in: δ = 0.06 m.
As a result, for the experiments with a constant downstream water level, the bed level drops to z_b= 1.18-0.21-0.06 = L.B.F. +0.91 m.
If experiments are done with variable downstream water levels, the bed level can go down even further. An extra margin of 11 cm is therefore taken into account, so that the bottom of the sand bed is located at L.B.F. +0.80 m. At this level a thin concrete floor is cast (see figure 10.5), on top of which the sand with appropriate grain diameter is placed.

10.8 Initial values for experimentation

10.8.1 Introduction

Even though all of the parameters involved in the model are variable, the model was designed with a certain "basic" experiment in mind. The details of this experiment are given in the following section. This is followed by the possible alterations of the applied parameters.

10.8.2 The basic experiment

As can been seen in the Detailed Design (Den Dekker and Van Voorthuizen, 1993) the model, and the basic experiment, were designed to "fit" into the local circumstances of the laboratory. The determining factor of this design was the capacity of the sandfeeders, which was then assumed to be a given constant. A review of this design process is given here.
The Chézy roughness coefficient is assumed to be C = 30 m^{½}/s. Moreover, a bed slope i=10^{-3} is taken into account. The available sandfeeding capacity (18 kg/hour) is thus assumed to be constant. The resulting necessary flow velocity is found with the Engelund-Hansen formula:

$$S = B\frac{0.084}{D_{50}\sqrt{g}\Delta^2 C^3}u^5 \quad \Leftrightarrow \quad u = \left(\frac{SD_{50}\sqrt{g}\Delta^2 C^3}{0.084B}\right)^{\frac{1}{5}} \tag{10.5}$$

With this flow velocity the resulting adaptation time T is found with Eq. (9.7). This is done for several grain sizes, until a grain diameter is found for which there is no suspended load ($\rightarrow u_*/W \leq 1$) and for which the adaptation time is acceptable within the time schedule of experimentation. A necessary grain diameter D_{50}= 300 μm results from these computations.

Sand was bought at the market, which eventually led to D_{50} = 270 μm. Considering the minor influence of the grain size on the adaptation time this sand type is considered acceptable (see Eq. (9.7)). The resulting experimental parameters for the input of branch 0 are:

S_0 = 18 kg/hour = 3.14 10^{-6} m^3/s;

D_{50} = 270 μm;

u_0 = 0.30 m/s;

Q_0 = 30 l/s;

T = 25 hours.

10.8.3 Domain of alterations

Obviously the values found for the basic experiment will vary according to the demands of each experiment. The time T is only an estimate of the actual adaptation time that will occur during experimentation. If it turns out that the experiments take longer than anticipated, the processes can be speeded up by increasing S, or increasing Q.

The increase of S is governed by the maximum capacity of the sandfeeder, which is indicated in Section 11.3.

As can be found in Section 11.2, the discharge Q can be increased to a maximum of 60 l/s. The resulting increase in the flow velocity u (see Eq. (9.3)) must, however, be limited if suspended load occurs.

Chapter 11 - Specifications of the test rig

11.1 Introduction

As mentioned before the model consists of a temporary and a permanent part. The latter is the subject of this chapter and can be seen as the hardware of the test rig. It provides the running of all experiments. This permanent part can be divided into three elements:
- the water supply system;
- the sediment supply system;
- the regulating and measuring system of the test rig.

During the design proces a lot of problems were encountered considering the three elements with their functions and requirements. To fulfill these demands specific constructions were necessary. The following sections deal with the three elements in more detail, especially by reproducing part of the technical drawings and photographs made by the writers during their stay at BUET in Dhaka.

11.2 The water supply system

11.2.1 General description

The circulation of the water within the test rig is a closed system. From the downstream reservoir the water is transported by means of the pipeline to the upstream reservoir. Consequently it flows through the experimental model (the temporary part of the test rig). Via the regulating and measuring facilities, the water returns into the downstream reservoir (see figure 11.1).

To ensure smooth experiments and valuable results, a controlled inflow into the experimental model is absolutely necessary. Due to bothersome irregularities in the water supply at BUET it is essential to have a closed self-sufficient water circulation system. This especially has consequences for the size of the downstream reservoir.

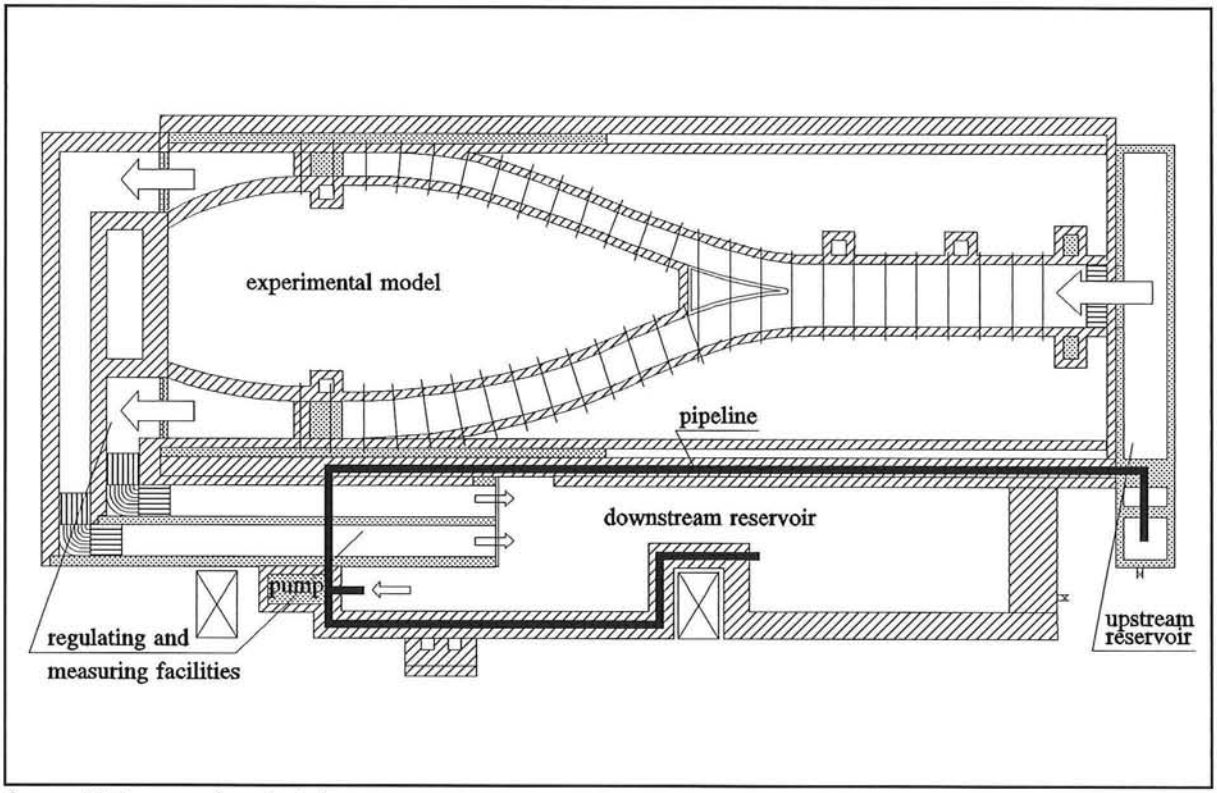

figure 11.1 - overview test rig

11.2.2 Downstream reservoir

The configuration of the downstream reservoir is defined by the following factors:

- The required suction head needed for the pump. Hence, as mentioned in Section 10.7, the minimum water level maintained in the reservoir during experimentation has to be L.B.F. + 0.50 m.
- The demand of an independent water supply. Taking into account that the experimentation will not be continued during night time the necessary storage of the downstream reservoir is determined by the water amount in the pipeline and the water layer in the guiding flumes and the approach channels above the Rehbock weir. If a safety margin of 20 percent is taken into account, the volume to be stored in the reservoir is about 3.10 m^3.
- The position of the approach channels. The water flow over the Rehbock weirs must end in the downstream reservoir to close the water circulation. The Rehbock weirs and their approach channels have to be constructed according to ISO 1975 (see Section 11.4).
- The available space in the laboratory. Together with existing drains and pillars in the laboratory, the necessary thickness of the brick walls (resulting from the horizontal

hydraulic forces) determines the required area for the downstream reservoir. The thickness leads to a maximum water level of L.B.F. + 0.77 m and consequently to a maximum allowable storage height.

These factors result in the configuration of the downstream reservoir as can be seen in figure 11.2.

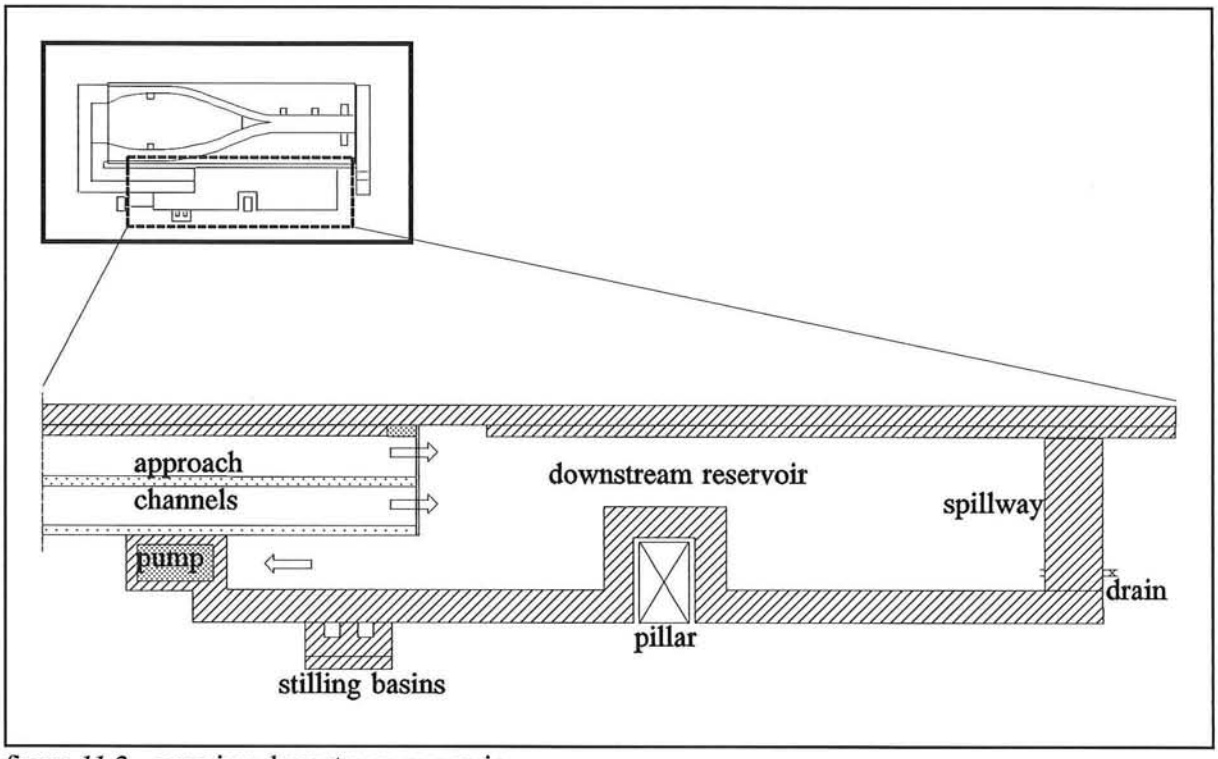

figure 11.2 - overview downstream reservoir

As mentioned before, besides a minimum water level there is also a maximum allowed water level of L.B.F. + 0.77 m following from the strength of the surrounding walls. To make sure this water level is not exceeded (in case of a power failure of the pump, a large amount of water will flow into the downstream reservoir) a spillway is built (see figure 11.3).

Due to the necessary volume of the spillway to withstand the horizontal forces, it turned out to be impossible to build such a spillway entirely according to the prescriptions on this kind of structures. For maintenance purposes the test rig can be emptied using a small valve in the spillway.

11.2.3 The pipeline system

The transport of water is taken care of by the pipeline system. The pump sucks the water from the downstream reservoir into the pipeline. The T-joint on top of the pump divides the water over the excess pipe and the delivery or supply pipe, depending on the

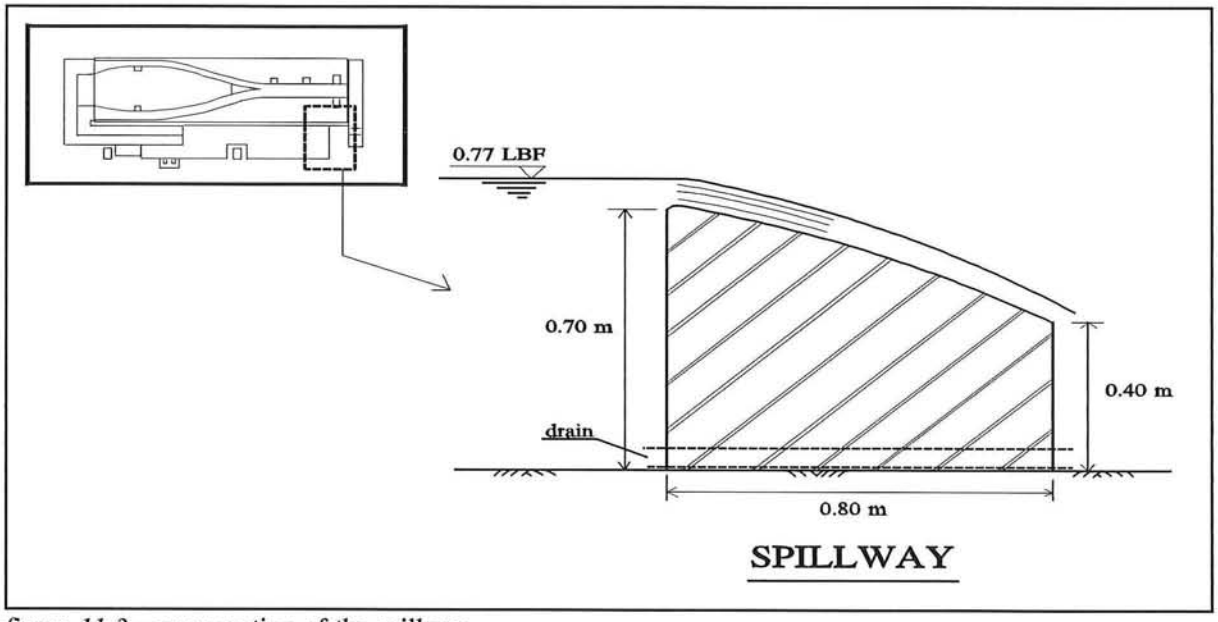

figure 11.3 - cross-section of the spillway

installation of the valves in the respective pipes (see figure 11.4). As the pump delivers a constant discharge, the required discharge through the model must be supplied operating these valves.

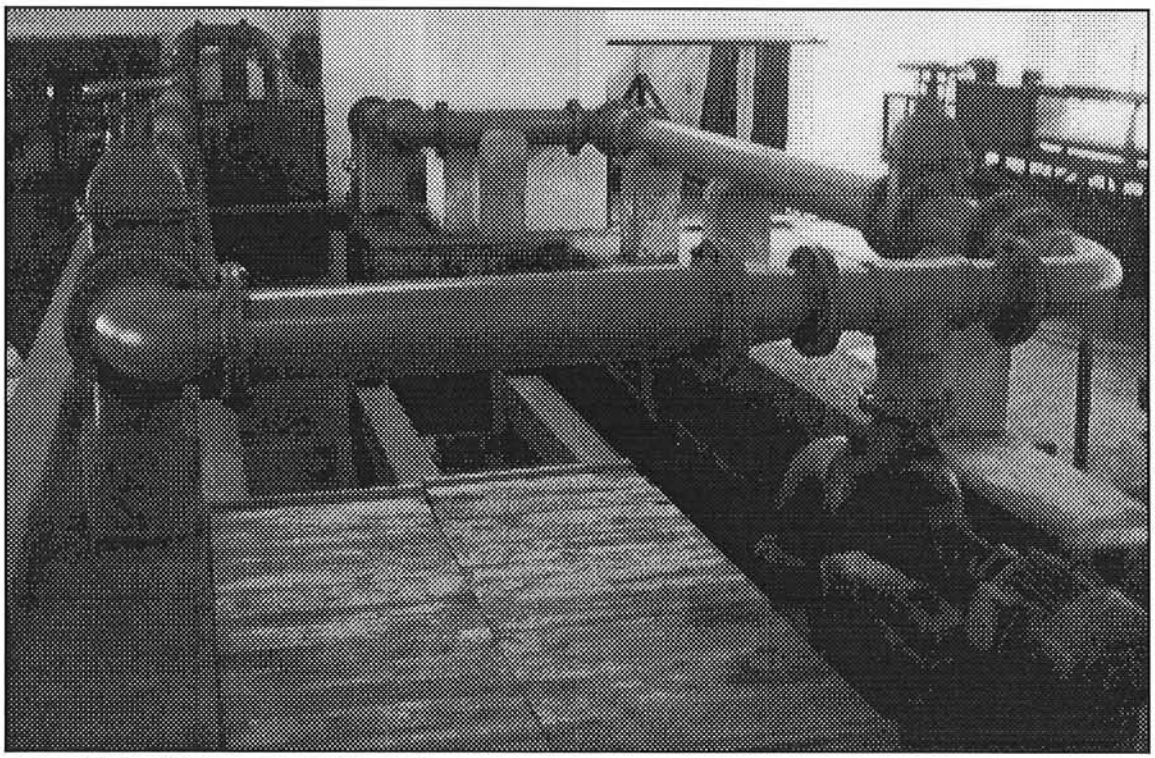

figure 11.4 - view on the pipeline system

The excess pipe dumps the water back into the downstream reservoir. The delivery pipe transports the water to the upstream reservoir. In this part of the pipe the flow rate is measured. At first this will only be done by means of measuring the pressure difference over an orifice. For a rating table on the orifice, see Appendix A. In the future also an electromagnetic Foxboro-meter can be implemented. The dimensions of the adjacent pipe parts are determined taking into account this possibility. To apply these measuring devices certain installation requirements have to be fulfilled, for example considering straight lenghts up- and downstream of the device. Both the orifice and the Foxboro are constructed and positioned acccording to ISO 1980. Moreover the availibility of pipe parts in the laboratory of the desired pipe diameter resulted in a rather strange mixture of the different pipe lenghts.
The possibility of air occuring behind the orifice and thus an incorrect reading has been prevented by an upward bend in the pipeline just behind the orifice. When the pipeline is filled slowly at the very beginning of an experiment, the air gets the chance to escape and by means of the upward bend the pipe stays filled during non-running periods.
At the end of the delivery pipe the water falls vertically into the stilling reservoir of the upstream reservoir. For an overview of the whole pipeline system, see figure 11.5. For further details of the pipeline system see Appendix B.

11.2.4 The upstream reservoir

The upstream reservoir consists of two basins. As mentioned before the water from the pipeline enters the upstream reservoir in the stilling reservoir. The function of this small rectangular basin is to dampen the turbulence in the water caused by all the bends in the pipeline. The stilling reservoir is seperated by a wall from the larger basin of the upstream reservoir (see figure 11.6).
To create a smooth inflow into this basin and hence to the experimental model, two holes are incorporated in the wall. The area of these openings is designed in accordance with the maximum possible discharge in the test rig of 60 l/s. To reduce the turbulence once more, the water inflow into the model passes by a cross-section filled with small PVC-pipes (see also Section 10.2).
For maintenance purposes the upstream reservoir can be emptied through a small pipe with a valve, incorporated in one of the walls. By opening the valve the water flows away into an existing drain in the laboratory (see figure 11.6).

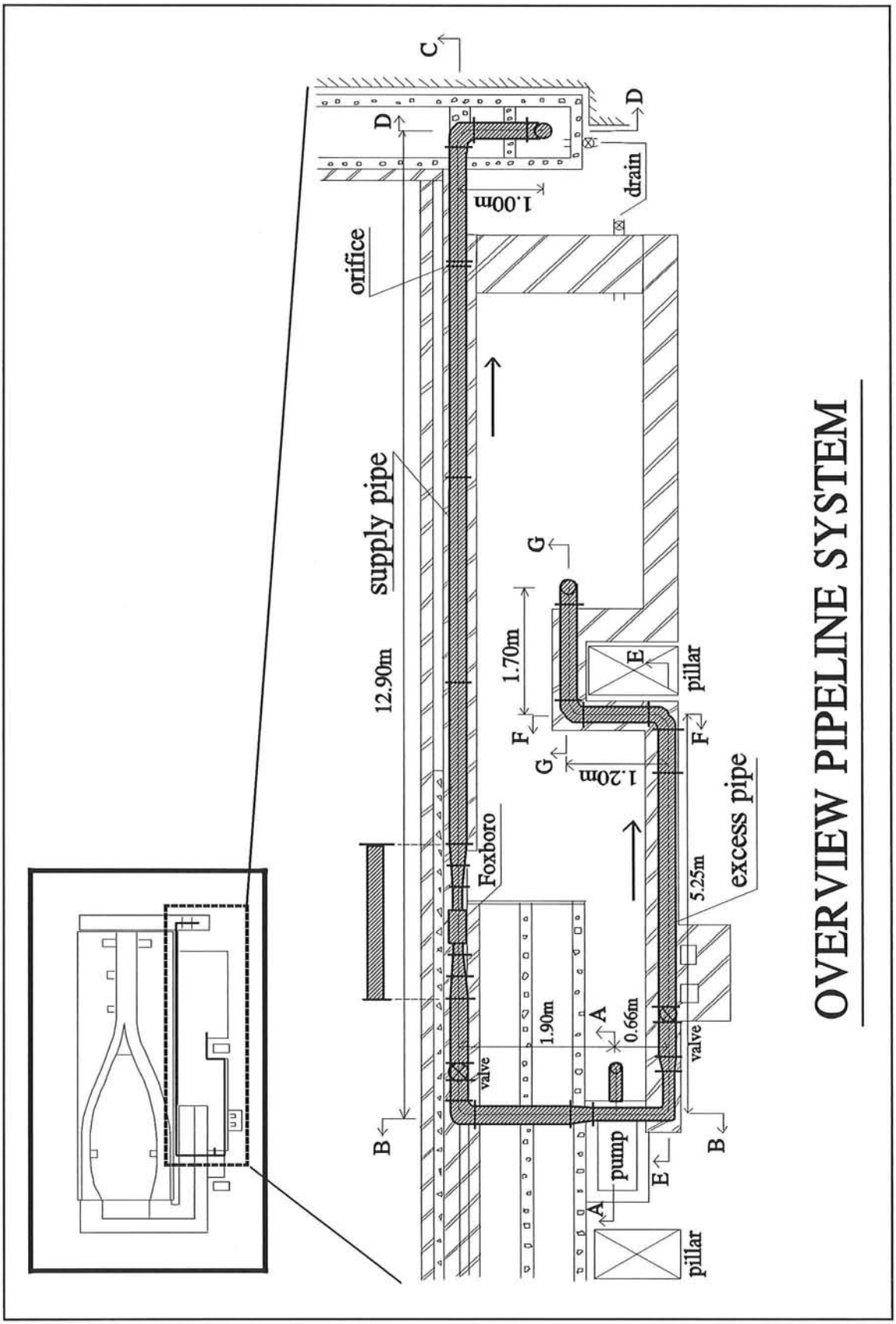

figure 11.5 - configuration of the pipeline system

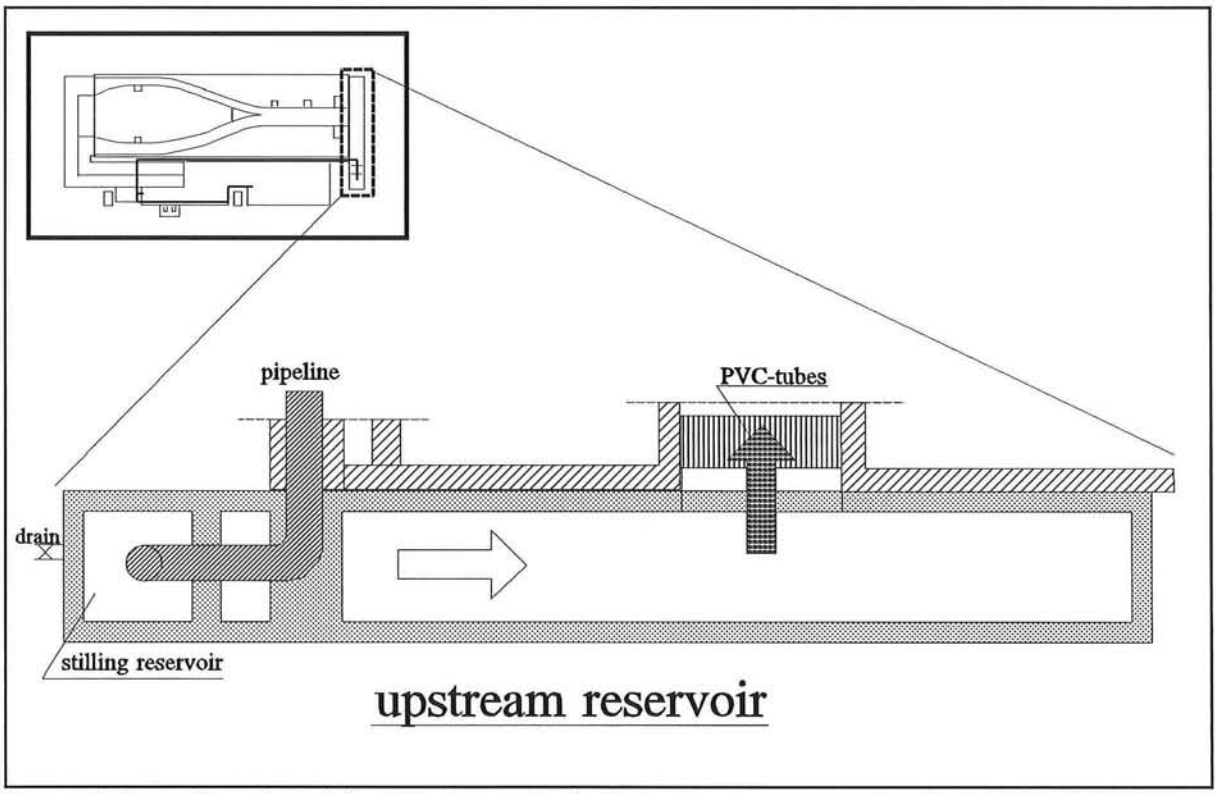

figure 11.6 - configuration of the upstream reservoir

11.3 The sediment supply system

In a research on morphological changes it is clear that sediment plays an important role in the experiments. Just as the water, also the sediment circulates during an experiment. At the beginning of an experiment, an initial bed level is placed in the model. This means that a certain layer of sand is put in the branches, according to calculations on possible bed level fluctuations (see Section 10.7).
Starting the model introduces a sediment transport as a result of the flow velocity. Sand is transported downstream and has to be refilled from upstream. Therefore two sandfeeders (see figure 11.7), placed at the beginning of branch 0, provide for the supply of sand.
The amount of sediment supply depends on the equilibrium state in branch 0. During the first hours of an experiment, the bed level in this branch has to be watched closely, in order to supply an adequate amount of sediment.
The sandfeeder on the right, which is fabricated at BUET, has a wide capacity-range with a maximum of about 85 kg/h, wherein the sand can be provided. This is concluded from a calibration, resulting in a rating curve for this particular sandfeeder. The other

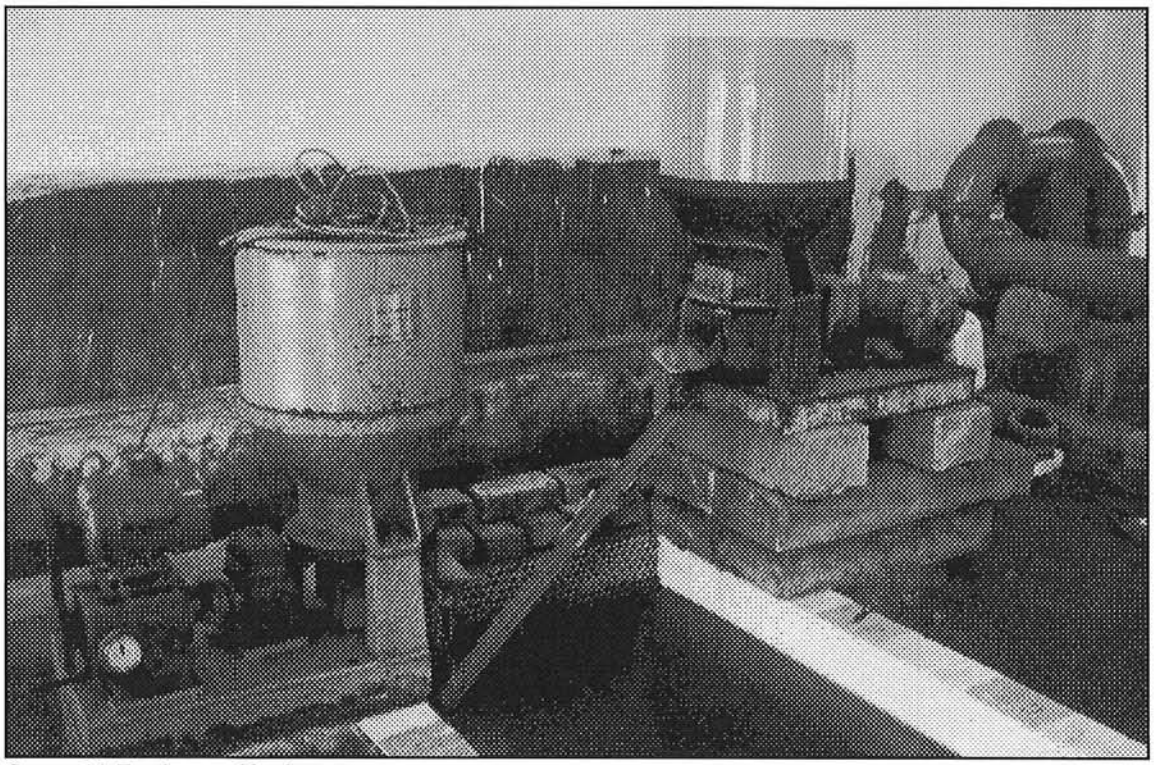

figure 11.7 - the sandfeeders

sandfeeder has a restricted range with a maximum of 18 kg/h. Attention has to be paid to an equal distribution over the width of branch 0, otherwise unwanted bed forms are created.

The transported sediment finally falls into the sand traps, both situated at the end of the downstream branches 1 and 2. The amount of sand captured in the sand traps can be measured in various ways, as mentioned in Section 12.3. It has to be removed from the sand traps every now and then to maintain a reliable efficiency of the sand traps, which in fact means maintaining enough water depth. Consequently the wet sand has to be dried in order to prepare it for recycling in the model. Only the use of dry sand as input for the sandfeeder makes the rating curve accurate.

11.4 The regulating and measuring system

11.4.1 Background

In the report concerning the detailed design of the test rig (Den Dekker & Van Voorthuizen, 1993) the conclusion was drawn that the regulating and measuring functions of the test rig could not be combined in one structure (see Appendix D). Hence

they are separated, resulting in quite a few structures, which are placed in a rather extended downstream end (see figure 11.8).

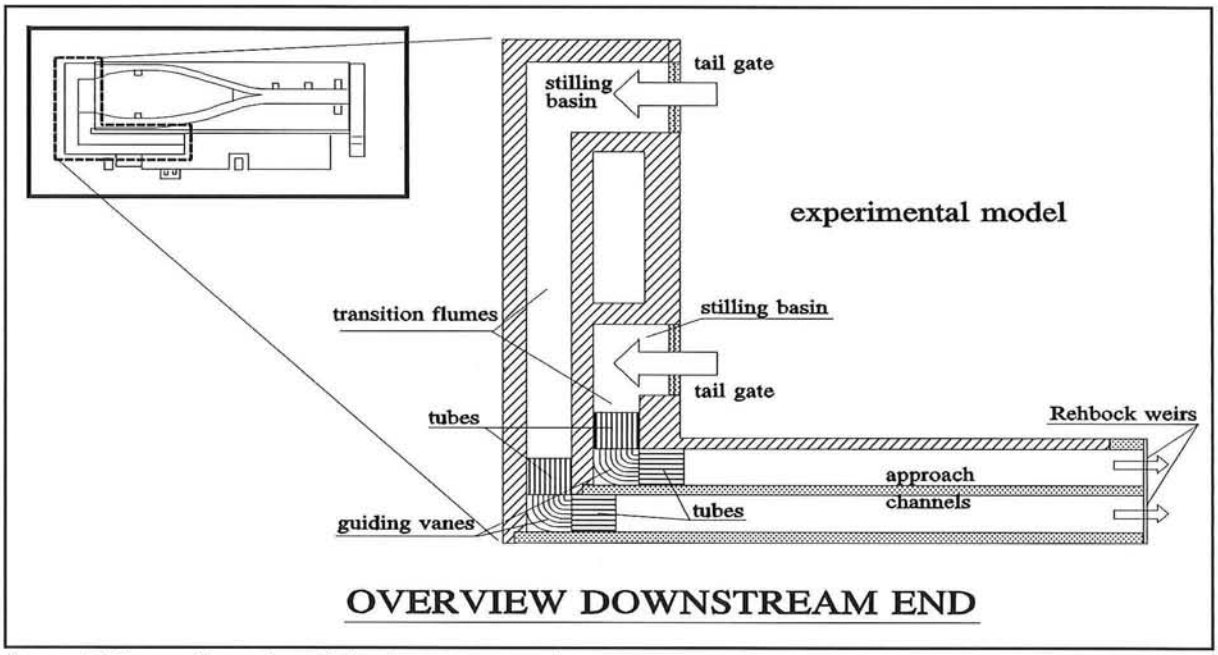

figure 11.8 - configuration of the downstream end

11.4.2 The tail gates

The regulating function of the downstream end is provided by two tail gates. In fact they belong to the temporary part of the test rig; the configuration of the experimental model determines the necessity and the position of the tail gates. The tail gates, however, are important structures and are therefore dealt with in this chapter (see figure 11.9).
The tail gates rotate around a horizontal axis. They represent the downstream boundary condition which follows from the situation to be reproduced. The flow over the tail gate is expressed by the next relation

$$Q = mB\frac{2}{3}H\sqrt{\frac{2}{3}gH} \qquad (11.1)$$

The enlargement of the downstream width of the sand traps (1.00 m for both sand traps, although the effective width of a tail gate is approximately 0.90 m due to the rubber flaps) also has positive consequences for the water height over the tail gates, as can be deduced from the above relation. A smaller water height over the tail gates, also reduces the total height of the test rig.
To ensure a smooth and representative flow over the tail gates, there must exist an atmospheric pressure behind the tail gates. A small air pipe underneath the tail gates

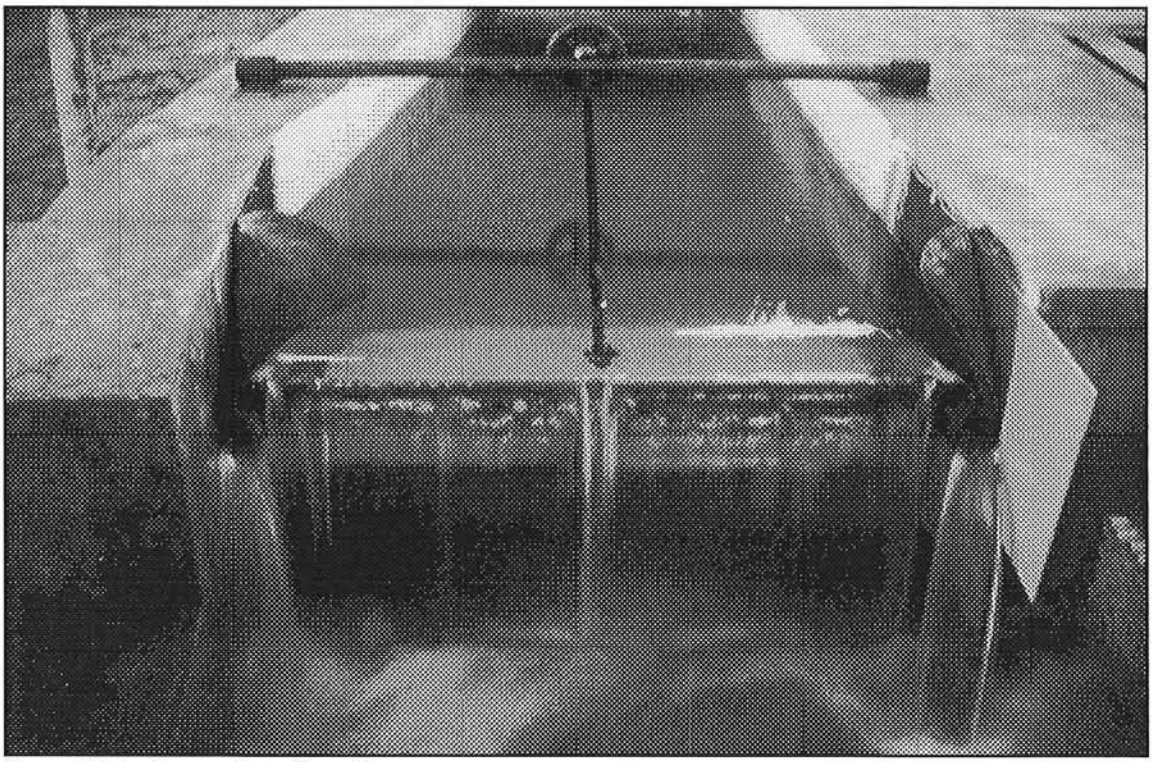

figure 11.9 - impression of a tailgate

provides this atmospheric pressure (see for details figure 11.10). The presence of atmospheric pressure is, however, not as important as it is in case of the Rehbock weirs (see Section 11.4.6).

An important function of the tail gates is to close the model during non-running periods. The tail gates prevent the water from flowing away, which would cause an unacceptable dry bed. The watertightness is reached using large rubber flaps, connecting the vertical side of the tail gate with the nearest wall (see Section 10.6).

11.4.3 The stilling basins and transition flumes

Behind the tail gates the water falls into a stilling basin. In case of the water from branch 1 this a larger basin than in case of branch 2. This difference is caused due to the available space. The water from branch 2 has to follow a more narrow turn. This also holds for the transition flumes. The flume behind branch 1 is much longer. The width of these transition flumes is already equal to the width of the approach channels (see Section 11.4.4), which is 0.50 m in both cases. Besides transporting the water to the measuring part of the permanent facility, already a lot of turbulence is destroyed in the stilling basins as well as in the transition flumes (see figure 11.8).

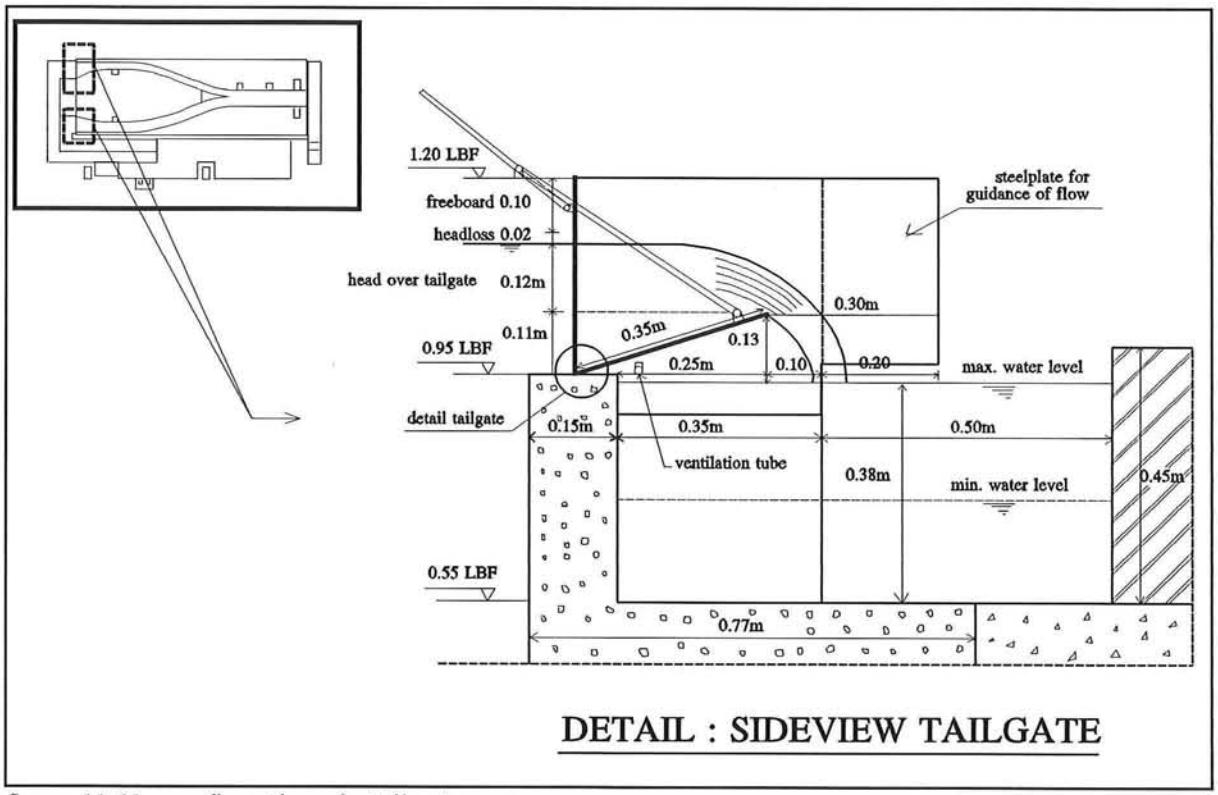

figure 11.10 - configuration of a tail gate

11.4.4 The guiding vanes and tubes

To ensure a more smooth flow towards the approach channels, between the transition flumes and the approach channels (making a perpendicular angle as can be seen from figure 11.8) guiding vanes are placed. These vanes guide the water around the corner. In order to prevent creation of extra unwanted turbulence in the approach channels, on both the upstream and downstream side of the guiding vanes PVC-tubes are fixed (see figure 11.11 and figure 11.12).

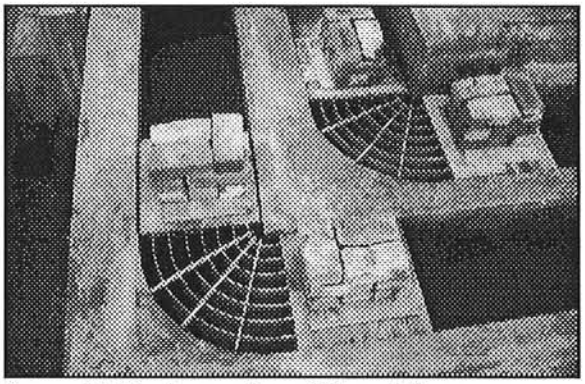

figure 11.11 - impression of the guiding vanes

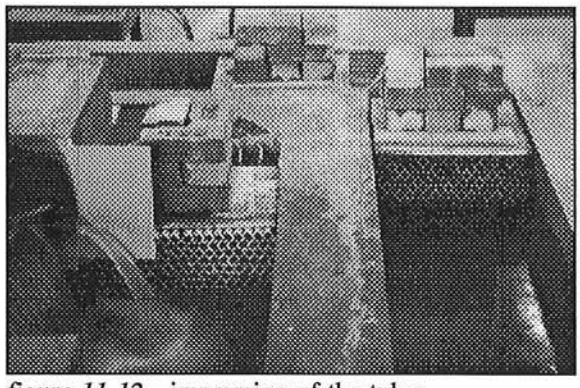

figure 11.12 - impression of the tubes

11.4.5 The approach channels

The only task of both approach channels is to reduce the turbulence in the water. According to ISO 1975 the channels are of sufficient length to develop the normal (uniform flow) velocity distribution for all discharges. The length and width are prescribed dependent on the width of the Rehbock weir used. The width of the channel must be equal to the width of the weir ($B_c=B_w$) over at least a length of ten times the width of the weir ($L_c=10*B_c$). A lot of attention is paid to make the walls as smooth as possible. This dimensional demand is satisfied, as is indicated by figure 11.8. For an impression of the approach channels see figure 11.13.

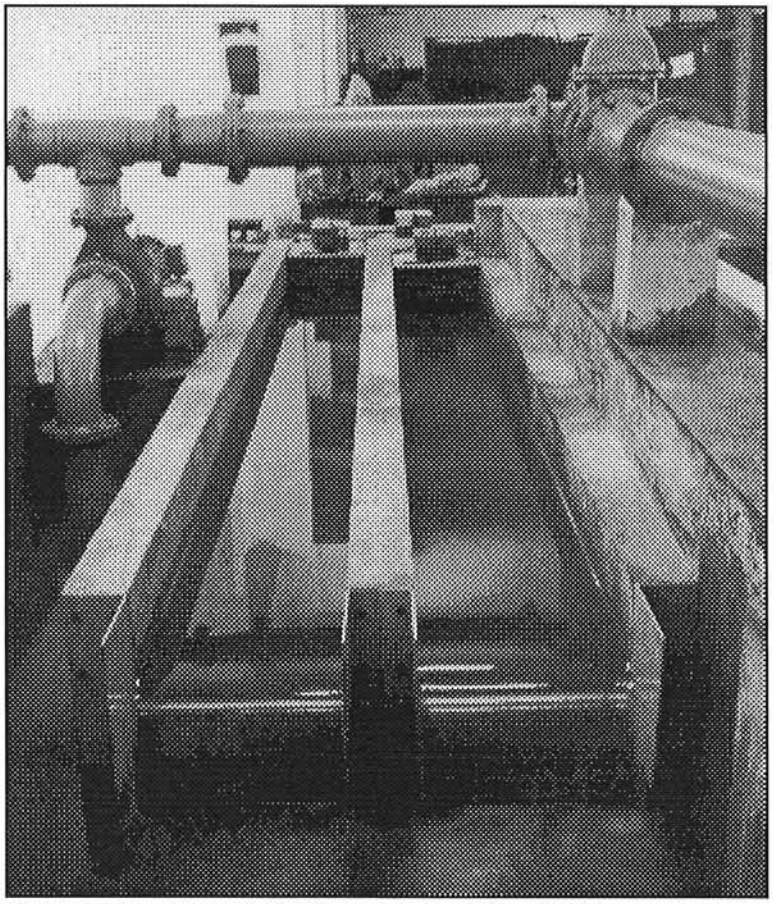

figure 11.13 - view on the approach channels and Rehbock weirs

11.4.6 The Rehbock weirs

The Rehbock weirs form the measuring facility of the test rig. Here the discharge distribution over branch 1 and 2 is measured. The weirs are placed at the downstream end of the approach channels. The construction of the weirs is rather complicated. They are fixed on a steel frame, which is incorporated in the reinforced concrete walls of the approach channels. Via this construction method the water is able to fall freely into the

downstream reservoir. That is very essential considering the absolute requirement of having an atmospheric pressure distribution under the weir. Otherwise the head-discharge equation of the Rehbock weir is not reliable, leading to inaccurate readings. The accuracy of the Rehbock weirs is the subject of Section 12.2; for specifications see Appendix E. To guide the flow over the weirs, so-called guiding plates are installed just behind and aside the weirs. These plates are also necessary in view of reliable measurements of the discharge. Attention has to be paid to the water level in the downstream reservoir. This level may not reach the guiding plates, because then atmospheric pressure is not assured anymore.
In figure 11.14 a view on the Rehbock weirs is given in running condition.

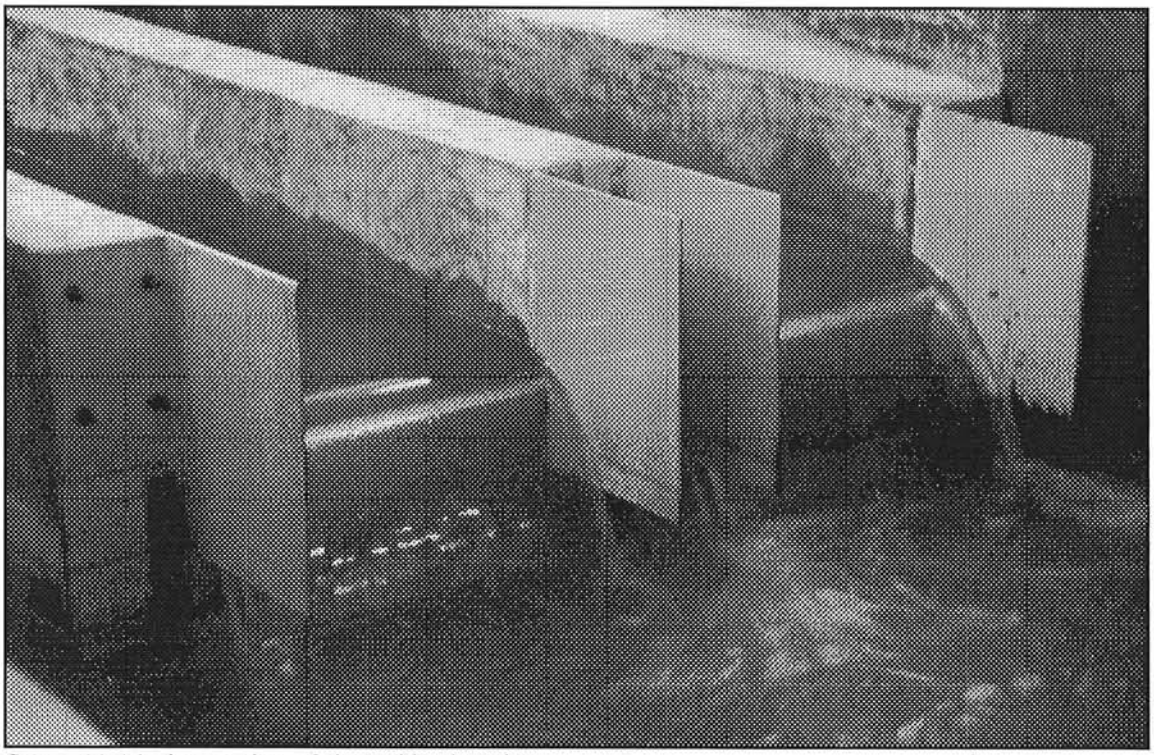

figure 11.14 - impression of the Rehbock weirs

11.4.7 The stilling basins connected with Rehbock weirs

For the measurement of the water height above the Rehbock weirs two stilling basins are built along the downstream reservoir. Due to lack of space it was not possible to construct them next to the weirs. According to ISO 1975, the water level has to be measured at a position 3 to 4 times the maximum level above the crest of the weir upstream of the place of the weir. Hence, at this spot, a hole is implemented in the floor of the approach channel, through which a pipeline was fixed. The pipeline (diameter $\varnothing = 1.5$ cm) connects the approach channel with the stilling basin (see figure 11.15). The

water level in the stilling basin is representative for the water level at the Rehbock weir. In the stilling basin the water level is measured with a point gauge.

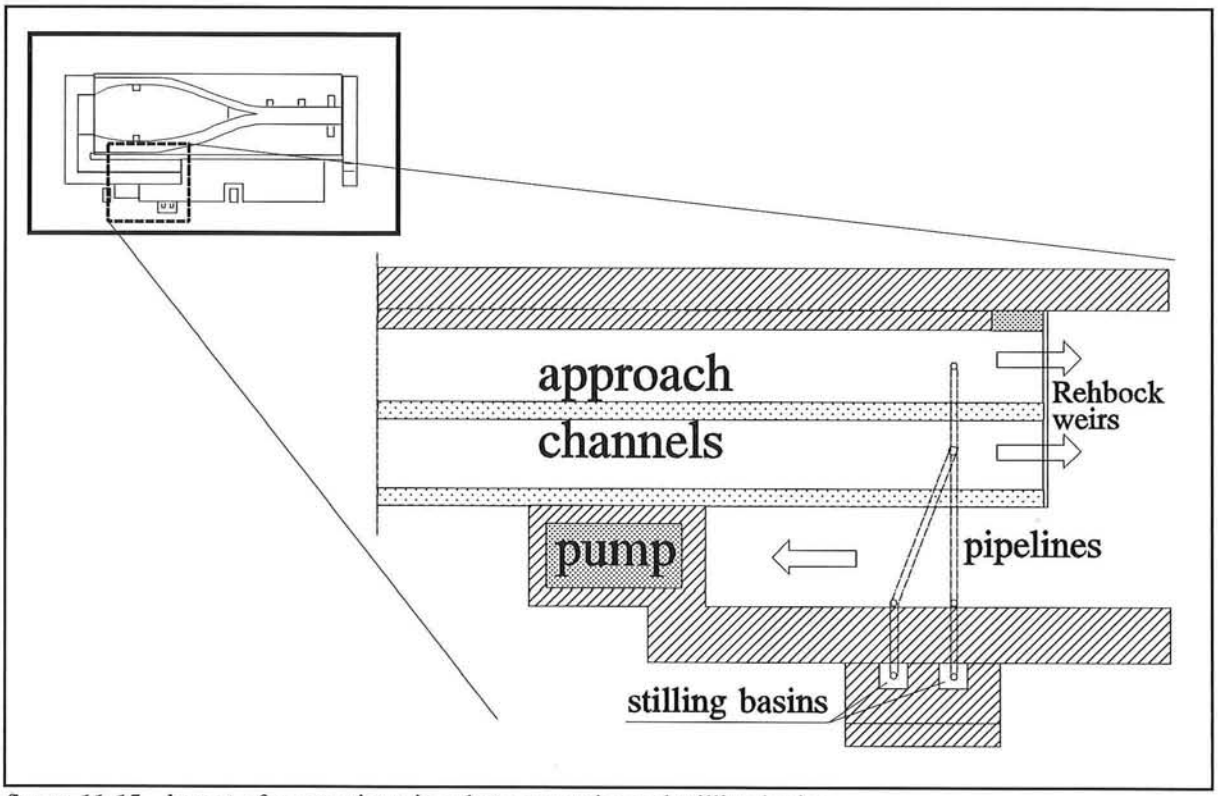

figure 11.15 - layout of connection pipes between weirs and stilling basins

Chapter 12 - Measurements

12.1 Parameters describing the system

In this chapter the measurements to be made during experimentation are discussed. Measurements will have to be made of the parameters describing a bifurcation. A list of these parameters is given here; the measurement *methods* applied are given in the following sections.

One of the aims of the experiments is to study the distribution of the sediment transport rates at a bifurcation, which can be theoretically described by a number of nodal-point relations. As seen in Part I, Wang et al.(1993) worked with the following general nodal point relation:

$$\frac{S_1}{S_2} = \left[\frac{Q_1}{Q_2}\right]^m \left[\frac{B_1}{B_2}\right]^{1-m} \tag{12.1}$$

B_1 and B_2 are known constants in the case of the model.

The unknown parameters S_1, S_2, Q_1 and Q_2 have to be measured; the methods applied are described in Sections 12.2 and 12.3.

The measurements of the water level (Section 12.4) and of the bed level (Section 12.5) are also necessary for several reasons:

* The factor m is dependent on the geometry of the bifurcation, and will most probably vary with the local width and depth of the branches. The depth is obtained by subtracting the water level from the bed level.
* The morphological behaviour of the branches, as a function of the shape of the bifurcation, is of great interest. For this reason the bed level in the branches must be measured at regular intervals. The final equilibrium slopes in the branches can also be determined by measuring the water level at the upstream and downstream ends of the branches.
* The measurements of the water levels at the ends of branches 1 and 2 are necessary for the setting of the downstream boundary conditions.

12.2 Discharge measurements

12.2.1 Introduction

The discharge is measured at two places: in the delivery pipe, where the inflow of the model is measured, and at the Rehbock weirs where the outflow is measured. The difference between these two discharges should be: $Q_{in} - Q_{out}=0$. If this is not the case then:
- there is a leak in the model which should be fixed;
- or, one of the two measuring devices (or both) is defective and should be fixed.

12.2.2 Measurement of the inflow

The discharge at the inflow is measured with an orifice installed according to the installation requirements found in ISO (1980). The discharge measured here represents the discharge Q_0 in branch 0. Specifications of the orifice dimensions are given in Appendix A.

12.2.3 Measurement of the outflow

As seen in Section 11.4 the individual discharges of branches 1 and 2 are measured with the respective Rehbock weirs. These weirs were made locally according to the specifications mentioned in ISO (1975). Details of the Rehbock dimensions are given in Appendix A. The water level at the crest of the weirs is measured in stilling basins (see Section 11.4) with point gauges, with an accuracy of 0.05 mm. The zeros of the point gauges were set by filling the two approach channels with water, up to the crest level of the weirs; the point gauges were then adjusted, and the zeros fixed.

12.2.4 Accuracies

The orifice was not yet fully operational, so no specific evaluation can be made of the accuracy of the measurements. However, the method to be used for the determination of the accuracy is given in Appendix F, including the sensitivity of the accuracy for the sources of possible errors.

The Rehbock weirs can measure the discharge properly up to a discharge of 60 l/s, with an accuracy (in the worst case) of 1.8 %. This is detailed in Appendix E.

12.3 Sediment transport measurements

12.3.1 Introduction

The sediment transport rates in branches 1 and 2 are determined with the help of the sand traps located at the end of each branch. These sand traps intercept all sediment transported through the branches. Once a sand trap is emptied and its content measured, the average sediment transport rate for the preceding branch is computed for the time-interval observed. This is done by dividing the amount of sediment by the time elapsed.

12.3.2 Volume of the sand traps

As can be found in Section 10.5 the storage capacities of the sand traps are:

- $V_{s1} = 0.63$ m^3;
- $V_{s2} = 0.72$ m^3.

Since the sediment transport is $S = 3.14\ 10^{-6}$ m^3/s (see Section 10.8), the maximum time interval for which the sediment transport rate can be determined is

$T_m = 0.63/3.14\ 10^{-6} = 200636$ s $= 55$ hours.

Obviously, the sand traps do not have to be filled completely. It is actually strongly recommended not to do so, since the value for the rate obtained would be insignificant: the shorter the time interval, the more information is obtained on the sediment transport (see below in Section 12.3.5). The only important thing is to keep track of the time elapsed for the sand trap to fill to the point that it will be emptied.

12.3.3 Emptying methods

The sand traps can be emptied once the model is put to a standstill. Water is always present in the model (see Section 10.6), so sediment can be siphoned out of the sand traps with a hose. The sediment concentration in the water being siphoned out is about 10 %. An alternative way of removing sediment from the sand traps is to place stop logs in the slots directly upstream of the sand traps, siphon out the water, and then scoop out the sediment by hand. This method is more time-consuming, but may be necessary if visibility in the water is too restricted: in that case, when siphoning out the sediment, it would not be possible to judge whether the sand trap has been completely emptied.

12.3.4 Measurement of collected sand

Once removed from the sand trap, the sediment is spread in a thin layer across the floor of the laboratory to let it dry; drying takes about four days (see also figure 13.2). The sediment is then weighed on a scale. This weight is translated into a volume (density of sand ρ_s= 2650 kg/m^3, porosity p= 40 %).

12.3.5 Accuracies

It is useless to define an accuracy for the sediment transport because the transport rate is an *average* for the time interval chosen. The transport rate will vary continuously, but it is not possible to measure these variations. The only way to get more detailed information on the *changes* in transport rates is to shorten the time intervals for which the sediment transport rates are determined.

12.4 Water level measurements

12.4.1 Introduction

The water level is measured at four places in the model, in stilling basins placed at the beginning and end of each branch (see figure 12.1). A description of the stilling basins and of the measurement methods applied is given in the following.

12.4.2 Stilling basins

The stilling basins I, III and IV are "fixed" stilling basins: they render the water level present in a fixed place of the adjacent branch, namely the water level immediately in front of it. As can be seen in figure 12.2 the water seeps through a hole in a wooden plate fixed in the wall of the branch. This wooden plate can be moved up and down to ensure that the seepage hole is always located between the water level and bed level. Stilling basin II, which is located near the bifurcation, is a "flexible" stilling basin : water levels at different places in the vicinity of the stilling basin can be measured. As can be seen in figure 12.3 the stilling basin is completely closed (i.e there is no connecting hole from basin to branch). The water is siphoned into the stilling basin via a Pitot tube mounted on a frame laid across the width of the channel. The Pitot tube can be moved to different spots in the channel so that it is possible to measure the water level at different places near the bifurcation. This may be necessary since different shapes of "noses" (see Section 14.2) will be applied which each induce different local flow patterns. It must be

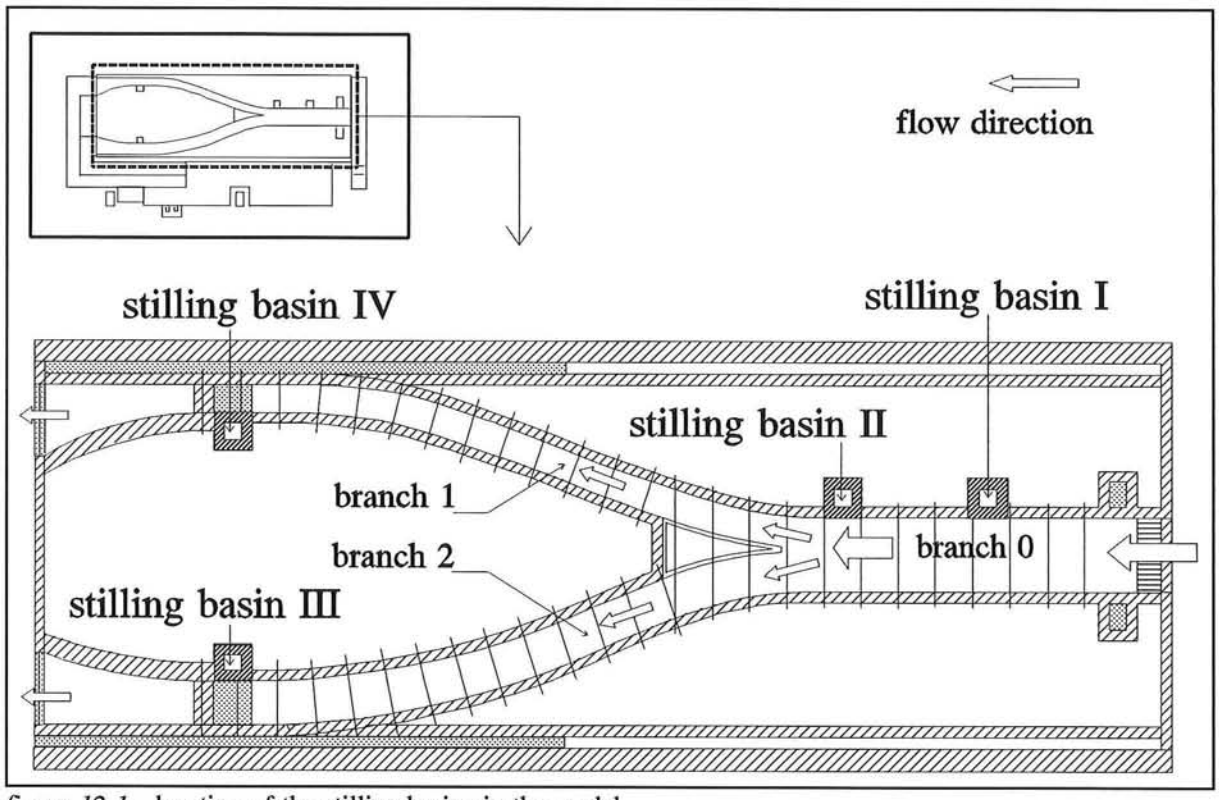

figure 12.1 - location of the stilling basins in the model

noted that the Pitot tube is merely used as a siphon, and not as a measuring device: the readings are done with a point gauge in the stilling basin (see Section 12.4.4), which gives more accurate readings.

12.4.3 Adjustment of desired water level

Stilling basins III and IV are placed directly upstream of the sand traps. They are used together with the tail gates to regulate the downstream water level. This water level must be checked at regular intervals during experimentation to ensure that the correct downstream boundary condition is being induced.

12.4.4 Measurement of the water level

The water level in a stilling basin is measured with a point gauge. The zeros of the four point gauges were set by filling the branches of the model with water, which made a horizontal reference-level to which all four gauges were related.

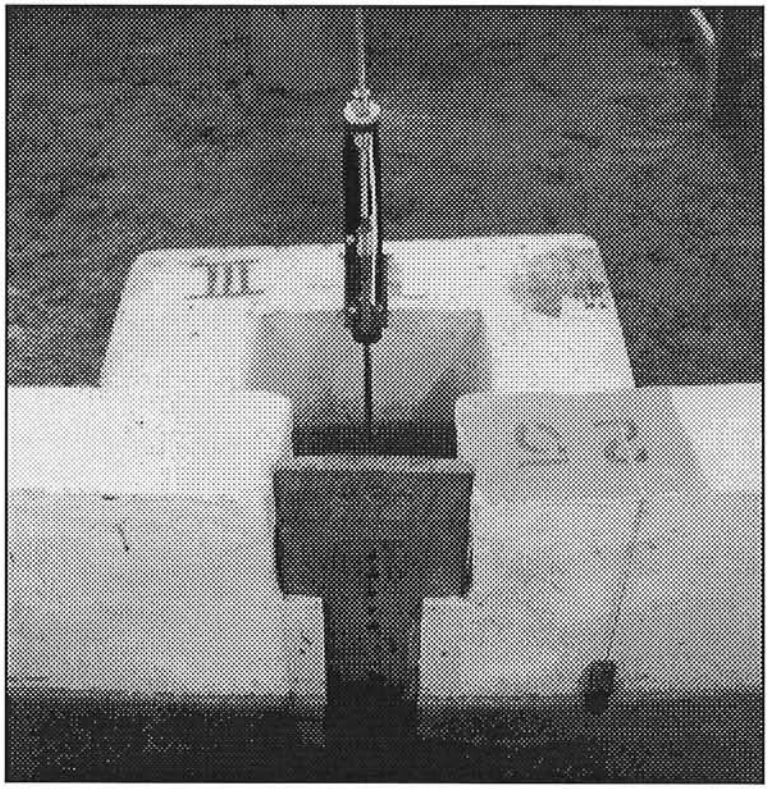

figure 12.2 - "fixed" stilling basin with a wooden plate through which the water seeps

12.4.5 Accuracies

The accuracy of the water level measurements is determined by the accuracy of the readings and the accuracy with which the zero was set. The error in h is defined as:

$$\epsilon_h = \sqrt{\epsilon_r^2+\epsilon_z^2+4\sigma_m^2} \tag{12.2}$$

where ϵ_r is the error made in the reading;

ϵ_z is the error made in the setting of the zero;

$2\sigma_m$ is the error in the mean of the readings.

The point gauges have a Vernier (i.e. Nonius) scale, so $\epsilon_r = 0.05$ mm and $\epsilon_z = 0.05$ mm.
The standard deviation in the mean of ten readings was $\sigma_m = 0.03$ mm.
As a result the water level can be measured with an accuracy $\epsilon_h = 0.09$ mm.

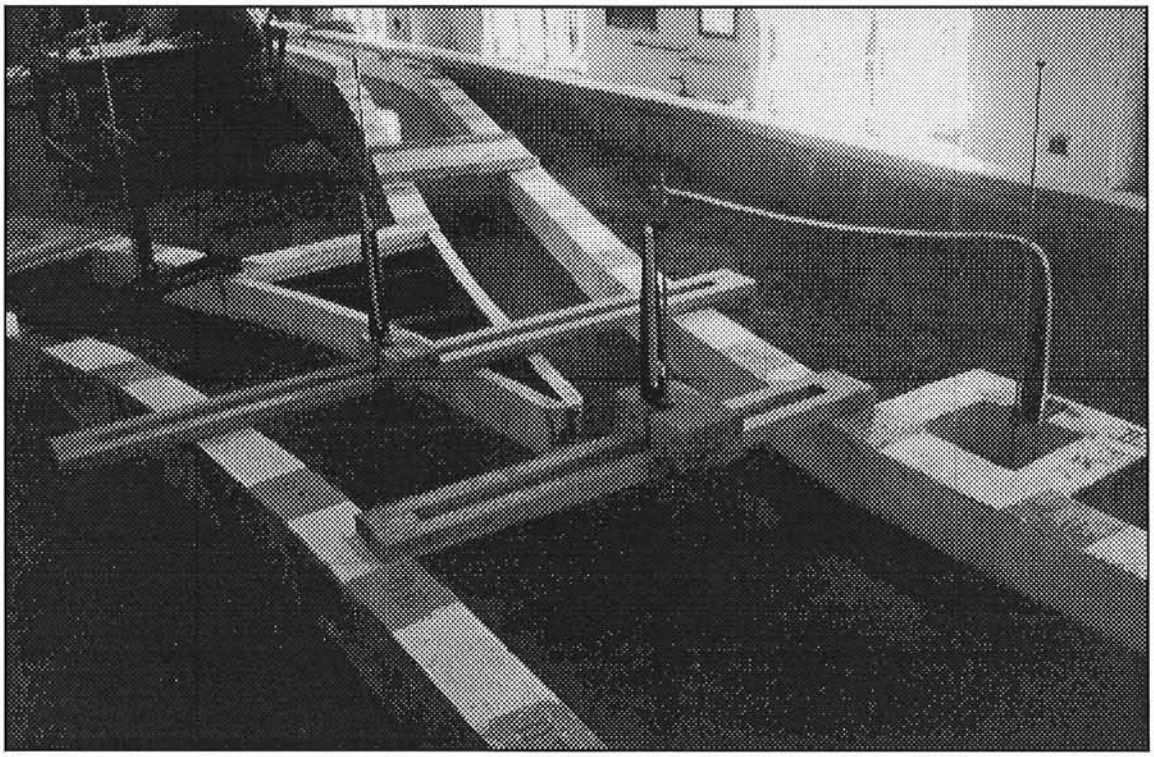

figure 12.3 - at right: "flexible" stilling basin with Pitot tube connection; at left: support structure of the bed level measuring gauge.

12.5 Bed level measurements

12.5.1 Introduction

The bed level is measured with a point gauge in which a special pin is used. A square plate of 2×2 cm^2 is fixed to the point of the pin to prevent it from sinking too deep into the sand bed. The gauge is mounted on a frame which is laid across the channel on the branch walls. A more detailed description of the measuring device and location of the measurements is given in the following.

12.5.2 Location of the measurements

The bed level is measured at intervals of 0.5 m ,in 39 marked cross-sections of the three branches (see figure 12.4). In branch 0 the bed level is measured in 5 points of each cross-section. In branches 1 and 2 the bed level is measured in 3 points of each cross-section.

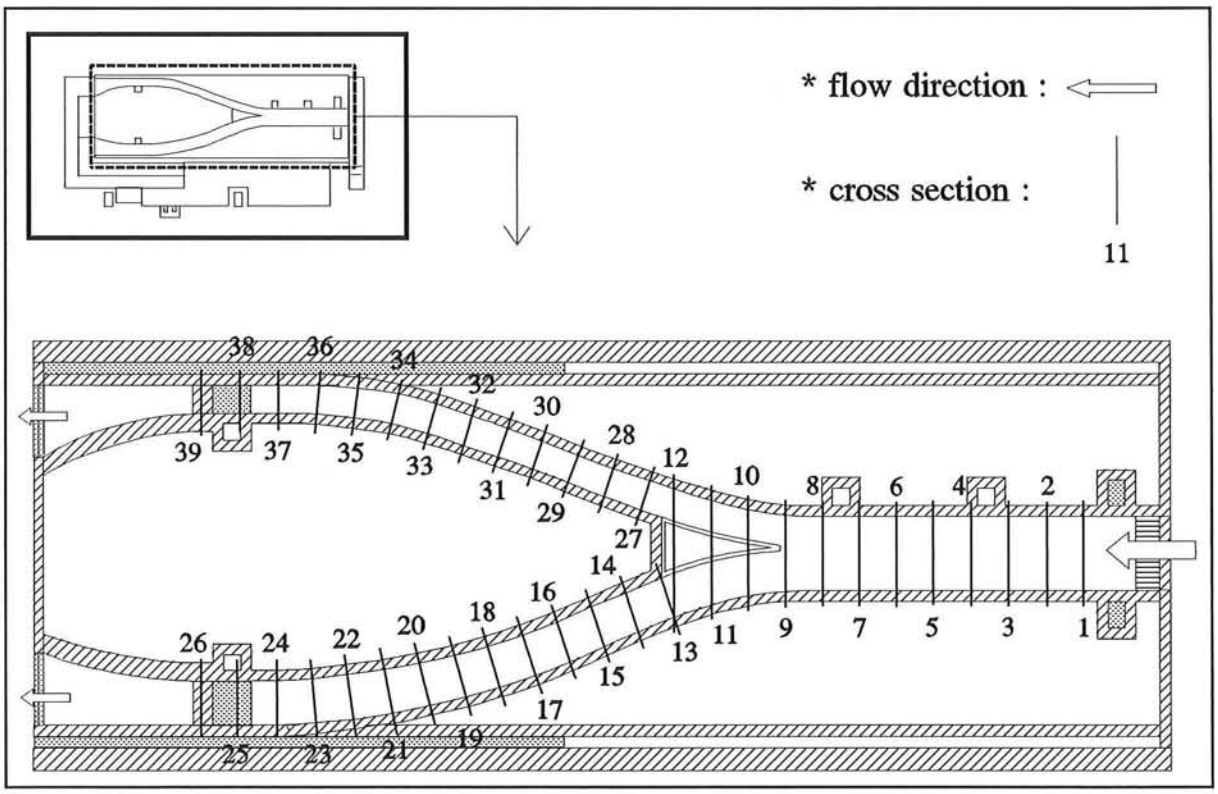

figure 12.4 - cross-sections where the bed level measurements are made

The measurements in the eight cross-sections of branch 0 are done more often than in the other cross-sections. The reason for this is that from the results of these measurements it can be checked whether an acceptable ratio between the upstream discharge and sediment supply from the sandfeeders is being put in at the upstream end. If this is not the case (e.g. branch 0 is silting-up quickly) then the necessary changes can be made (e.g. Q should be increased or S decreased).

12.5.3 Frequency of the measurements

At the outset of the experiments the interest of the writers is primarily focused on the course of the bed level once equilibrium is reached, and a general impression of the changes in time. It is therefore not necessary to measure the bed level at *all* cross-sections during the span of an experiment. It should be enough to make readings in only half of the cross-sections of branches 1 and 2 (the readings in branch 0 should *all* be done; see Section 12.5.2). The total time necessitated for the measurements is greatly reduced in this way. However, care must be taken to make readings at *all* the measurement points once equilibrium is reached.

Equilibrium is reached once:

* $S_{in} = S_{out}$;

* the bed level throughout the model is unchanging in time.

If the time-dependent morphological changes in the model become the main interest in later experiments, it will obviously be possible to make readings of the bed level in *all* cross-sections at all times.

12.5.4 Support structure

The measuring gauge is placed on a wooden frame which is laid across the width of the channel at one of the cross-sections previously mentioned (see figure 12.3). The gauge can slide on the frame across the width of the channel in order to make a measurement at the desired point of the cross-section. The frame is made of wood, which deflects slightly when placed across the channel. This deflection is in the order of 0.5 mm, which is considered negligible compared with the ultimate accuracy with which the bed level is measured (see Section 12.5.7).

12.5.5 Reference level

The supporting frame is placed on the walls of the branches. These, however, are not perfectly horizontal. Therefore the height of the walls at every cross-section was measured with a level with an accuracy of 0.1 mm, so that a virtual reference level could be made. The deviation Δh of the height of a particular cross-section from the reference level is simply added to the reading to get a correct measurement.

12.5.6 Range of the point gauges with pins

As seen in Section 10.7 the lowest possible bed level is L.B.F. +0.80 m. The highest possible bed level is L.B.F. +1.20 m; this is the bed level of a branch that is completely silted up to the surface of the water. Thus the range of bed levels to be measured is about 0.40 m. Since the available point gauges have a maximum range of 0.32 m, two different pins (see Section 12.5.1) with different lengths were made: one with a length of 0.05 m, and another with a length of 0.20 m (see figure 12.5).

This way an extra height of 0.20-0.05=0.15 m is available for the bed level measurements. As a result, the range for the bed level measurements is:

0.32+0.15=0.47 m.

The zero of the point gauge for the bed level measurements was set with the short pin. Care must therefore be taken to note which pin is being used when a measurement is made. If the long pin is used, then the "extra" length of 0.15 m must be discounted from the reading.

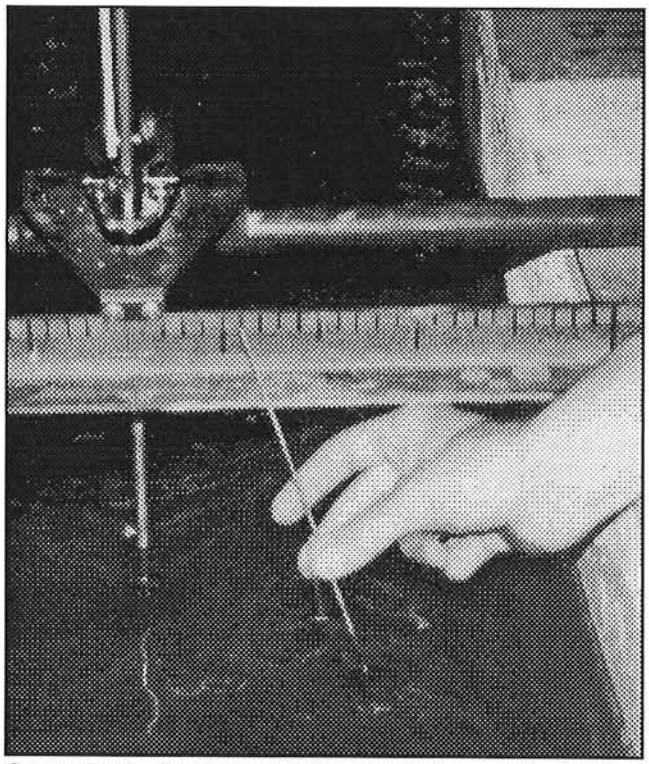

figure 12.5 - the long and the short pin used in the bed level measuring gauge

12.5.7 Sinking-in of pins

As already mentioned the pins have a 2×2 cm^2 plate fixed to the point. This plate was meant to prevent the gauge from sinking very deep into the bed of the river. Despite this plate, the pin still sunk into the sand quite a bit.

With the advice of a supervisor an attempt was made to measure the bed level in a consistent way, in order to obtain a "constant" sinking-in which could be discounted from the readings. The method applied turned out not to be very successful, as can be seen in the following.

The pin of the gauge was dropped onto the bed from a fixed height so that it might land on the bed with a constant impact. Ten readings for each pin were made in this way at places where the actual bed level was also carefully measured. The reading subtracted from the actual bed level gave the unknown sinking-in of the pin Δz. From these ten readings an average $\Delta\overline{z}$ and a standard deviation σ for each pin was determined:

* for the short pin $\Delta\ \overline{z}_s = 16.7$ mm
  $\sigma_s = 4{,}5$ mm
* for the long pin $\Delta\ \overline{z}_l = 24.2$ mm
  $\sigma_l = 6.9$ mm

These standard deviations are obviously very large, leading to unacceptably large errors in the readings. The measurement method for the bed level must therefore be improved; suggestions are given in the following.

12.5.8 Accuracies

The standard deviations of the sinking-in are too large. The local water depth is about 0.10 m; as a result the relative error for the water depth is at least X_a=0.0045/0.10= 4.5 %, when considering *only* the error made with the sinking-in. This error is unacceptable and must therefore be reduced.
In order to improve the measurements, the standard deviations of the sinking-in must be minimized. In the next section the *causes* of the inconsistencies in the sinking-in are given, as well as alternative solutions for the measurement methods.

12.5.9 Improvement of the accuracy

There are two problems with the chosen bed level measurement method.

- The first problem lies in the design of the pin applied to the point gauge. The square plate at the point of the pins is *fixed* to the pins, at a 90° angle with the pin. Due to the presence of the bed forms in the sand bed, the bed and the plate will not always be parallel (see figure 12.6). Thus the weight of the pin will not always be distributed over the same plate area. Consequently different sinking-in depths occur, as can be seen from the standard deviations of the two pins. A remedy for this problem is to make a flexible joint between the plate and the pin, so that the plate can follow the slope of the bedform. A fixed plate was originally chosen because it was relatively simple to make. Whether a flexible joint can be made in Dhaka will have to figured out locally. A drawback of this design, however, is that, as a result of the flexibility of the joint, the fixation of the plate with the pin is loose; this goes to the expense of accuracy.

- The second problem with the measurement method applied is the fact that the pin is *dropped* onto the bed. The method *was* consistently applied (see above); however, the packing of the sand is not constant throughout the branches. If the sand is loosely packed at one point (e.g. on a steep bed form slope), then the pin will sink in deeper than at another place where the sand may be more densely packed (e.g. the trough between two bed forms), even though the pin is dropped from the same height. To improve the accuracy of the measurement with respect to this problem the pin can be lowered to the bed level slowly by hand, until bottom resistance is felt, at which point the reading is made. This method is more time-consuming, and within the scope of the experiments *may*

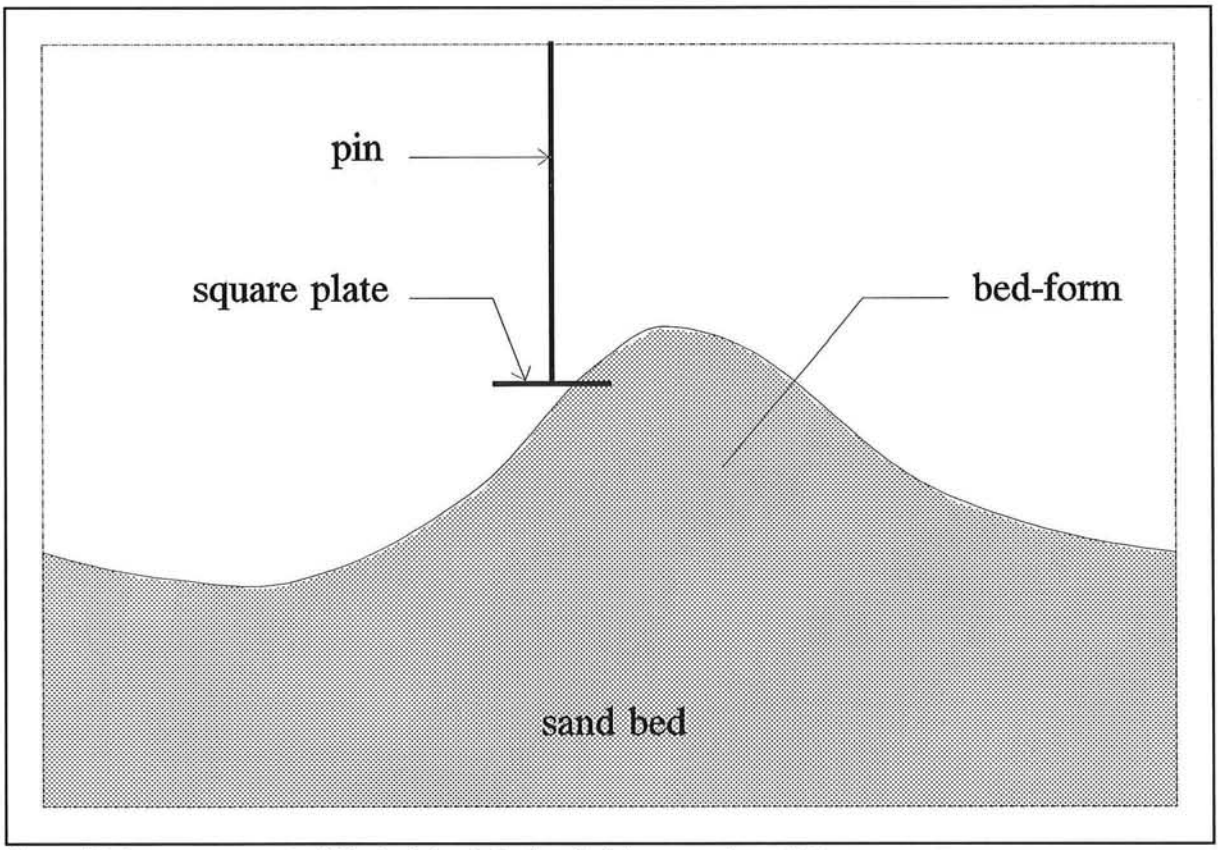

figure 12.6 - measurement of the bed level: bed and plate are not parallel

result in the necessity to reduce the amount of bed level measurement points. This, of course, depends on how much more time-consuming the new method is.
For the record it can be noted here that the best bed level measurements are generally made when using a electronic *Profile Indicator*, which was developed by DELFT HYDRAULICS. This is a fully automatic measuring device which can give a continuous reading of the bed level along the length of the branches, with an accuracy in the order of magnitude of the sediment-grain diameter. However, because of high costs and significant maintenance requirements, it is not feasible to place a Profile Indicator in the Laboratory at BUET for the time being.

Chapter 13 - The running of the model

13.1 Introduction

Smooth experimentation asks for an adequate handling of both the temporary (the experimental model) and the permanent part of the test rig. To provide a satisfactory running of an experiment a lot of information about the test rig is required. After two weeks experience the writers gained some knowledge themselves on running the particular test rig. Together with the advice and remarks of people experienced in experimental research present in Dhaka, this knowledge has resulted in a sort of *manual*. The information is roughly divided into two items viz. information on *starting the test rig* and information on *running experiments*. These items are described in the following sections. Some remarks have already been mentioned in previous chapters.

13.2 Starting the test rig

13.2.1 The reason for a starting procedure

As mentioned earlier it is not possible to continue an experiment at night, due to reasons of safety as well as lack of occupation of the model. Moreover, taking measurements would have to be continued during the night, which is not recommendable because that results in different working shifts. This makes it necessary to get started every day again. Starting the test rig includes fulfilling a list of successive operations. This procedure concerns the handling of some elements of the experimental test rig.

13.2.2 The pump

Before starting, the pump first needs to be *primed*. Priming of the pump means filling the suction head and the volume of the pump itself with water to prevent a refusal while starting the pump due to suction of air. Attention must be paid to a small valve on the pump, which should be closed. Otherwise suction of air via this valve results in a reduction of the capacity of the pump, thus delivering a lower discharge.
Despite maintaining a water level in the downstream reservoir above the minimum allowed water level, suction of air through the suction pipe connected at the pump is still possible. This can be concluded from a visible vortex. The resulting problem of a

decrease in maximum discharge is easily overcome by placing wooden boards on the water surface around the suction pipe to prevent the vortex from reaching the water surface.

13.2.3 The valves

Both the excess and the supply pipe have a valve for the regulation of the discharge. A valve influences the flow rate by changing the flow area locally. This happens via the vertical movement of a round steel plate inside the valve. A wheel on top of the valve is turned to determine the vertical position of the steel plate and thus to determine the discharge. The T-joint above the pump divides the water over the two pipe lines proportionally to the installation of the two valves. In combination with the orifice in the supply pipe the desired discharge for the experiment is delivered by adjusting the valves in the correct position.
After starting the pump first all the water goes through the excess pipe (see figure 11.5). By turning the valves smoothly the discharge through the supply pipe and hence in the model will increase until the desired inflow is reached.

13.2.4 The tail gates

At the end of an experimental session the pump is stopped and the tail gates are raised to prevent the water within the model from flowing away and hence causing a dry bed. This has unacceptable consequences for the bed level (see also section 10.6). While starting the test rig, the tail gates are lowered in combination with the increasing inflow of water. This adjustment must happen smoothly, as no disturbances in the bed level may be initialised. Otherwise the bed level measurements will be influenced.
The tail gates can be seen as the representation of a downstream boundary condition. The tail gates are adjusted according to the desired downstream water level. When the discharge is increasing during the start of an experimental session, a first idea of the desired water level is derived from a small wooden block which (lowest point) is positioned at this level. These wooden blocks are hung in front of the sand trap. Further on, each of the tail gates is adjusted according to a reading of the water level in the stilling basin of the particular branch (see figure 13.1).

13.2.5 The sandfeeders

Depending on the calculated sediment transport a choice as to which sandfeeder is applied has to be made. The sandfeeder, manufactured by BUET, has a wide range of possible capacities. When starting the experiment and consequently the sandfeeder, it is necessary

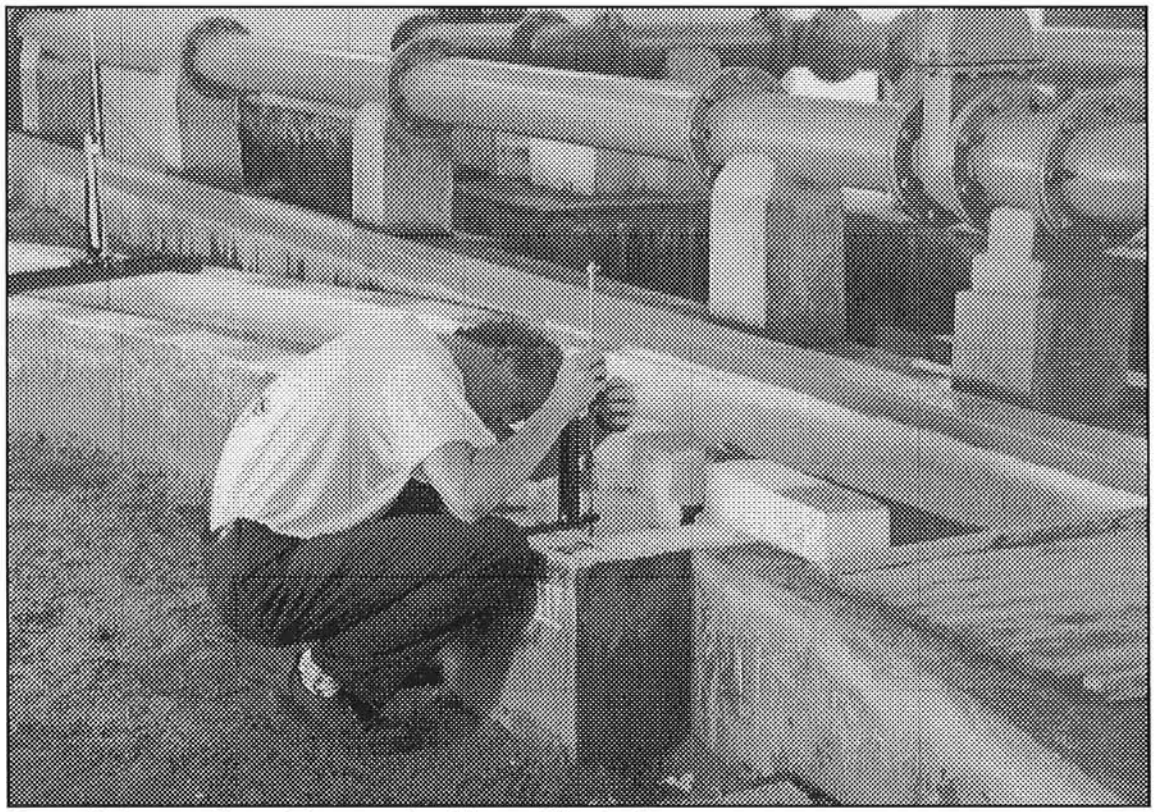

figure 13.1 - a reading of the water level in a stilling basin

to check if there is enough sand available in the stock cylinder of the sandfeeder.

13.2.6 Sequence of operations

Starting the test rig means fulfilling a list of successive operations. First of all the tail gates are placed in the lowest position possible without losing water from the model. At the same time the pump is primed. After ensuring that the valve in the supply pipe is closed, the pump is started. Consequently this valve is opened slightly to fill the supply pipe slowly so that the air behind the orifice can escape. When water is flowing in the upstream reservoir the water will also enter the model and thus the tail gates are lowered. The proces of almost simultaneously opening the valve in the supply pipe and closing the valve in the excess pipe, together with lowering the tail gates, must happen very gradually. The valves are turned until the desired discharge is reached. The position of the tail gates is correct if the imposed downstream waterlevel is present. When the water flow is satisfactorily installed, the sandfeeders can be switched on. This completes the starting procedure.

13.3 Running experiments

13.3.1 Twofold division

After starting the test rig, attention has to be paid to keep it going without creating any discontinuities in the experimentation. Also some advice and suggestions for the measurements of the different physical parameters are given.

13.3.2 Keep the model running

To secure a smooth and steady running of the model the following things need to be checked every now and then:

- The stock cylinder of the sandfeeder has to be filled at time intervals dependent on the desired sediment transport rate, to assure a constant input of sand into the model. The sand which will be used for the experiments has to be dried. In case new sand will be put in the sandfeeder it is very important to first wash this sand. This prevents the presence of much wash load in the whole test rig and consequently having a very dirty model and test rig as well (see figure 13.2).

figure 13.2 - drying of the sand

Controlling an equal distribution of sand over the width of the upstream branch is very essential for creating an acceptable bed form at the beginning of the experimental model.

- The occurrence of a vortex near the suction pipe in the downstream reservoir has to be checked. As already mentioned, wooden boards on the water surface prevents this vortex.
- Despite the idea of having all the bed load captured in the sand traps some sand might get in the guiding and approach channels. This sand can cause a few problems. The guiding vanes and the tubes in between these flumes may silt up after some time. Also the connection pipes between the approach channels and the stilling basins to measure the water height above the Rehbock weirs must be free of sand. These two points have to be checked (see figure 13.3).

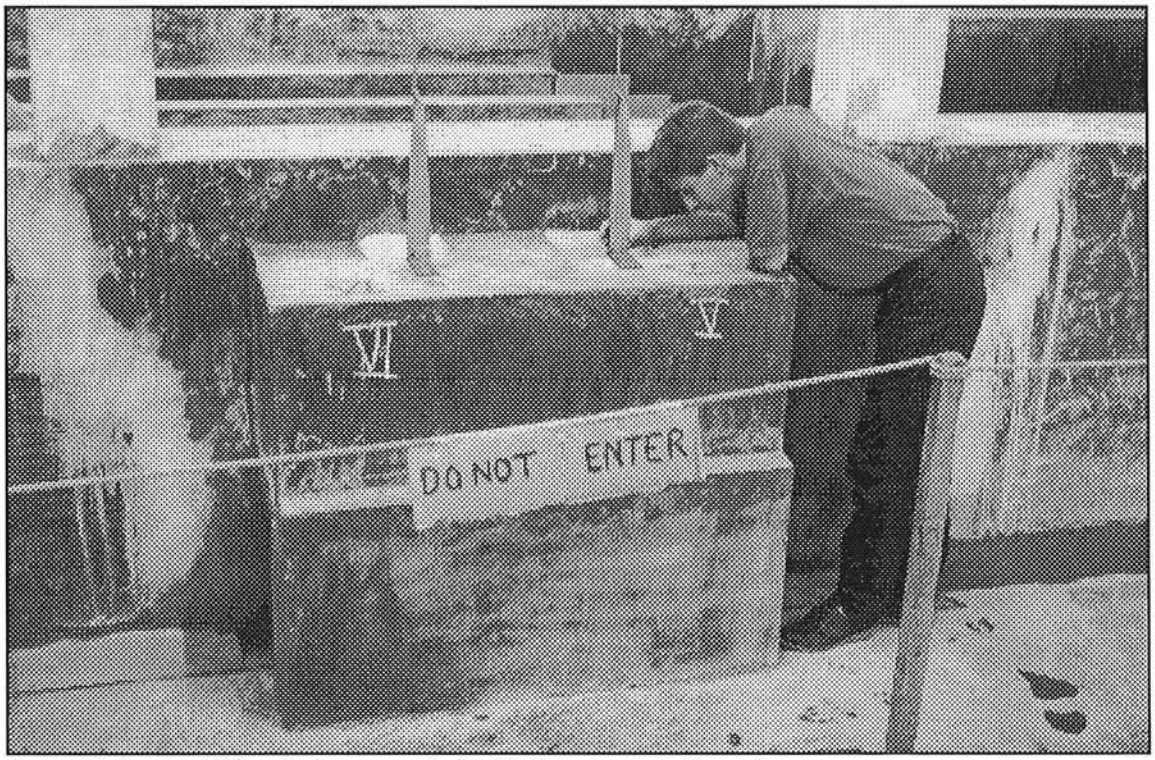

figure 13.3 - the stilling basins connected with the approach channels

- Important for having an acceptable flow over both tail gates and the Rehbock weirs is the presence of atmospheric pressure under these structures. This especially holds for the Rehbock weirs because the absence of atmospheric pressure will affect the water flow over the weirs, thus giving a wrong impression of the discharge in the respective branches. Any deviation of this atmospheric pressure must be prevented.
- The Rehbock weirs are placed in a steel U-frame. For a correct water level measurement, there should not be any leakage. Therefore so-called *pudding*, a soft kind of clay, is used to close the openings between the weir and the frame. The adhesion of this pudding has to be checked once in a while.

- The previous point also holds for the tail gates. Here pudding is applied to prevent leakage resulting in an empty model the next day.

13.3.3 Doing experiments

Keeping the model running is a different matter then carrying out experiments. Considering these experiments one has to think of some aspects next to the things mentioned in the previous section:

- The use of standard forms for the physical parameters to be measured makes the monitoring of the morphological processes in the model much easier. These parameters are the bed level, the water level and the discharge. The different standard forms made by the writers are presented in Appendix G.
- Depending on the goals of the experiment the tail gates have to be adjusted every now and then. If the downstream boundary condition (e.g. the tail gates) must represent a sea level, then the water level at the stilling basins in front of the sand traps have to be kept constant in time.
- The character of the experiments on bifurcations makes it essential to maintain an equilibrium situation in the upstream branch 0. This implies a constant bed level. Hence, especially during the first hours of an experiment, the bed level in branch 0 has to be measured more frequently. Dependent on a situation with erosion or sedimentation, the supply by the sandfeeder is increased or decreased respectively.
- Attention has to be paid to the type of sand used during the experiments. As the sand is bought on the local sand market, one is dependent on the available sand types. The average grain size of these sand types has no constant value. In case it is necessary to buy more sand, it will be impossible to buy sand with the same D_{50}. This demands a thorough estimate of the total amount of sand necessary for the running of the experiments.
- Also important is to check whether the discharge delivered by the pump is constant or not. Perhaps the discharge can be irregular due to variations in the electricity supply to the WRE-building.
- The water levels as well as the bed levels are measured by means of a point gauge. As mentioned in Chapter 12 a point gauge has a reference level which is installed by setting the zero at the beginning of an experiment. In case this zero level is disturbed, the next measurements are useless. To know whether the reference level is changed these levels have to be sealed. This can be done by putting paint over the reference zero marker. When the seal is broken, one must be suspicious about the measurements.

- For the sake of running smooth experiments the test rig should also be kept as clean as possible. Therefore several wooden boards are made making it easy to walk over the branches in the test rig. No step should be taken on the walls of the experimental model. Persuading everyone to walk on the prescribed paths is in the interest of succesful experiments. Prof. de Vries suggested to paint the concrete walls of the test rig in white. This makes maintenance much easier.

13.4 Stopping the model

At the end of an experimental session the test rig is stopped. The discharge through the model is therefore gradually decreased to zero. At the same time the tail gates are raised to keep the sand bed filled with water. The next procedure has to be followed:

- First the sandfeeder is stopped;
- The valve in the supply pipe is closed and the valve in the excess pipe opened;
- Simultaneously with the previous point the tail gates are raised;
- Finally the pump is stopped.

Chapter 14 - Recommendations for possible experiments

14.1 General

As the term *temporary* part of the model already indicates, the experimental model applied in the test rig can be adapted to the desires of the user. Consequently countless possible experiments can be carried out. During this thesis work the writers only focus on bifurcations and in particular on experiments with the bifurcation model as built in the WRE-laboratory in Dhaka. Although the writers have not been in the position to experiment themselves, they have considered a number of possible experiments.
As already mentioned in Part I the local three-dimensional flow pattern around the bifurcation determines the sediment distribution (Bulle, 1926). The distribution of water over the two branches is determined by the bathymetry of the downstream branches. The writers' main interest concerns the research of the sediment distribution dependent on the shape of the bifurcation.

14.2 Experiments with different bifurcation tips

To investigate the influence of the shape of the bifurcation on the sediment distribution three different tips or noses have been designed:

- one symmetrical nose (see figure 14.1);
- two asymmetrical noses from which one tip is directed towards branch 1 reducing the inflow area of this branch with 50 percent with respect to the symmetrical tip (see figure 14.2); the second tip is directed opposite and reduces the entrance of branch 2 by 50 percent (see figure 14.3).During the experiments with these three different noses, the sediment transport and the discharge in both the downstream branches are measured. Eventually the experimental results may lead to a better insight in the relation of the shape of the bifurcation to the sediment distribution over the downstream branches as a function of time. And finally may lead to a better understanding of islands in rivers. Also the experiments treated in the next section can add to the knowledge on this matter.

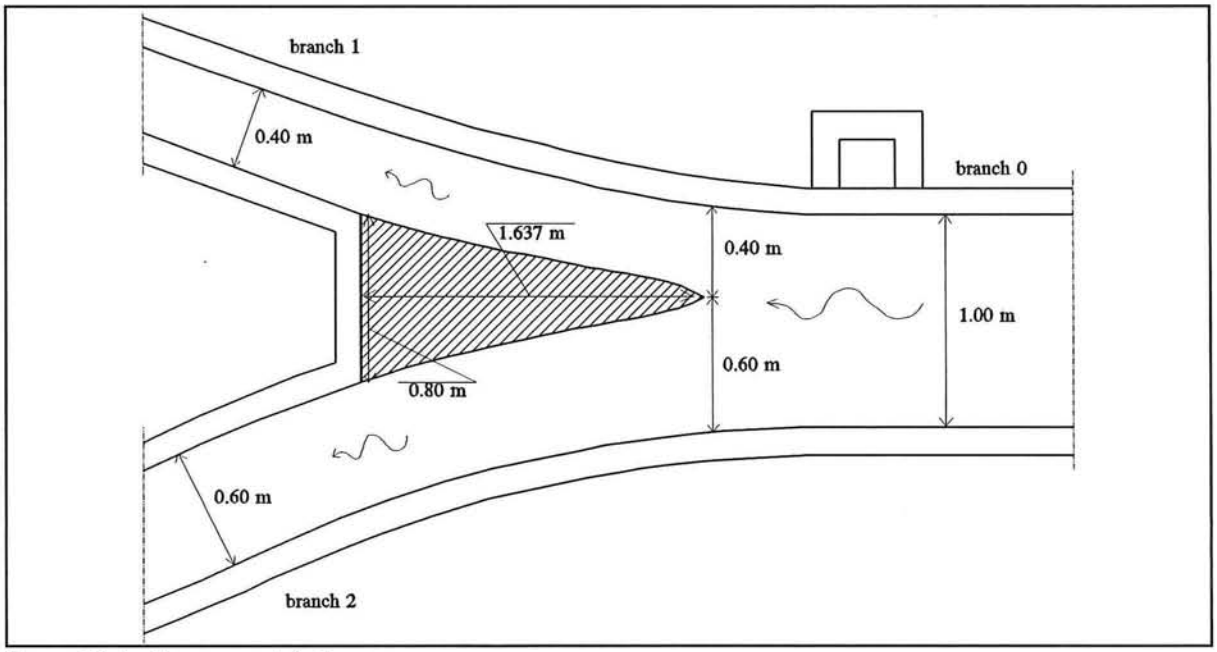

figure 14.1 - the symmetrical nose

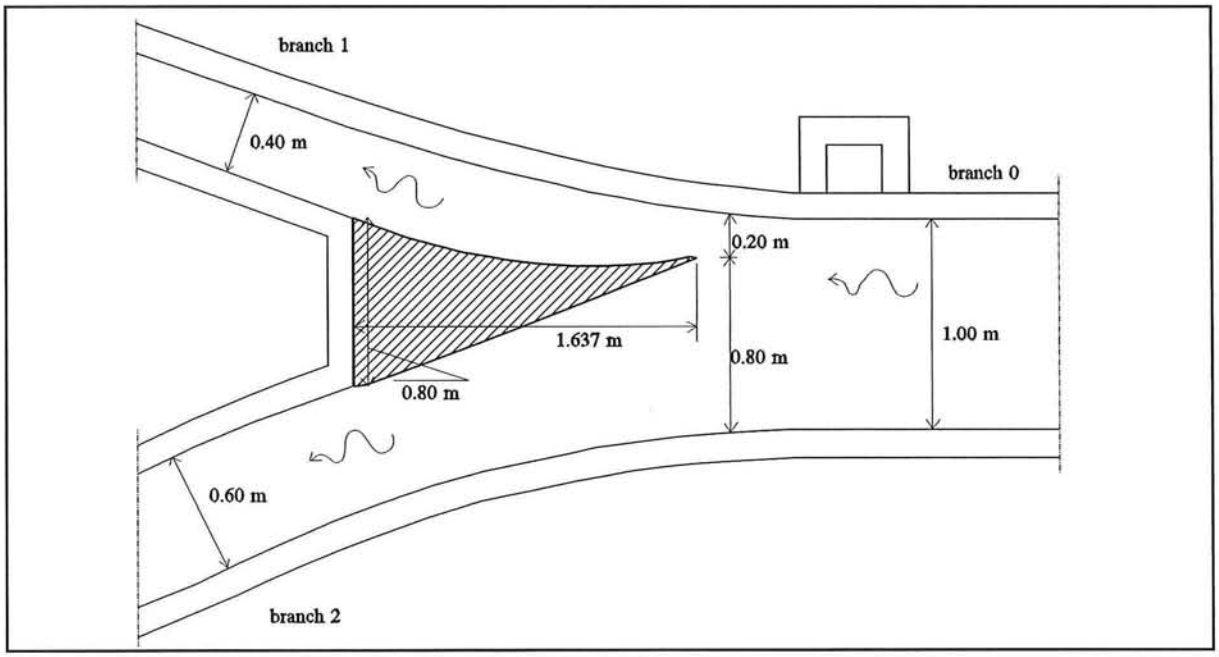

figure 14.2 - the asymmetrical nose directed towards branch 1

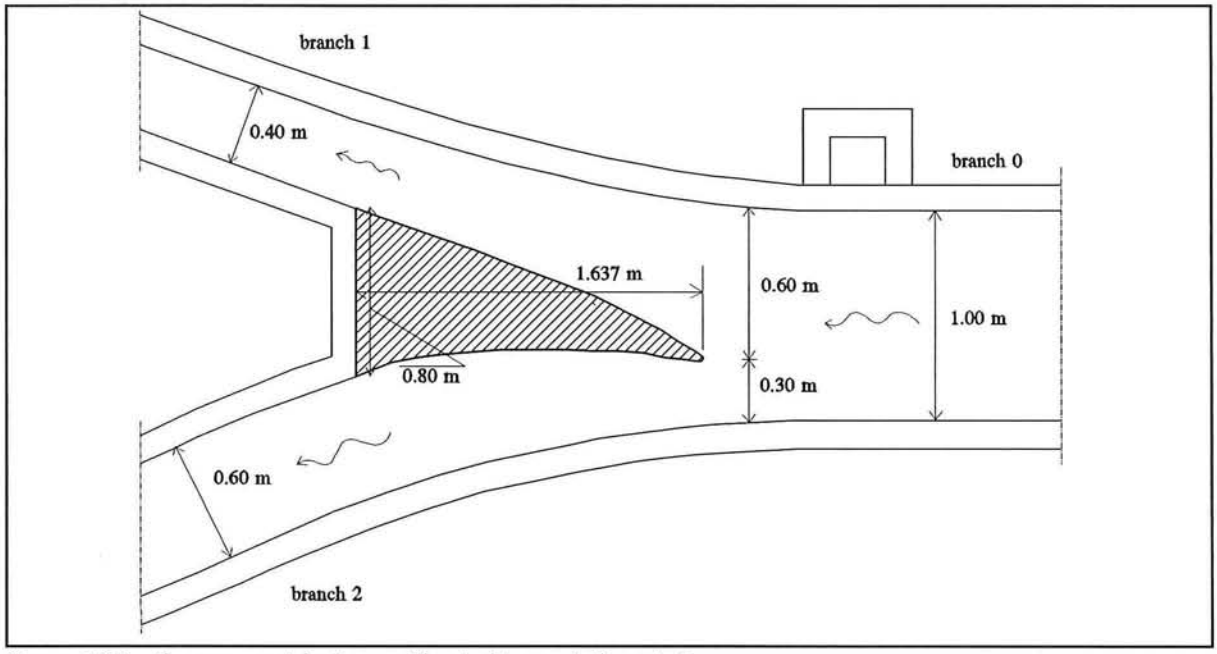

figure 14.3 - the asymmetrical nose directed towards branch 2

14.3 Other possible experiments

Besides the experiments with the different noses, more possibilities exist to vary the experiments. Altering for example the bathymetry of the downstream branches influences the morphological process and thus the bed level development. Each of these changes can be applied independent of the bifurcation tip used in the particular experiment. In order to acquire a complete view on the behaviour of bifurcations a number of essential variations have to be applied. These variations are discussed below:

- First of all the tail gates give the possibility to introduce different lengths of the two branches. This is represented by a different (constant) water level over each of the tail gates. Hence the equilibrium slope in the branches is not the same. In this way an infinite number of situations can be introduced.
- Instead of maintaining a constant downstream water level during an experiment, implying an outflow of the branches in a sea, the water levels also can be changed constantly during an experiment. This application introduces an experiment in which the model, although resembling half an island, actually represents the case of a whole island. Hence the tail gates are placed at a position somewhere along the island. That implies the presence of continuously varying water levels dependent on the

morphological developments. The adjustment of the water levels is obtained by adapting the position of the tail gates. This option is a very complicated one, because the necessary water levels have to be computed with the use of a numerical model. In that case the following sequence of actions must be followed:

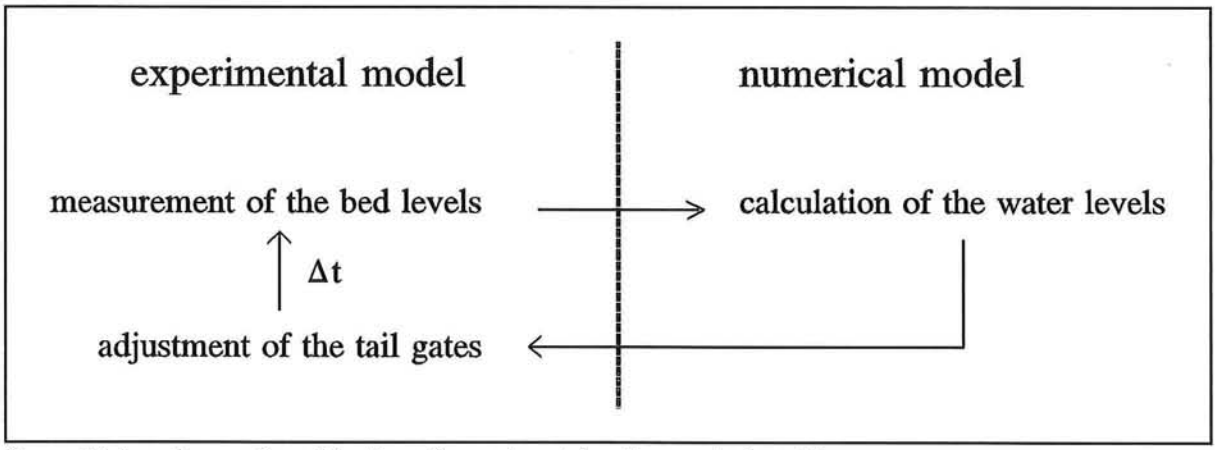

figure 14.4 - scheme of combination of experimental and numerical model

- Changing the bathymetry is possible in many ways. Easy to construct is a change of width. In that way a groyne can be represented. Also the initial bed level can be varied. Hence the morphological development will be different.

14.4 Conclusion

In order to have a total view on the morphological processes around islands in rivers, the writers recommend an experimental program in which the prescribed variations will be implemented. Such a thorough research on the bifurcation problem hopefully leads to valuable results making the use of numerical programs more convenient and reliable. In other words, these experiments hopefully give a more reliable general nodal-point relation, which for example can be adapted to local circumstances with the use of specific parameters.
This can be clarified with the next two examples of nodal-point relations, applied in the numerical program Wendy.
The first formula is

$$\frac{S_1}{S_2} = \alpha\left[\frac{Q_1}{Q_2}\right]+\beta \tag{14.1}$$

One has to think of a prescribed value of α and β dependent on the shape of a bifurcation. Perhaps, as the geometrical features around the bifurcation and the downstream branches vary in time, also the values of α and β are a function of time.

Also used is

$$\frac{S_1}{S_2} = \left[\frac{Q_1}{Q_2}\right]^m \left[\frac{B_1}{B_2}\right]^{1-m} \tag{14.2}$$

In this case the value of m can be related to a specific shape and situation. The value of m will probably be a function of time as well. As seen in Part II, the link between the value of m in Eq. (14.2) and the physical configuration of the bifurcation can be done via computations in the computer program WENDY. The scaled dimensions of the experimental model are used as an input in WENDY; the program is then run for different values of m, keeping track of the resulting morphological time-scale. When the same morphological time-scale is found in WENDY as in the experiments, the calibration is complete, and a link is made between theory and experiments. For a flow chart of this process see figure 14.5.

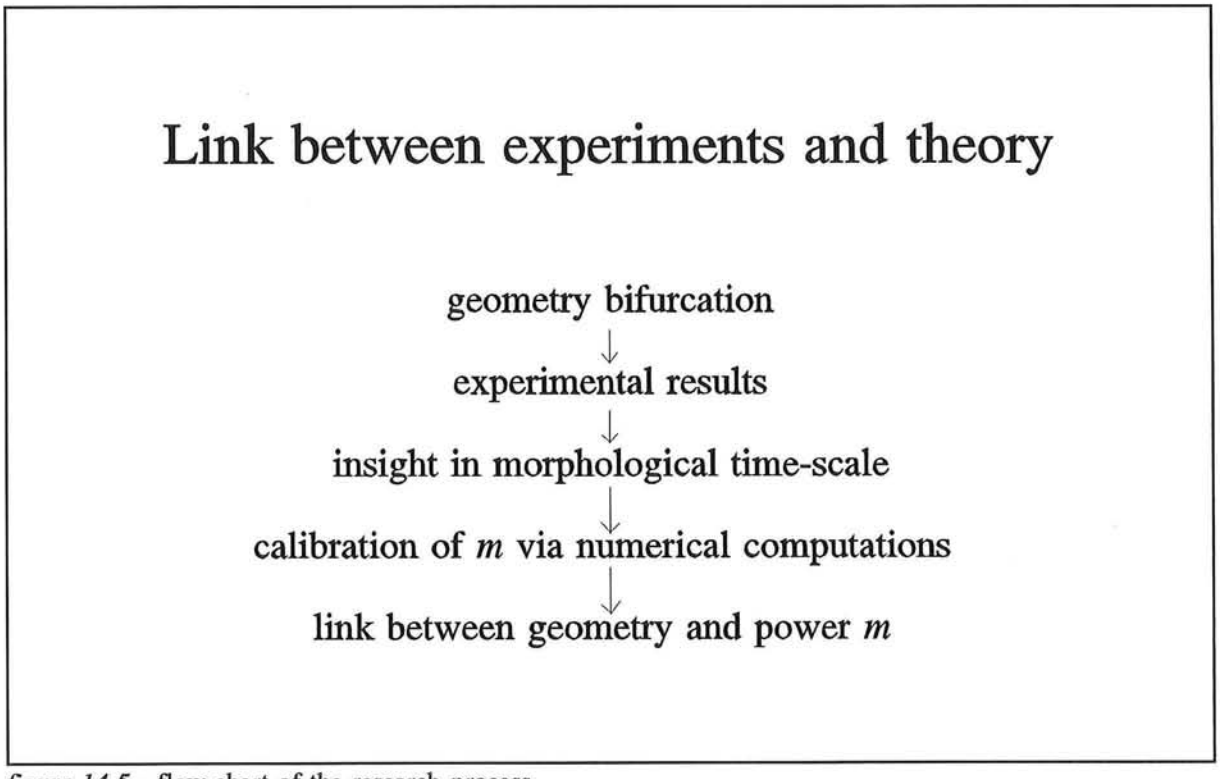

figure 14.5 - flow chart of the research process

One has to realize that a complete view on this subject can only be obtained after a great number of different experiments. Even then one must realize that these experiments are done with a physical model in a laboratory, which is still a schematization of a real-life situation. Nevertheless, with the results of these experiments it could be possible to develop a reliable nodal-point relation which can be used for numerical 1D-modelling.
If this leads to good results, the more extensive development of a 3D-model (the ultimate solution) would not be necessary.
The continuation of this research project is therefore strongly recommended; hopefully the results obtained by the next set of students going to Dhaka will lead to some interesting conclusions.

References

Bos, M.G. (1989). *Discharge measurement structures* (3rd edn.). ILRI, Wageningen.

Boreli, M. and S. Bruck (1957). *Note on the stability of river branches for the design of diversions* (in French). Proceedings of the IAHR Congress, Lisbon.

Bulle, H. (1926). *Investigations on the trapping of bed-load in branching rivers* (in German). VDI-Verlag, Forschungsarbeit auf dem Gebiet des Ing. wesens, Berlin, Heft 283.

Dekker, P. den & J.M. van Voorthuizen (1993). *Detailed design for an experimental research on bifurcations.* Preliminary studies for MSc. thesis-work; unpublished manuscript.

Engelund, F. and E. Hansen (1967). *A monograph on sediment transport in alluvial streams.* Teknisk Forlag, Copenhagen.

Flokstra, C. (1985). *The influence of nodal-point relations on the bed level at bifurcations - 'Report mathematical analysis'* (in Dutch). Report R2166, DELFT HYDRAULICS.

Gasser, M.M., A.F. Ahmed and M.T.K. Gaweesh (1990). *Scaling and calibration of a movable-bed model.* Proc. national conf. on hydraulic engineering, ASCE, Hydr. Div., San Diego, California.

Hütte (1955). *Der Ingenieurs Taschenbuch I, Theoretische Grundlagen* (28e Ausgabe). Berlin.

ISO (1975). *Liquid flow measurement in open channels using thin-plate weirs and venturi flumes.* ISO, Geneva.

ISO (1980). *Measurement method of fluid flow by means of orifice plates, nozzles and venturi tubes inserted in circular cross-section conduits running full.* ISO, Geneva.

Klaassen, G.J., E. Mosselman and H. Brühl (1993). *On the prediction of planform changes in braided sand-bed rivers*. Adv. in Hydro-Science and -Engineering, ed. S.S.Y. Wang, pp 134-146.

Rijn, L.C. van (1993). Unpublished manuscript, DELFT HYDRAULICS.

Vermeer, K. (1990). Fourth visit to Egypt of K. Vermeer; unpublished manuscript, DELFT HYDRAULICS.

Vries, M. de (1959). *Transients in bed-load transport (basic considerations)*. DELFT HYDRAULICS, Report No. R3.

Vries, M. de (1992). *River Engineering*. Delft University of Technology, Faculty of Civil Engineering. Lecture notes f10.

Vries, M. de (1993). *Note on river engineering for braided rivers*. Delft University of engineering, Faculty of Civil Engineering. Workshop on River Engineering, Dhaka, Bangladesh, January 1993.

Wang, Z.B. and R.J. Fokkink (1993). *Study on fundamental aspects of 1D network morphodynamic models;* Report Z654, DELFT HYDRAULICS.

List of main symbols

Symbol	*description*	*dimension*
a	water depth	[L]
B	width	[L]
c	celerity of a disturbance	[LT^{-1}]
C	Chézy-value	[$L^{½}T^{-1}$]
d_s	depth of the sandtrap	[L]
D_{50}	grain diameter	[L]
Fr	Froude-number = $u/\sqrt{ga}$	[-]
g	acceleration of gravity	[LT^{-2}]
H	water level	[L]
i	slope of the bed	[-]
L_i	length of branch i	[L]
n	exponent of transport (power) law $s = mu^n$	[-]
p	porosity	[-]
q	discharge per unit width	[L^2T^{-1}]
Q	discharge	[L^3T^{-1}]
R	hydraulic radius	[L]
Re	Reynolds number	[-]
s	sediment transport per unit width (bulk volume)	[L^2T^{-1}]
S	sediment transport over the entire width (bulk volume)	[L^3T^{-1}]
T	adaptation time	[T]
u	flow velocity	[LT^{-1}]
u_*	shear stress velocity	[LT^{-1}]
$V_{s,i}$	volume of sand trap i	[L^3]
W	fall velocity	[LT^{-1}]
Δ	relative density = $(\rho_s-\rho)/\rho$	[-]
ν	kinematic viscosity	[L^2T^{-1}]
δ	height of a bed form	[L]
ρ_s	density of sediment	[ML^{-3}]

Appendices

Appendix A - Specifications of the orifice and of the Rehbock weir

A.1 The orifice

The function of the orifice in the test rig is to measure the discharge through the delivery pipe which is the inflow in the experimental model. The pressure difference (Δp) at the orifice follows from a reading of the pressure difference meter, connected to the orifice, and now the discharge equation of the orifice can be applied (ISO, 1980):

$$Q_O = \alpha \frac{\pi}{4} d^2 \sqrt{\frac{2\ \Delta p}{\rho}} = C \frac{D^2}{\sqrt{D^4 - d^4}} \frac{\pi}{4} d^2 \sqrt{\frac{2\ \Delta p}{\rho}} \qquad \text{(A.1)}$$

where Q_O is the discharge measured with the orifice;
α is the flow coefficient;
C is the discharge coefficient;
d is the diameter of the orifice;
D is the upstream internal pipe-diameter;
Δp is the pressure difference measured at the orifice;
ρ is the density of water.

The specifications of the orifice are:

d = 0.1309 m;
D = 0.2027 m;
Q_o = 250 m^3/h;
Δp = 30 kN/m^2.

With these specifications, the discharge equation turns into: $Q_o = 4.01.10^{-4}(\Delta p)^{½}$ m^3/s. The pressure difference meter is filled with mercury (ρ=13,6 kg/m^3).

The following rating table is now obtained:

reading Δh (mm)	Δp (N/m^2)	Q_o (l/s)
...	...	...

A.2 The Rehbock weir

The discharge distribution over the two branches downstream of the bifurcation is measured by the use of two Rehbock weirs. The discharge equation of a Rehbock weir is (ISO, 1975):

$$Q_R = C_e \frac{2}{3}\sqrt{2g} b h_e^{\frac{3}{2}} \qquad (A.2)$$

with $h_e = h + k_h = h + 0.0012$

$C_e = 0.602 + 0.083 h/p$

where

Q_R is the discharge measured over the Rehbock weir;

C_e is the coefficient of discharge;

b is the measured width of the weir;

h_e is the *effective* piezometric head with respect to the level of the crest;

h is the *measured* head;

k_h is an experimentally determined quantity which compensates for the influence of surface tension and viscosity;

p is the apex height in meters.

The width and the apex height of both Rehbock weirs are measured:

- Rehbock weir right: - p = 0.1719 m;
  - b = 0.4969 m.
- Rehbock weir left: - p = 0.1753 m;
  - b = 0.4978 m.

Now a rating table for the Rehbock weir can be made, from which directly the discharge is derived dependent on the measured head h.

Appendix B - Specifications of the pipeline

In order to give a more complete view on the pipeline system, as mentioned in Chapter 11, this appendix specifies the exact dimensions of the pipeline via several cross-sections of the overview of the pipeline system (see figure 11.5). The drawings are not to scale.

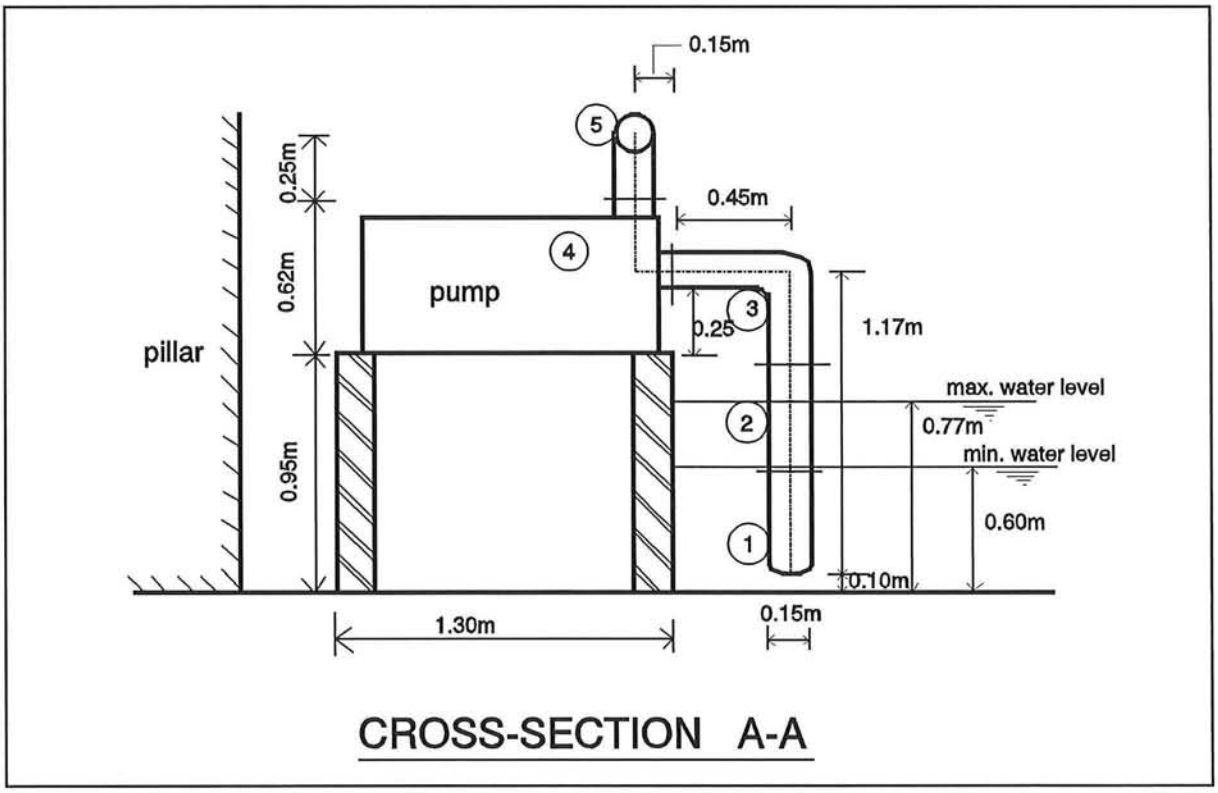

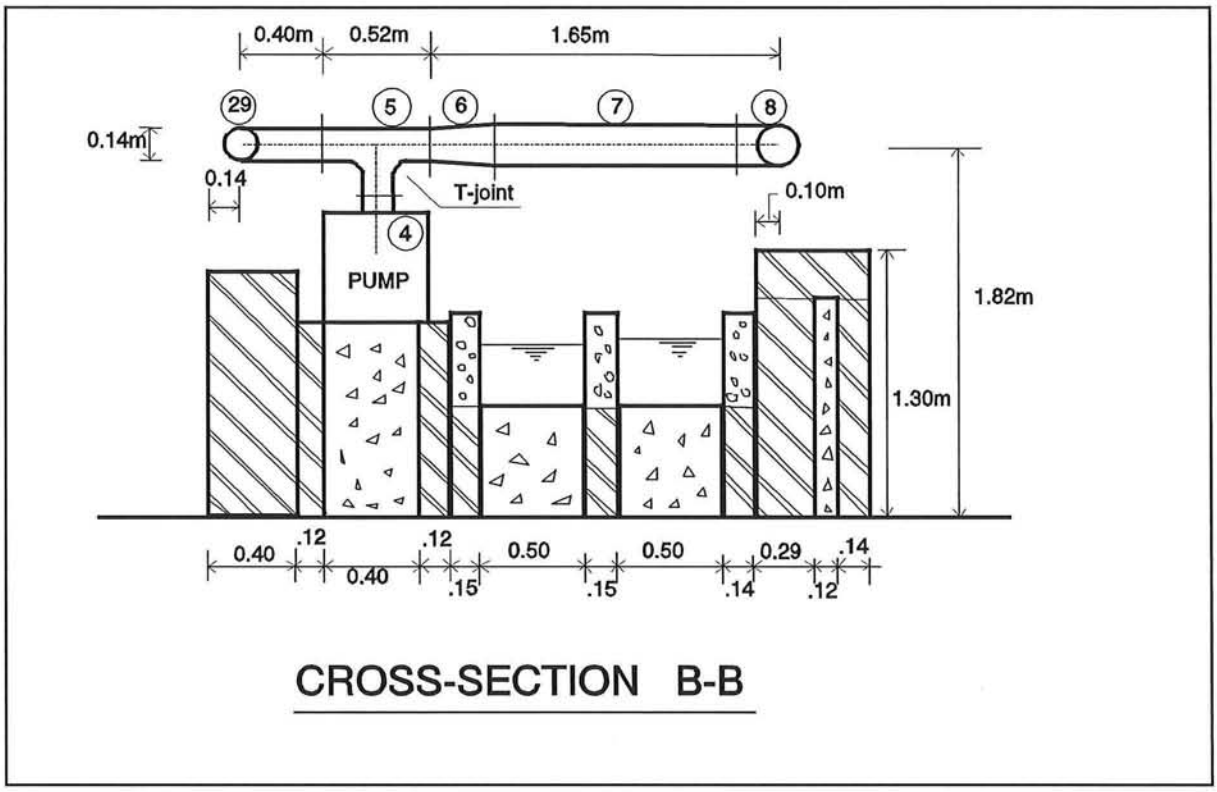

CROSS-SECTION B-B

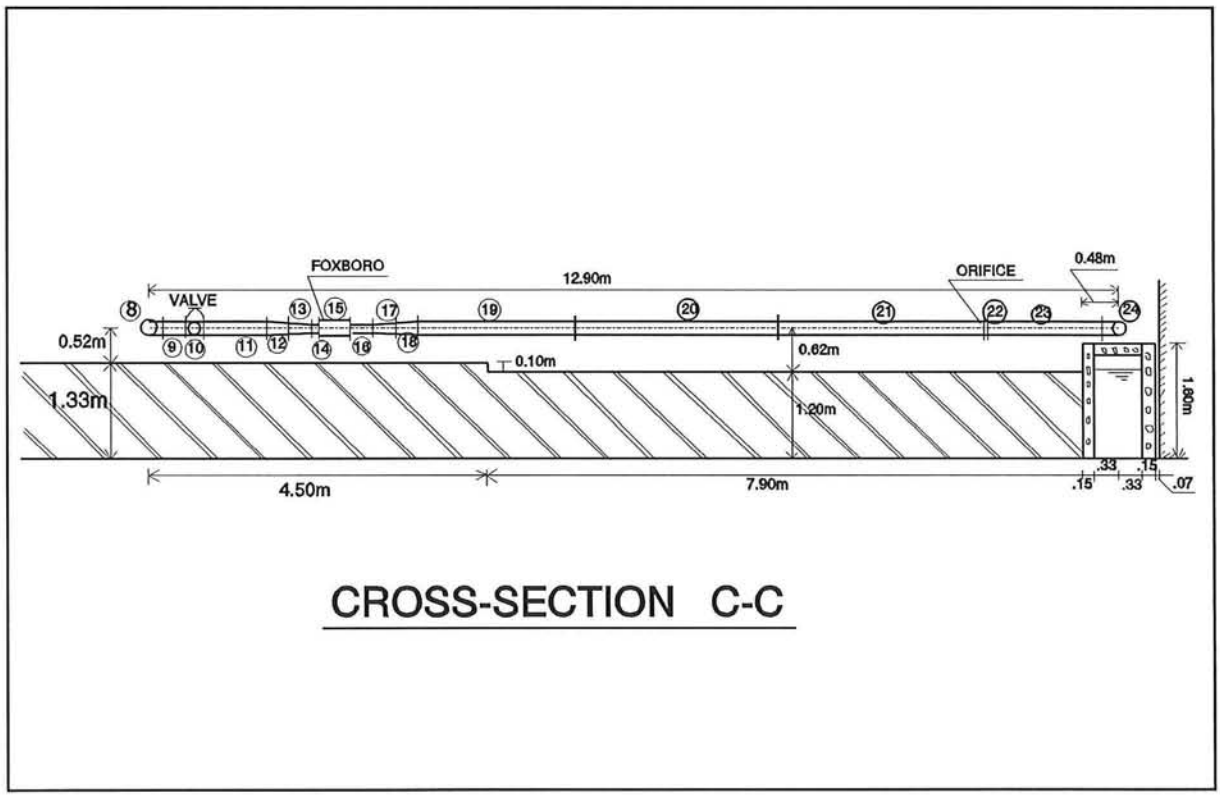

CROSS-SECTION C-C

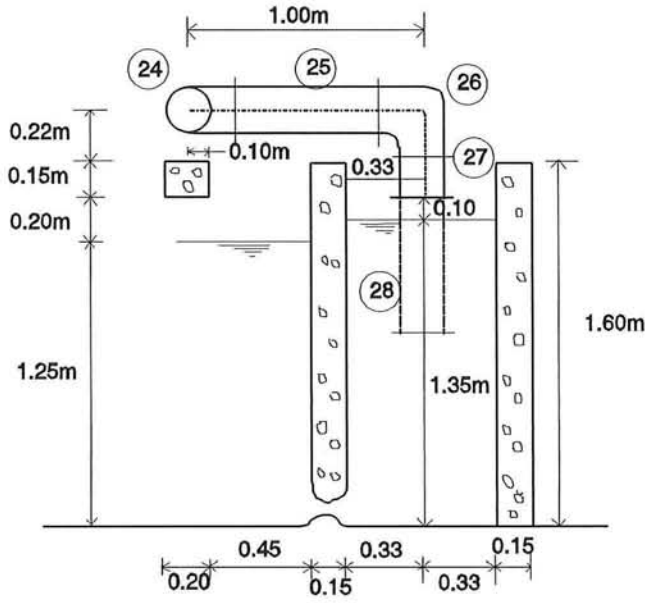

CROSS-SECTION D-D

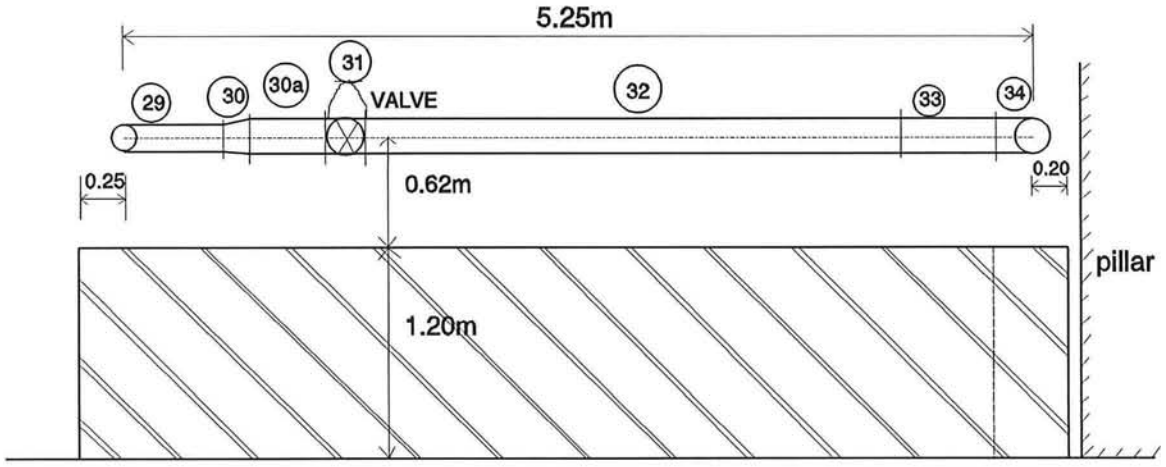

CROSS-SECTION E-E

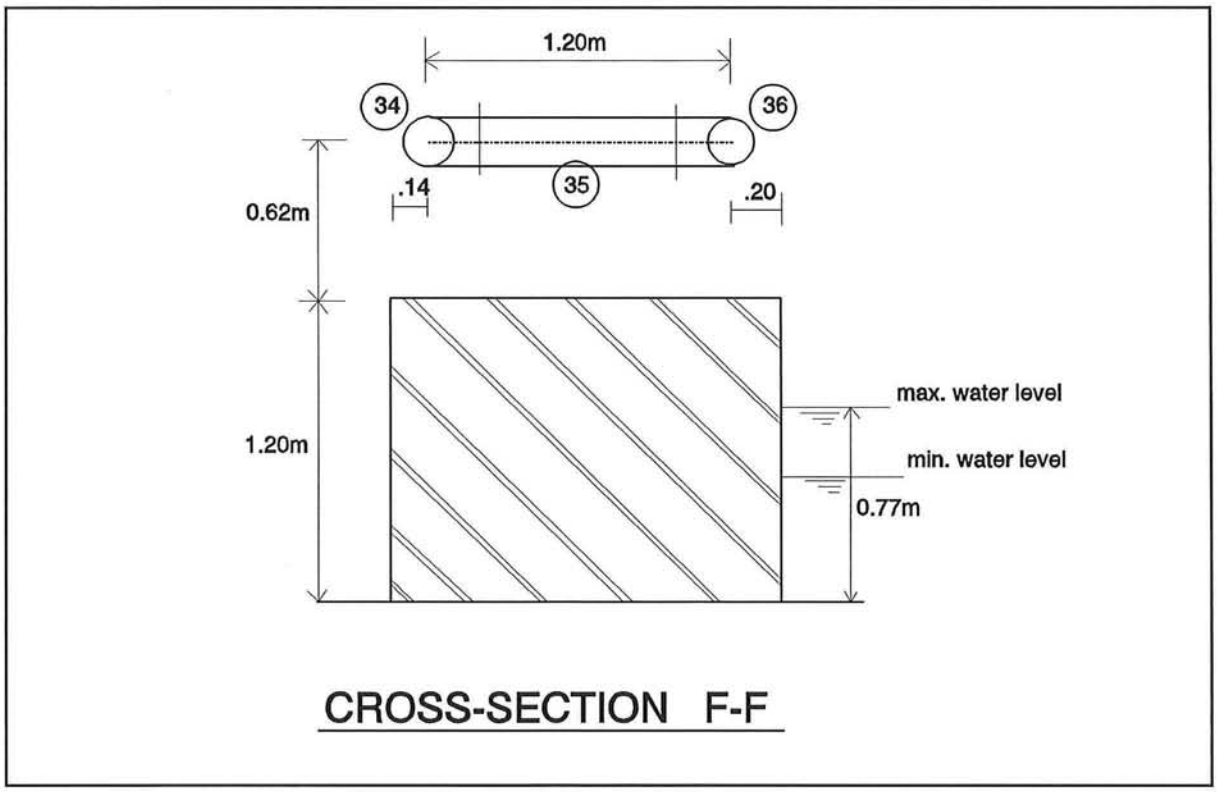

CROSS-SECTION F-F

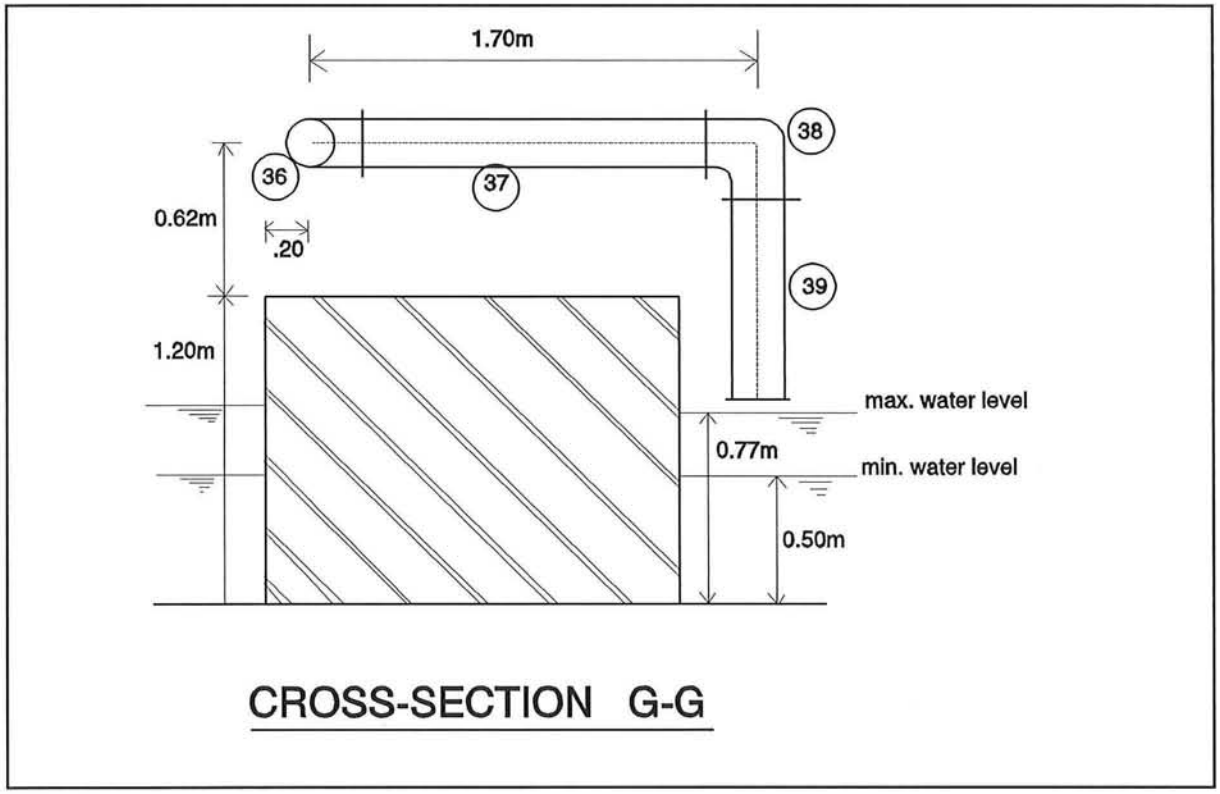

CROSS-SECTION G-G

Appendix C - Regulating and measuring functions of the test rig

This appendix is taken directly from a preliminary study performed by the writers (see Den Dekker and Van Voorthuizen, 1993); it deals with the process of determining the configuration of the regulating and measuring functions of the test rig.
The purposes of the downstream end are to measure the discharge and to regulate the water level in the respective branches. Because of the little space available behind the sand traps the first idea was to combine both purposes in one weir. The first purpose requires that the weir stays in a fixed position during the experimentation in order to avoid leakage, which results in unacceptable inaccuracies in the measured discharge. Considering the second purpose it is essential to use a weir with a shape which follows the water level fluctuations of the river, so that the weir can stay in a fixed position. Taking into account that the 'river' has a discharge equation following $Q \sim h^{3/2}$, a Cipoletti-weir (Bos, 1989) with an essential characteristic of $Q \sim h^{3/2}$ seems a good possibility. The head-discharge equation of this weir type is:

$$Q=C_D C_V \frac{2}{3}\sqrt{2g} b_c h^{\frac{3}{2}} \tag{C.1}$$

in which $C_D C_V 2/3(2g)^{½} \approx 1.86$ m^{½}/s is a good approximation.

In order to know whether the Q/h-curve of a fixed Cipoletti-weir is able to give a satisfactory representation of the real Q/h-curve it is necessary to determine the behaviour of the water level in the situation of a constant water level downstream (De Vries, 1992). At the bifurcation there is continuity with respect to water and sediment. Hence the following equations can be applied:

$$Q_0=Q_1+Q_2 \tag{C.2}$$

and

$$S_0=S_1+S_2 \tag{C.3}$$

Knowing that for the two branches the same water level is present at the bifurcation:

$$Q_1^{-1} S_1^{\frac{3}{n}} B_0^{1-\frac{3}{n}} L_0 = Q_2^{-1} S_2^{\frac{3}{n}} B_2^{1-\frac{3}{n}} L_2 \tag{C.4}$$

and considering the definitions $\xi = Q_2/Q_0$, $\sigma = S_2/S_0$, $\beta = B_2/B_0$ and $\lambda = L_2/L_0$, it is possible to combine the last three equations into

$$(1-\xi)^{-1}(1-\sigma)^{\frac{3}{n}} = \xi^{-1}\sigma^{\frac{3}{n}}(\beta^{1-\frac{3}{n}}\lambda) \tag{C.5}$$

For

$$\beta^{1-\frac{3}{n}}\lambda = \gamma \tag{C.6}$$

this becomes

$$\left[\frac{1-\sigma}{\sigma}\right]^{\frac{3}{n}} = \gamma\left[\frac{1-\xi}{\xi}\right] \tag{C.7}$$

The change of the water level is

$$\eta = \frac{\Delta H_1}{\Delta H_0} = \frac{Q_1^{-1}}{Q_0^{-1}} \frac{S_1^{\frac{3}{n}}}{S_0^{\frac{3}{n}}} = \frac{(1-\sigma)^{\frac{3}{n}}}{1-\xi} \tag{C.8}$$

Combination of the last two equations gives

$$\eta = (1-\sigma)^{\frac{3}{n}} + \gamma\sigma^{\frac{3}{n}} \tag{C.9}$$

Instead of $\eta = f(\sigma)$ it is necessary to have $\eta = f(\xi)$ in order to compare the real situation with the Cipoletti-weir. With

$$\sigma = \frac{1}{\gamma^{\frac{n}{3}}\left[\frac{1-\xi}{\xi}\right]^{\frac{n}{3}} + 1} \tag{C.10}$$

η is expressed as a function of ξ (= the water movement):

$$\eta = \frac{\gamma}{\xi} \frac{1}{\left(\gamma^{\frac{n}{3}}\left[\frac{1-\xi}{\xi}\right]^{\frac{n}{3}} + 1\right)^{\frac{3}{n}}} \tag{C.11}$$

Taking into account that the relation η can also be seen as a relation between two different equilibrium stages in one branch:

$$\eta = \frac{\Delta H_1}{\Delta H_0} = \frac{\Delta H_{new}}{\Delta H_{old}} \tag{C.12}$$

Hence

$$\frac{\Delta H_{new}}{\Delta H_{old}} = \gamma \frac{Q_0}{Q_2} \frac{1}{\left(\gamma^{\frac{n}{3}} \left[\frac{Q_0}{Q_2} - 1 \right]^{\frac{n}{3}} + 1 \right)^{\frac{3}{n}}} \tag{C.13}$$

Now that the water level fluctuations in a real situation has been described, a comparison with the behaviour of a Cipoletti-weir can be made.

Figure 1 shows that:

$$\left(\frac{\partial h}{\partial Q} \right)_{weir} = \left(\frac{\partial \Delta H}{\partial Q} \right)_{reality} \tag{C.14}$$

with

$$\left(\frac{\partial h}{\partial Q} \right)_{weir} = \frac{2}{3} \left(\frac{1}{1.86 b_c} \right)^{\frac{2}{3}} \frac{1}{Q^{\frac{1}{3}}} \tag{C.15}$$

and

$$\left(\frac{\partial \Delta H}{\partial Q} \right)_{reality} = -\gamma \frac{Q_0}{Q_2} \frac{1}{\left(\gamma^{\frac{n}{3}} \left[\frac{Q_0}{Q_2} - 1 \right]^{\frac{n}{3}} + 1 \right)^{\frac{3}{n}}} + \gamma^{\frac{n}{3}+1} \frac{Q_0^2}{Q_2^3} \frac{\left(\frac{Q_0}{Q_2} - 1 \right)^{\frac{n}{3}-1}}{\left(\gamma^{\frac{n}{3}} \left[\frac{Q_0}{Q_2} - 1 \right]^{\frac{n}{3}} + 1 \right)^{\frac{3}{n}+1}} \tag{C.16}$$

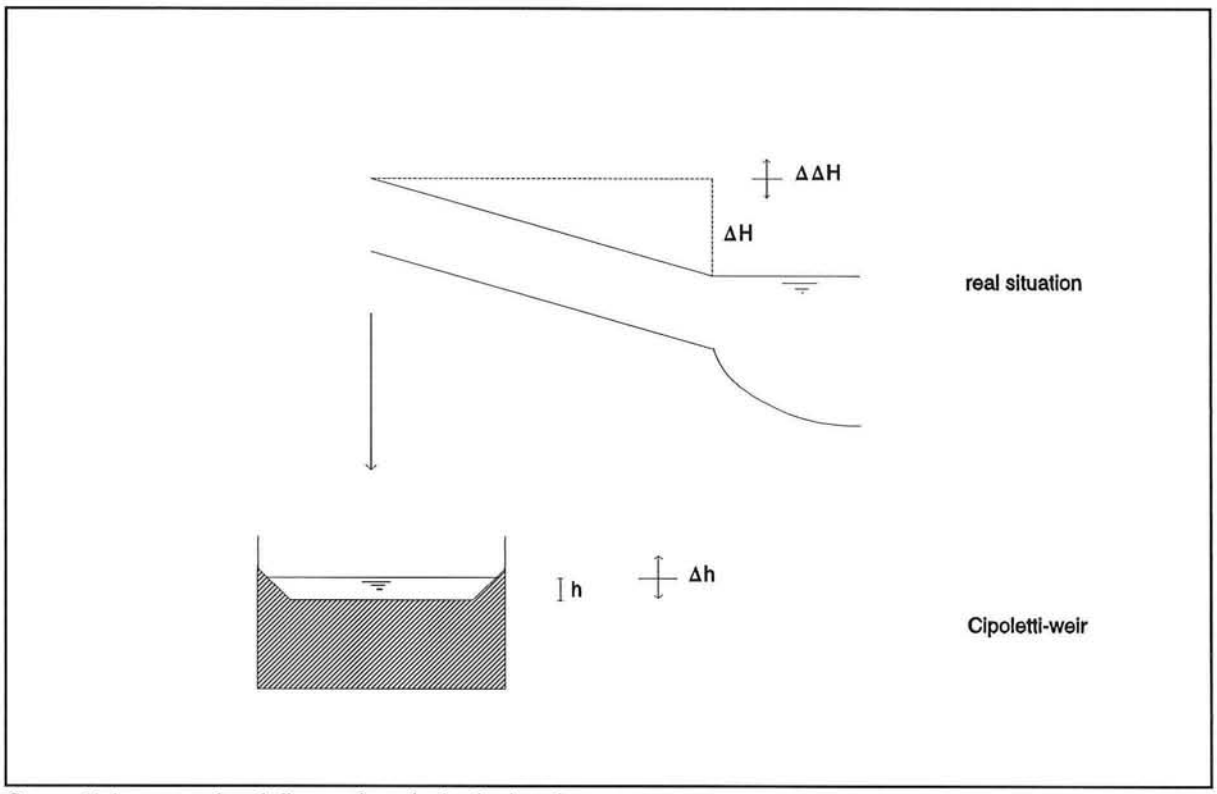

figure C.1 - water level fluctuations in both situations

The relation of Eq. (D14) has been tried to fit with different crest widths b_c but this proved to be impossible.
The conclusion is that the water level fluctuations in reality cannot be represented by a fixed (Cipoletti) weir. This results in the decision to separate the regulating and measuring function.
This led to the construction of a tail gate followed by a Rehbock weir as can be seen in Chapter 11.

Appendix D - Accuracy of the Rehbock weirs

The accuracy of the Rehbock weirs was determined according to well-known statistical methods for the propagation of errors.

D.1 Discharge equation

The discharge equation of a Rehbock weir is (ISO, 1975):

$$Q_R = C_e \frac{2}{3}\sqrt{2g} b h_e^{\frac{3}{2}} \qquad (D.1)$$

with $h_e = h + k_h = h + 0.0012$

$C_e = 0.602 + 0.083 h/p$

where

Q_R is the discharge measured over the Rehbock weir;

C_e is the coefficient of discharge;

b is the measured width of the weir;

h_e is the *effective* piezometric head with respect to the level of the crest;

h is the *measured* head;

k_h is an experimentally determined quantity which compensates for the influence of surface tension and viscosity;

p is the apex height in meters.

D.2 Sources of possible error

The sources of possible error can be identified by examining Eq. (D1); these sources are:

- the discharge coefficient C_e;
- the dimensional measurement of b;
- the measured head h;
- the corrective term k_h.

The total error results from a contribution of all these errors. According to the *quadratic error propagation* method the relative error on the rate of flow is calculated with:

$$X_{Q_R} = \pm\sqrt{X_{C_e}^2 + X_b^2 + \left(\frac{3}{2}X_{h_e}\right)^2} \qquad \text{(D.2)}$$

where X_{Q_R} is the relative error in Q_R;

X_{C_e} is the relative error in C_e;

X_b is the relative error in b;

X_{h_e} is the relative error in h_e.

D.3 Estimate of the total error

As can be seen in Eq. (D2) the total relative error can be calculated once the individual relative errors are found.

Error in C_e:

In ISO (1975) it can be found that the relative error in the coefficient of discharge can be expected to be $X_{C_e} = \pm 1.0$ %.

Error in b:

In Eq. (D2) X_b is defined as:

$$X_b = \frac{\epsilon_b}{b} \qquad \text{(E.3)}$$

where ϵ_{b_e} is the error in the measurement of width b.

The width b was measured with a ruler divided into 1 mm intervals; therefore $\epsilon_b = \pm 0.5$ mm.

From Eq. (D3) it can now be found that $X_b = \pm(0.5/500) = \pm 0.1$ %.

Given this small value, the contribution of X_b to the total error (see Eq. (D2) is considered to be negligeable.

Error in h_e:

In Eq. (D2) the relative error in h_e is used:

$$X_{h_e} = \frac{\sqrt{\epsilon_{h_1}^2 + \epsilon_{h_2}^2 + \ldots + \epsilon_{k_h}^2 + 4\sigma_m^2}}{h_e} \qquad \text{(E.4)}$$

where - ϵ_{h_1}, ϵ_{h_2}, ... are the errors in the measurement of head h;

- ϵ_{k_h} is the error in the k_h term;
- $2\sigma_m$ is the error in the mean of the readings of the head measurement.

- According to ISO (1975): $\epsilon_{k_h} = 0.3$ mm.
- The head-measuring device was divided into 0.1 mm intervals. The head h was therefore read to $\epsilon_{h_1} = \pm 0.05$ mm; the zero was set to within $\epsilon_{h_2} = \pm 0.05$ mm.
- The standard deviation in the mean of ten head measurements proved to be $\sigma_m = 0.03$ mm.

It should be realized that X_{h_e}, and therefore also X_{Q_R}, is not single-valued for a weir: it will vary with the discharge. A worst-case value can however be given: ISO (1975) sets a minimum value for h: $h \geq 0.03$ m. As a result:

$$h_e \geq 0.03 + 0.0012 = 0.0312 \text{ m} \qquad \text{(see Eq. (D1))}$$

$$\Rightarrow X_{h_e} \leq \pm 1.0\ \%.$$

Total error:

With the results of the various contributions, the total relative error made for the rate of flow (in the worst-case) can now be calculated using Eq. (D2).

$$X_{Q_R} = \pm\sqrt{1.0^2 + \left(\frac{3}{2}1.0\right)^2} = \pm 1.8\ \% \qquad \text{(E.5)}$$

Appendix E - Accuracy of the orifice

The accuracy of the orifice was determined according to well-known statistical methods for the propagation of errors.

E.1 Discharge equation

The discharge equation of the orifice is (ISO, 1980):

$$Q_O = \alpha \frac{\pi}{4} d^2 \sqrt{\frac{2\ \Delta p}{\rho}} = C \frac{D^2}{\sqrt{D^4 - d^4}} \frac{\pi}{4} d^2 \sqrt{\frac{2\ \Delta p}{\rho}} \qquad \text{(E.1)}$$

where Q_O is the discharge measured with the orifice;
α is the flow coefficient;
C is the discharge coefficient;
d is the diameter of the orifice;
D is the upstream internal pipe-diameter;
Δp is the pressure difference measured at the orifice;
ρ is the density of water.

E.2 Sources of possible error

The sources of possible error are found by examining Eq. (E1); these sources are:

- the discharge coefficient C;
- the dimensional measurement of d;
- the dimensional measurement of D;
- the measured pressure difference Δp;
- the variation in density ρ.

The total error results from a contribution from all these errors. According to the *quadratic error propagation* method this gives by approximation:
where ϵ_i are the errors made for the different variables.

$$\epsilon_Q^2 = (\epsilon_C \frac{\partial Q}{\partial C})^2 + (\epsilon_d \frac{\partial Q}{\partial d})^2 + (\epsilon_D \frac{\partial Q}{\partial D})^2 + (\epsilon_{\Delta p} \frac{\partial Q}{\partial \Delta p})^2 + (\epsilon_\rho \frac{\partial Q}{\partial \rho})^2 \quad \text{(E.2)}$$

After some algebraic manipulation an expression for the relative errors can be found:

$$X_Q = \sqrt{X_C^2 + \frac{1}{4}X_{\Delta p}^2 + \frac{1}{4}X_\rho^2 + 4\left(\frac{1}{1-\beta^4}\right)^2 X_d^2 + 4\left(\frac{\beta^4}{1-\beta^4}\right)^2 X_D^2} \quad \text{(E.3)}$$

where $X_i = \epsilon_i / i$ is the relative error in the variable i;

$\beta = d/D = 0.1309/0.2027 = 0.6458$.

Numerically this gives:

$$X_Q = \sqrt{X_C^2 + 0.25X_{\Delta p}^2 + 0.25X_\rho^2 + 5.86X_d^2 + 0.18X_D^2} \quad \text{(E.4)}$$

E.3 Estimate of total error

As can be seen in Eq. (E4) the total relative error can be determined once the individual relative errors are found.

Error in C:

An expression for C is given in ISO (1980):

$$C = 0.5959 + 0.0312\beta^{2.1} - 0.184\beta^8 + 0.0029\beta^{2.5}\left[\frac{10^6}{Re_D}\right]^{0.75} \quad \text{(E.5)}$$

with $Re_D = uD/\nu$

where

u is the mean axial velocity of the water in the pipe;

ν is the kinematic viscosity of the fluid.

According to ISO: $X_C = \beta\% + 0.3\%$[1]

As a result it can now be found that $X_C = 0.9458$ %.

Error in ρ:

With the help of tables (Hütte, 1955) an estimate can be made for the variation of ρ with the temperature. In extreme circumstances it can be estimated that $X_\rho = 0.2$ %.

When substituted in Eq. (E4) it can be seen that the contribution of ρ to the total error is negligible.

[1] It is assumed here that the *relative roughness k/D* and the *circularity of the pipe* are in conformity with the limits imposed by ISO (1980). This should be checked to make sure that no additional uncertainty factors have to be added to X_C.

Error in d:

The measuring device used to measure d was divided in 0.1 mm intervals. The diameter of the orifice was therefore measured with an accuracy $\epsilon_d = \pm 0.05$ mm.

As a result $X_d = \pm 0.05/130.9 = \pm 0.04$ %.

This can also be considered negligible when substituted in Eq. (E4).

Error in D:

The measuring device used to measure D was divided in 1 mm intervals. The diameter of the pipe was therefore measured with an accuracy $\epsilon_D = \pm 0.5$ mm.

As a result $X_D = \pm 0.5/202.7 = \pm 0.25$ %.

Combined with the very small factor (see Eq. (E4)) this can also be considered negligible.

Error in Δp:

The orifice was not operational, so a reading of Δp could not be made. Consequently a definite expression for $X_{\Delta p}$ cannot be given; only the sensitivity of Eq. (E4) for variations in $X_{\Delta p}$ can be indicated (see next paragraph).

Total error:

Most of the terms in Eq. (E4) are negligible, so that it can be simplified to the following expression:

$$X_Q = \sqrt{X_C^2 + 0.25 X_{\Delta p}^2} \tag{E.6}$$

An indication of the influence of $X_{\Delta p}$ on X_Q can now be given by substituting in different values for $X_{\Delta p}$:

- $X_{\Delta p} = 1.0$ % $\Rightarrow$ $X_Q = 1.1$ %;
- $X_{\Delta p} = 5.0$ % $\Rightarrow$ $X_Q = 2.7$ %.

If the maximum acceptable error for Q is taken to be $X_Q = 2.0$ %, it follows that the maximum acceptable error in Δp is: $X_{\Delta p} = 3.5$ %.

Appendix F - Standard forms

While conducting experiments it is practical to use standard forms for the physical parameters to be measured. This makes the monitoring of the morphological processes in the model an easier task.
The forms made by the writers are presented below; there are forms for the bed level, the water level and the discharge. Moreover, it is important to keep a good track of the starting and finishing time of the different runs; this is necessary for example for the computation of the average sediment transport - the duration of the run is then needed (see also Chapter 12).

Form 1:

Experiment I: Experimentation time

date :
starting of the pump :
closing of the pump :
experimentation time :

total experimentation time :_____

date :
starting of the pump :
closing of the pump :
experimentation time :

total experimentation time :_____

Form 2:

Experiment I: bed level measurements

date :

cross.sec.	level(mm)					time	exp. time
	1=l	2	3=m	4	5=r		
01							
02							
03							
04							
05							
06							
07							
08							

cross-sec.	level(mm)			time	exp. time
	1(left)	3(middle)	5(right)		
09(0.6m)					
09(0.4m)					
10(0.6m)					
10(0.4m)					
11(0.6m)					

11(0.4m)					
12(0.6m)					
12(0.4m)					
13					
14					
15					
16					
17					
18					
19					
20					
21					
22					
23					
24					
25					
26					
27					
28					
29					
30					
31					
32					
33					
34					

35					
36					
37					
38					
39					

Form 3:

Experiment I: water level measurements

date :

stilling basin	level(cm)	time	experimentation time
I			
II			
III			
IV			

The position of the pitot-tube connected with stilling basin 2 is _____ m up/downstream of the stilling basin.
This table is reproduced many times and is used several times a day, every time a water level measurement is made.

Form 4:

Experiment I: discharge measurements

date :

orifice:

△h (mm Hg)	discharge (l/s)	time	exp. time

Rehbock weirs:

stilling basin	level(cm)	discharge(l/s)	time	exp. time
V				
VI				

These tables can all be reproduced so that one is available every time a measurement is made.